

Grid-edge Monitoring and Control for Enhancement of LV Network Performance with High Renewable Energy Penetration

Citation for published version (APA):

Tâm, M. T. (2022). *Grid-edge Monitoring and Control for Enhancement of LV Network Performance with High Renewable Energy Penetration*. [Phd Thesis 1 (Research TU/e / Graduation TU/e), Electrical Engineering]. Eindhoven University of Technology.

Document status and date:

Published: 07/06/2022

Document Version:

Publisher's PDF, also known as Version of Record (includes final page, issue and volume numbers)

Please check the document version of this publication:

- A submitted manuscript is the version of the article upon submission and before peer-review. There can be important differences between the submitted version and the official published version of record. People interested in the research are advised to contact the author for the final version of the publication, or visit the DOI to the publisher's website.
- The final author version and the galley proof are versions of the publication after peer review.
- The final published version features the final layout of the paper including the volume, issue and page numbers.

[Link to publication](#)

General rights

Copyright and moral rights for the publications made accessible in the public portal are retained by the authors and/or other copyright owners and it is a condition of accessing publications that users recognise and abide by the legal requirements associated with these rights.

- Users may download and print one copy of any publication from the public portal for the purpose of private study or research.
- You may not further distribute the material or use it for any profit-making activity or commercial gain
- You may freely distribute the URL identifying the publication in the public portal.

If the publication is distributed under the terms of Article 25fa of the Dutch Copyright Act, indicated by the "Taverne" license above, please follow below link for the End User Agreement:

www.tue.nl/taverne

Take down policy

If you believe that this document breaches copyright please contact us at:

openaccess@tue.nl

providing details and we will investigate your claim.

Grid-edge Monitoring and Control for Enhancement of LV Network Performance with High Renewable Energy Penetration

PROEFSCHRIFT

ter verkrijging van de graad van doctor
aan de Technische Universiteit Eindhoven,
op gezag van de Rector Magnificus, prof. dr. ir. F.P.T. Baaijens,
voor een commissie aangewezen door het College voor Promoties
in het openbaar te verdedigen
op 07 juni 2022 om 13:30 uur

door

Mai Thanh Tâm

geboren te Nam Dinh, Vietnam

Dit proefschrift is goedgekeurd door de promotoren en de samenstelling van de promotiecommissie is als volgt:

Voorzitter:

prof. dr. ir. M. Mischi

1^{ste} Promotor:

dr. H.P. Nguyen

2^{de} Promotor:

prof. dr. ing. A.J.M. Pemen

Copromotor:

dr. A.N.M.M. Haque

Leden:

prof. dr. P.F. Ribeiro (Universidade Federal de Itajubá)

prof. dr. ir. J.J.L. Driessen (Katholieke Universiteit Leuven)

prof. dr. ir. J.F.G. Cobben

Adviseur:

dr. ir. A. Le (Chalmers University of Technology)

Het onderzoek of ontwerp dat in dit proefschrift wordt beschreven is uitgevoerd in overeenstemming met de TUIe Gedragscode Wetenschapsbeoefening.

*To my parents
To my wife, Hai, and my sons, Pisu and Mon*

This research is supported by Netherlands Organisation for Scientific Research (Nederlandse Organisatie voor Wetenschappelijk Onderzoek - NWO) under the project m2M-GRID - Interaction of microgrids in Active Distribution Networks.

A catalogue record is available from the Eindhoven University of Technology Library.

ISBN: 978-90-386-5513-0

NUR: 959

Printed by Ipskamp Drukkers, Enschede.

Cover design by T.T. Mai, Eindhoven.

Copyright © 2022 by T.T. Mai

All rights reserved.

Summary

Driven by sustainable development targets, the energy transition is taking place in the electrical distribution networks with increasing integration of renewable energy sources (RES), especially solar photovoltaic (PV). However, the intermittency and randomness of RES introduce operational difficulties to the distribution system operators (DSOs) in terms of voltage limit violations and transformer overloading. The PV inverters can curtail the power generation, leading to the loss of energy yield of the PV owners. These adverse impacts become significant barriers to further deployments of RES in the distribution networks, especially at the low-voltage (LV) level. Furthermore, the distribution network reinforcements will require a substantial investment given the large scale of the networks. The investment might not be cost-effective when the problems caused by RES occur not very often.

The recent adoption of advanced sensors, smart meters, and information and communication technology at the grid edges, i.e., interface points between the LV networks and the end-user installations, principally paves the way to deploy the emerging monitoring and control functionalities. Therefore, this thesis investigates the observability and controllability of these grid-edge technologies to assist the LV distribution networks in accommodating a higher share of RES.

The grid-edge monitoring, which uses the available measurement data from smart meters, is explored in Chapter 3. A local energy community (LEC) concept is adopted to perform the proposed monitoring functions, enabling a relief to DSOs regarding investment and operation of the distribution transformer monitoring systems. A data-driven approach is developed based on a critical set of smart meter data (including measurement of voltage magnitudes) collected from LECs. The proposed approach adopts machine learning-based regression models to determine relationships between the estimated transformer loading and measured voltage magnitudes. To this end, a comprehensive framework is provided to implement, validate and compare different machine learning algorithms. Simulation results highlight that the proposed approach can effectively determine the transformer loading using only a limited set of the smart meter measurements provided by the LECs while preserving customers' privacy rights.

In Chapter 4, a sequential control mechanism is formulated at the local control level to miti-

gate the voltage rise problems resulting from the surplus power generation from PV systems. The sequential integration of $Q - V$ and $P - V$ droop control into this mechanism allows PV unit to operate in reactive power priority mode. This mode enables voltage regulation to be first attempted through reactive power absorption (RPA). Then, active power curtailment (APC) is triggered only if the voltage levels cannot be maintained below the threshold value using RPA, which will reduce the curtailed energy of PV systems. However, the droop parameters of such sequential control mechanism have significant technical and economic impacts for the PV owners and the DSOs. Therefore, a Monte Carlo-based method is developed to comprehensively assess the cost-effectiveness of the sequential control mechanism by using a series of economic and technical metrics.

Chapter 5 presents a centralised coordination paradigm for multiple local controllers of PV inverters to cope with the voltage rise problems. Given the radial LV network structure, applying the droop-based local control with the static, same parameter values in voltage rise conditions causes the deficient employment of RPA capacity of PV inverters. This deficiency refers to PV units connected closer to the transformer operating with limited or even no reactive power absorption. Meanwhile, other PV units, e.g., connected toward the end of the feeder, can still bear a high share of RPA. Therefore, an optimisation problem is formulated together with the sensitivity matrix concept to regularly update the droop parameters of the local controllers of various PV inverters during the voltage rise conditions. The objective is to optimise RPA capacity for reducing APC. Finally, the centralised control algorithm is executed to solve the optimisation problem, which is successfully verified through simulations on a typical Dutch LV network.

In Chapter 6, a distributed coordination control strategy is proposed that adapts sequential droop control-based local control for PV inverters with advancement in the effective use of RPA and a fair APC. The distributed control, i.e., requiring neither a central control nor extensive communications, is developed to periodically adapt the parameters of both $Q - V$ and $P - V$ droop control in the sequential control mechanism. To this end, the consensus algorithm and sparse communication are adopted. This distributed control is superior to the centralised one in terms of scalability and reliability when considering the widespread integration of PV systems in LV networks. Furthermore, the epsilon-decomposition technique is employed to decouple the network into multiple control areas. Finally, the proposed control strategy is implemented to significantly reduce the amount of APC and simultaneously obtain an effective contribution of RPA among all PV units toward voltage rise mitigation.

In short, the thesis demonstrates the importance of grid-edge monitoring and control strategies that will help stimulate the integration of RES, such as PV systems in LV distribution networks and support the networks in its operation. The developed grid-edge monitoring and control strategy focuses on solving the transformer overloading and voltage rise problems by exploiting the RES controllability and digital transformation. The energy transition in the distribution networks, hence, can be facilitated.

Samenvatting

In de elektriciteitsdistributienetten vindt de energietransitie plaats met toenemende integratie van duurzame energiebronnen (RES, renewable energy sources), vooral fotonvoltaïsche zonneënergie (solar PV, photovoltaics). De fluctuerende en willekeurige opwekkingspatroon van RES levert voor de distributienetbeheerders (DSOs, distribution system operators) operationele moeilijkheden op in termen van overschrijding van spanningslimieten en overbelasting van transformatoren. Deze nadelige effecten worden belangrijke barrières voor de verdere aansluiting van RES op de distributienetten, vooral op het laagspanningsniveau (LV, low voltage). Bovendien vereisen de benodigde netverzwaringen een belangrijke investering, die gezien de uitgebreidheid van de netten niet kosteneffectief is.

Recente toepassing van geavanceerde sensoren, slimme meters en informatie- en communicatietechnologie aan de “grid edges”, dat wil zeggen de laagspanningszijden van de netstations, maakt opkomende monitoring- en regelfuncties mogelijk. Dit proefschrift onderzoekt de observeer- en regelbaarheid van deze “grid-edge”-technologieën bij het opnemen van een hoger aandeel RES in de laagspanningsnetten.

De “grid-edge”-monitoring, die gebruik maakt van meetgegevens uit slimme meters, wordt onderzocht in hoofdstuk 3. Een concept voor lokale energiegemeenschappen (LEC, local energy community) wordt gebruikt voor de voorgestelde monitoringfuncties, wat de DSOs investeringen en bedrijfsvoering uitspaart voor transformator-monitorsystemen. De ontwikkelde op data gebaseerde benadering maakt gebruik van een kritische set van slimme-meterdata (inclusief meting van de spanning) verzameld van LECs. De voorgestelde benadering gebruikt op machine-learning gebaseerde regressiemodellen om verbanden tussen de geschatte transformatorbelasting en de gemeten spanningen te bepalen. Een alomvattend kader wordt gegeven voor het implementeren, valideren en vergelijken van verschillende machine-learningsalgoritmes. Simulatieresultaten tonen dat de voorgestelde benadering de transformatorbelasting effectief kan bepalen, met slechts een beperkte set van de metingen van de slimme meters van de LECs en met behoud van de privacy van de klanten.

In hoofdstuk 4 wordt een sequentieel regelmechanisme op het lokale regelniveau geformuleerd teneinde de spanningsoprijvingsproblemen door het vermogenoverschot door de PV-opwekking te verminderen. Door sequentiële integratie van blindvermogens-spanningsr-

egeling en vermogens-spanningsregeling kan de PV-eenheid in blindvermogens-prioriteit-regelmodus werken. Deze regelmodus probeert spanningsregeling in eerste instantie te bereiken met blindvermogensabsorptie (RPA, reactive power absorption). In tweede instantie, alleen als RPA de spanning niet onder de drempelwaarde kan brengen, wordt vermogensbeperking (APC, active power curtailment) getriggerd. Een dergelijk sequentieel regelsysteem heeft een belangrijke technische en economische impact voor de eigenaren van PV-systemen en DSOs. Daarom is een Monte-Carlomethode ontwikkeld om de kosteneffectiviteit van het sequentiële regelmechanisme integraal te evalueren op een reeks economische technische aspecten.

Hoofdstuk 5 introduceert een paradigma voor gecentraliseerde coördinatie van meerdere lokale regelaars van PV-omvormers om de problemen met spanningsopdriving op te lossen. Gegeven het radiale karakter van het laagspanningsnet leidt lokale regeling met statische, onderling gelijke parameters onvoldoende gebruik van de RPA-capaciteit van de PV-omvormers: PV-eenheden dicht bij de transformator zullen weinig of zelfs geen blindvermogen opnemen, terwijl andere PV-eenheden aan het eind van een kabel een groot aandeel in RPA leveren. Daarom wordt een optimalisatieprobleem met gevoeligheidsmatrix geformeerd waarbij de spanningsregelparameters (statisch) van de verschillende PV-omvormers bij hoge spanning regelmatig geüpdate worden. Het doel is om de RPA-capaciteit te optimaliseren om APC te beperken. Tenslotte wordt het centrale regelalgoritme uitgevoerd om het optimalisatieprobleem op te lossen, wat succesvol getest is met simulaties aan een Nederlands laagspanningsnet.

In hoofdstuk 6 wordt een gedistribueerde coördinatieregelstrategie voorgesteld die sequentiële lokale regeling voor PV-omvormers aanpast met verbetering in het gebruik van RPA en een beperkte hoeveelheid APC. De gedistribueerde regeling, dat wil zeggen zonder centrale regeling en zonder uitgebreide communicatie, is ontwikkeld om de parameters van zowel blindvermogens-spanningsregeling als vermogens-spanningsregeling periodiek aan te passen. Hiertoe worden het consensusalgoritme en sparse communication gebruikt. Deze gedistribueerde regeling is superieur aan de gecentraliseerde regeling in termen van schaalbaarheid en betrouwbaarheid, gezien de wijdverbreide integratie van PV-systemen in laagspanningsnetten. Verder is de epsilon-decompositietechniek gebruikt om het net in verschillende regelgebieden te verdelen. De voorgestelde regelstrategie wordt geïmplementeerd om de hoeveelheid APC belangrijk te verminderen en tegelijkertijd RPA van alle PV-eenheden te verkrijgen om de spanning te beperken.

Kortgezegd toont dit proefschrift het belang aan van “grid-edge”-monitorings- en -regelstrategieën die een hogere integratie van RES, zoals PV in laagspanningsnetten zullen bevorderen, en die de bedrijfsvoering van distributienetten zullen ondersteunen. De ontwikkelde “grid-edge”-monitorings- en -regelstrategieën richt zich op het oplossen van de congestie- en spanningsproblemen door gebruikmaking van de regelbaarheid van RES en digitale transformatie. Aldus kan de energietransitie in de distributienetten worden gefaciliteerd.

Contents

Summary	v
Samenvatting	vii
1 Introduction	1
1.1 RES integration in electricity distribution networks	1
1.2 Motivation	2
1.3 Research objective and questions	4
1.3.1 Objective	4
1.3.2 Research questions	4
1.4 Research approach and thesis outline	5
1.4.1 Research approach and scope	5
1.4.2 Thesis outline	6
2 Overview of grid-edge monitoring and control	9
2.1 Introduction	9
2.1.1 Grid-edge monitoring and control concept	9
2.1.2 Challenges from high RES penetration	11
2.2 Grid-edge monitoring	14
2.3 Modelling and simulations of grid-edge control	15
2.3.1 From physics-based to data-driven models	15
2.3.2 From numerical to real-time simulation	16
2.4 Grid-edge control architecture, layers and strategies	17
2.4.1 Control architecture	17
2.4.2 Hierarchical control	18

2.4.3	Grid-edge control strategies	20
2.5	Particular use-cases for grid-edge control	21
2.5.1	Autonomous control	21
2.5.2	Coordinated control	26
2.6	Discussion	28
2.6.1	Advanced functionalities of RES	28
2.6.2	Distribution network monitoring improvement	28
2.6.3	Cybersecurity consideration	29
2.6.4	Regulatory/Framework consideration	29
2.6.5	Uses of Data-driven/Machine learning approaches	29
2.7	Summary	30
3	Transformer loading monitoring	31
3.1	Introduction	31
3.2	Problem definition	32
3.2.1	Transformer congestion monitoring	32
3.2.2	Residential smart meter data	33
3.2.3	Data-driven monitoring framework	33
3.3	Data pre-processing procedure	34
3.3.1	Training data generation	34
3.3.2	Exploratory data analysis	37
3.3.3	Feature selection	41
3.4	Model fitting and evaluation	43
3.4.1	ML algorithm list preparation	43
3.4.2	Model evaluation and selection	45
3.4.3	ML algorithm selection	47
3.5	Model deployment	50
3.5.1	Model set-up	51
3.5.2	Model performance analysis	51
3.6	Summary	54
4	Local control for voltage regulation	57
4.1	Introduction	58

4.2	Voltage rise issues	59
4.3	Droop control for voltage regulation	60
4.3.1	Active power curtailment (APC)	60
4.3.2	Reactive power absorption (RPA)	61
4.3.3	Proposed sequential droop control	61
4.4	Stochastic impact assessment	63
4.4.1	Assessment procedure	63
4.4.2	Metrics for impact assessment	64
4.5	Simulation setup	66
4.6	Numerical results	66
4.6.1	Impacts on LV distribution networks	68
4.6.2	Impacts on the PV owners	69
4.7	Summary	73
5	Centralised control for voltage regulation	75
5.1	Introduction	75
5.2	Centralised coordination control	76
5.2.1	Local control algorithm	77
5.2.2	Centralised control algorithm	78
5.2.3	Integration of local control and centralised control	81
5.3	Simulation setup	83
5.3.1	Case study	83
5.3.2	Simulation platform	85
5.4	Numerical results	86
5.4.1	Voltage control	86
5.4.2	Control of PV generation	89
5.4.3	Summary	91
6	Distributed control for voltage regulation	93
6.1	Introduction	94
6.2	Impact of PV generation on voltage regulation	95
6.3	Proposed control strategy	95
6.3.1	ε -Decomposition technique	96

6.3.2	Local control layer	98
6.3.3	Coordination control layer	98
6.4	Modelling and simulation	101
6.4.1	LV distribution network	101
6.4.2	Load profiles and PV system data	101
6.4.3	Simulation platform	101
6.5	Numerical results	103
6.5.1	Control area determination	103
6.5.2	Voltage rise mitigation	105
6.5.3	PV system contribution to voltage rise mitigation	108
6.5.4	Sensitivity analysis of different threshold values	110
6.5.5	Performance evaluation in different control areas	111
6.6	Summary	115
7	Conclusions	117
7.1	Research summary	117
7.1.1	Grid-edge monitoring and control	118
7.1.2	Transformer loading monitoring	119
7.1.3	Local control for voltage regulation	119
7.1.4	Centralised control for voltage regulation	120
7.1.5	Distributed control for voltage regulation	121
7.2	Contributions	121
7.3	Recommendations	123
7.3.1	Grid-edge monitoring in LV distribution networks	123
7.3.2	Grid-edge control in LV distribution networks	124
A	Load characteristics and PV capacity data	127
B	Results of exploratory data analysis	129
C	Additional results of the assessment of PV local voltage control	137
	References	137

List of Figures	161
List of Tables	167
List of Abbreviations	169
List of Publications	172
Acknowledgments	175
Curriculum Vitae	178

1

Introduction

1.1 RES integration in electricity distribution networks

In efforts to address climate change, the electricity power systems are undergoing the energy transition with the goal of reducing carbon dioxide emission and smarter use of resources. A main pillar for such transition is the integration of renewable energy sources (RES), such as wind and solar photovoltaic (PV), in the electricity distribution networks (see Fig. 1.1). Policies and support schemes have been issued to promote the RES integration. For instance, at the world-wide level, the 26th United Nation climate change conference of the parties (COP26) encourages countries in setting ambitious 2030 emissions reductions targets, e.g., by accelerating the coal-fired power plants phase-out and investing in RES [1]. At the continent level, the European Union (EU) set a target of 40% share of EU energy consumption being generated by RES by 2030 [2]. At national level, the Netherlands proposes to increase the EU 2030 target to 55% emission reduction [3]. The energy transition towards more environment-friendly operation based on electrification is also occurring in other energy sectors, such as the transport and heating/cooling [4]. Specifically, the former opts for the adoption of electric vehicles (EVs) to substitute the fossil-fuel vehicles, while the latter aims to replace gas-fired heaters by heat pumps (HPs).

The integration of RES at the customers' premises reduces the network power losses while

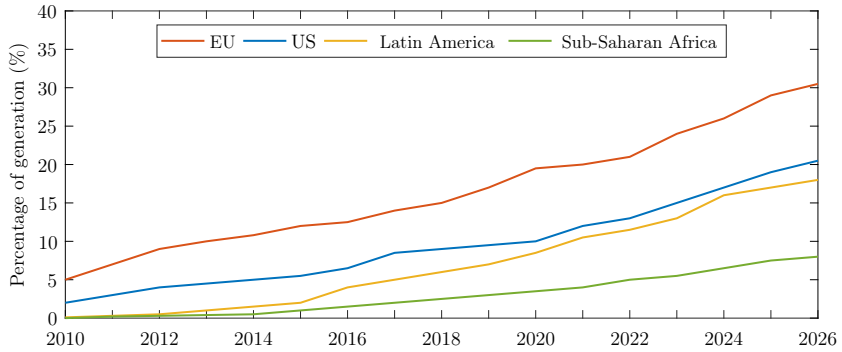


Figure 1.1: *Percentage of wind and solar PV in total electricity generation [5].*

increasing the end-users' control over their electricity consumption and enabling them to be actively involved in the electricity market [6]. Furthermore, RES in combination with energy storage systems (ESS) are capable of reshaping the energy generation, providing support for the network operation.

Despite all of these improvements, massive integration of RES in low-voltage (LV) and medium-voltage (MV) distribution networks cause several challenges for network operation and planning. The challenges have arisen from the nature of RES associated with the uncertainty and variability. For instance, the surplus power due to rapid expansion of wind and solar PV can lead to voltage rise and/or congestion problem. In several countries, the RES generation curtailment have already been implemented to ensure the system operation (see Fig. 1.2). A more detailed description of the challenges is given in Chapter 2. Addressing these adverse impacts involves changes in the network planning and operation, e.g., reinforcements of network components and operation of power quality supporting equipment, to increasingly accommodate RES while maintaining the overall quality of supply. These solutions, however, require a significantly high financial investment given the large scale of the networks. The investment, however, might not be cost-effective when the problems caused by RES occur not very often.

1.2 Motivation

As mentioned previously, the proliferation of RES systems in LV distribution networks has resulted in the burden on the network operation and the deterioration in power quality. Such adverse influences will spread out as RES are still foreseen to be increasingly integrated in the network. Additionally, the fact of limited online monitoring and real-time control

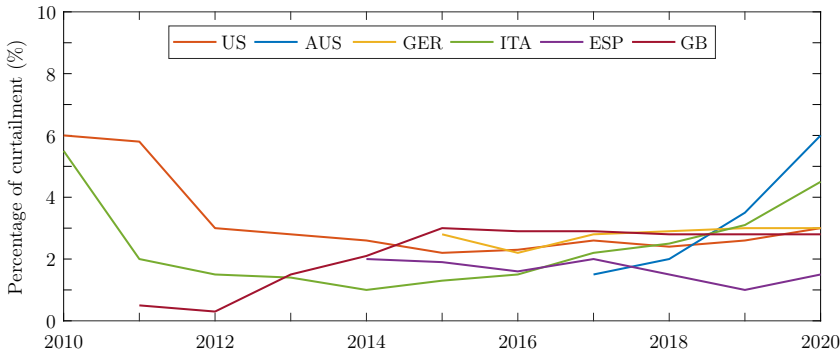


Figure 1.2: *Percentage of wind and solar PV generation curtailment [5].*

in LV distribution networks can worsen the adverse influences of RES. Suitable solutions to cope with these problems, thus, become necessary.

One of the traditional solutions is to reinforce the existing network infrastructure, that would enhance the overall hosting capacity of the network. This traditional solution, however, typically comes at great investment cost for DSOs. Furthermore, DSOs will need a substantial investment in developing an adequate monitoring and control in LV distribution networks for the network operation. Due to the large investment, these reinforcements and developments can be delayed and fail to support the network performance. It is, hence, desired to have the alternative solutions for the network monitoring and control, which involves not only DSOs but also RES systems.

The growing presence of RES with its built-in controllability in LV distribution networks offer great solutions to enhance the network operation. Thanks to the advanced power electronic interfaces used, RES have the control possibilities that can be exploited to aid the network operation. On the other hand, the growing integration of RES in the network enables its contributions towards managing the operation constraints to be more effective. Controlling RES, thus, has been widely proposed by the researchers to not only overcome the network operation issues but also allow more RES intergration.

Moreover, the rapid digital transformation in LV distribution networks can facilitate the control of RES, as well as the monitoring of the network. The digital transformation attributes to the installations of advanced sensors and smart meters (SM), and the applications of Internet-of-Things (IoT) with two-way communication. Such recent development at the grid edge aids in collecting the network operational data; therefore increase the observability of the networks. The digital transformation, additionally, promotes the exchange of information among the network components, which then assist the network control.

Hence, the combination of the digital transformation and the inherent controllability of RES, if properly designed, is expected to provide the promising solutions to enhance the performance of LV distribution networks with high RES penetration.

1.3 Research objective and questions

1.3.1 Objective

The main objective of this thesis is to devise appropriate grid-edge monitoring and control strategies, that can help to enhance the performance of LV distribution networks. The devised strategies should be able to deal with current issues in the power distribution networks due to the increasing penetration of RES. Moreover, such strategies also should be capable of exploiting the RES controllability in combination with communication and information availability in the LV distribution networks to provide the network support.

1.3.2 Research questions

To achieve the aforementioned objective, the following research questions are formulated and will be addressed in the subsequent chapters.

- Q1: What are key enabling technologies for grid-edge monitoring and control and how can they enhance the performance of the future LV distribution networks?
- Q2: How can the increasing availability of residential smart meter data be used for the monitoring of the distribution transformer loading?
- Q3: How can the residential PV control functions be properly designed to overcome voltage rise problems in LV distribution networks while reducing PV generation curtailment?
- Q4: What are the long-term effects of the local voltage control by the residential PV systems on LV distribution networks and the PV owners and how can the DSO quantify such effects?
- Q5: How can the available reactive power capacity be optimally coordinated among residential PV systems to solve voltage rise problems?
- Q6: How can the distributed control strategy be formulated to coordinate PV systems for voltage rise mitigation with more effective contribution and fair treatment of PV systems, without the need for a central controller?

1.4 Research approach and thesis outline

1.4.1 Research approach and scope

An appropriate approach is devised to achieve the research objective of formulating the effective grid-edge monitoring and control strategies. The challenges of the increasing integration of RES in LV distribution networks are explored first. Reviewing the monitoring and control in LV distribution networks is subsequently conducted, focusing on its role in the network operation support and the possible architectures, as well as the enabling functionalities related to distribution network monitoring and control.

Next, with the purpose of improving the congestion monitoring in the LV distribution network, the grid-edge monitoring approach is investigated leveraging the increasing availability of residential smart meter data. In this regard, the application of the machine learning techniques to estimate the distribution transformer loading is studied. To implement this data-driven approach, the role of the local energy communities (LECs) is also discussed. The efficiency of the proposed grid-edge monitoring approach is evaluated through simulations on the unbalanced European LV distribution network.

Then, the suitable grid-edge control strategies for supporting LV distribution network in voltage violation management are formulated. Since the voltage violation is a local problem, the voltage control methods need to be developed considering the widespread integration RES in distribution networks, as well as RES controllability. The local voltage control is implemented by every RES utilising the locally available information; thus no cost of investment and network modifications for DSOs. The local voltage control method is assessed on their long-term technical and economical impact on the network and RES owners by running simulations on European LV distribution network. On the other hand, as the overall optimal operation of the networks and the proper utilisation of RES capacity are desired, formulating the coordinated control methods for multiple RES is essential. For this, the hierarchical control framework, i.e., with multiple control layers operating in different time intervals, are applied considering the sheer scale of LV networks. Accordingly, centralised and distributed control strategies are separately investigated for mitigating the voltage violation problems. The centralised control strategy is considered to coordinate the local voltage control of RES with optimally dispatching the RES power output. Solving such optimisation problem is performed by a centralised controller using the linear programming technique. Besides, the distributed control strategy coordinates the local voltage control of RES, aiming for the fairness of RES active power curtailment and the efficient uses of its reactive power capacity. To this end, the consensus algorithm and a sparse communication network are used, while the central controller is needless. The feasibility of the proposed centralised and distributed control strategies is verified through simulations on the typical LV distribution networks, respectively.

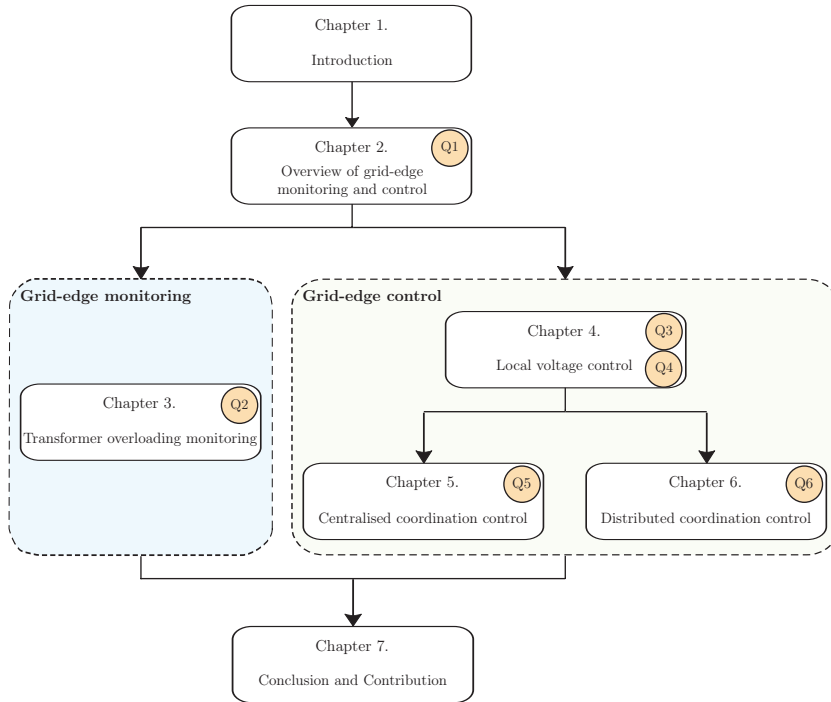


Figure 1.3: Visualisation of the thesis outline and the correlation between the chapters and the research questions (Q1 - Q6).

The above description indicates that exploring the controllability of residential-scale RES systems and exploiting the availability of residential customer consumption data fall within the scope of this research. It is assumed that the adequate communication infrastructure is available in the LV distribution networks to facilitate the grid-edge monitoring and control. The main focus of the research reported in this thesis is on evaluating the proposed strategies more in the operation phase. The development requirement and cost for the communication infrastructure is, hence, left out of the scope of this work.

1.4.2 Thesis outline

The rest of the thesis is organized in the following chapters, where the research questions (i.e., Q1 to Q6) described in the previous section are addressed. The thesis outline and the correlation between the chapters and the research questions are visualised in Fig. 1.3.

- **Chapter 2** describes an overview of grid-edge monitoring and control in LV distribution networks. First, the challenges resulted from the energy transition in LV distribution networks is presented. The context of grid-edge monitoring and control is then elaborated, including the role of these approaches in supporting distribution network operation. Next, technological aspects of grid-edge monitoring and control, including modelling, architecture, and strategies, are discussed.
- **Chapter 3** discusses the application of a data-driven approach for congestion monitoring of MV/LV transformers. It is proposed that this approach be implemented by the local energy communities, considering their ability to access the residential SMs. In this regard, data from these residential SMs in terms of voltage magnitudes is used as an input variable. Next, the relationships between residential SM data and the transformer loading are analysed. The machine learning-based regression models are subsequently adopted to estimate the transformer loading. To this end, a methodological framework to implement, validate and compare different machine learning algorithms is presented. This framework covers the essential stages for training data generation, exploratory data analysis, feature selection, model selection and algorithm selection.
- **Chapter 4** investigates the impact of local control methods for voltage rise problems on LV distribution networks and the PV owners. This local voltage control is performed by the residential-scale PV systems operating with the sequential droop control (SDC) mechanism and using local measurement. The SDC mechanism is comprised of reactive power absorption and active power curtailment schemes (based on the $Q - V$ and $P - V$ droop control, respectively), to regulate the PV generation for tackling voltage rise issues. A conditional multivariate Copula method is adopted to generate a large set of time series input data. A Monte Carlo-based stochastic approach and various impact metrics are subsequently used, that helps to achieve a comprehensive assessment of the long-term technical and economical impact.
- **Chapter 5** studies a coordinated voltage violation management in LV distribution networks with high PV penetration. This coordinated management approach is formulated by integrating the local voltage control of PV systems and the centralised control algorithm following a hierarchical control architecture. The sequential $Q - V$ and $P - V$ droop control (SDC) scheme is utilised in each PV inverter to address voltage rise problems. A centralised controller is assumed to manage the coordination of the local voltage control of PV systems. The concept of Jacobian matrix is adopted to estimate the linearised relationship between changes in powers injection at bus with changes in bus voltage. Given the computed Jacobian matrix, the centralised controller solves the optimisation problem of PV power output by using the linear programming technique. To this end, new control parameters for the local voltage control is calculated and then dispatched to PV inverters, enabling an increasing utilisation of its reactive power capacity and reduction in its active power curtailment.

- **Chapter 6** presents a distributed coordination control strategy for mitigating voltage rise problems in LV distribution networks. First, the ε -decomposition technique is employed to decouple the network into multiple control areas with the strong coupling nature of PV systems, where the proposed control strategy can be effectively implemented. Next, in each control area, the hierarchical control architecture is designed to incorporate the local voltage control and the distributed control of PV systems for voltage regulation support. The local voltage control makes use of the SDC mechanism discussed in Chapter 4. The distributed control is developed using the consensus algorithm and a sparse communication network with a low bandwidth requirement, while no need for a centralised controller. Based on a consensus among PV inverters within each control area, the distributed control periodically tunes and adapts the parameters of both $Q - V$ and $P - V$ droop control scheme of PV inverters. This distributed coordination control inherits the autonomous feature of the droop control for coping with voltage rise issues while helps achieving the fair active power curtailment and the efficient employment of reactive power absorption of PV systems. In addition, a sensitivity analysis of different control parameters as well as different ε values is conducted to further evaluate the performance of the proposed control strategy.
- **Chapter 7** concludes the thesis by summarizing the main findings, highlighting the general contributions and formulating recommendations for future research.

2

Overview of grid-edge monitoring and control

This chapter introduces a comprehensive overview of grid-edge monitoring and control for LV distribution networks. First, relevant aspects of the energy transition in LV distribution networks are presented, followed by the challenges originating from this recent development. Thereafter, the context of grid-edge monitoring and control is elaborated, including the role of the approach in supporting the distribution network operation. Technological aspects of grid-edge monitoring and control, including modelling, architecture, and strategies, are also discussed¹.

2.1 Introduction

2.1.1 Grid-edge monitoring and control concept

The penetration of RES is rapidly growing in both transmission and distribution power systems and posing several operational challenges. The monitoring of the system performance becomes a greater importance for transmission networks [9], as well as distribution networks;

¹This chapter is based on [7] and [8]

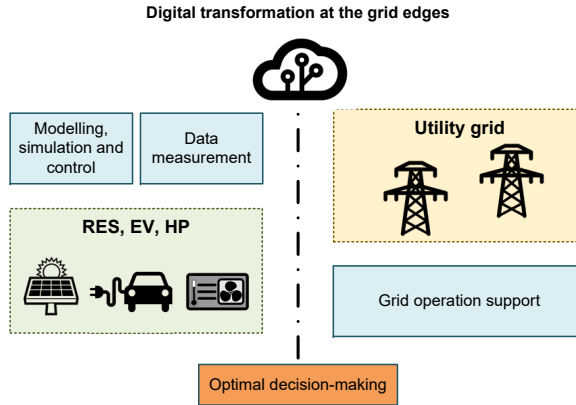


Figure 2.1: *The concept of the grid-edge monitoring and control.*

thus, the controlling actions can be properly executed. Distribution networks are evolving from the traditional, passive system into smart, active system, resulting from the rapid digital transformation at the grid edges, i.e., interface points between the LV networks and the end-user installations. The digital transformation arises from the adoption of advanced sensors, SM as well as the emerging development of IoT with two-way communication. For this, the key drivers are the technological development, i.e., data integrity, cyber-physical systems, artificial intelligence (machine learning), and digital twins for a secured, flexible, and efficient grid operation with cost reduction [10]. The digital transformation at the grid edges enables the LV distribution network to have digital structure, facilitating self-monitoring and self-healing capabilities [6]. Moreover, actively exploiting the advanced ICT can enhance the controllability of RES and the network [11]. The digital transformation at the grid edge, thus, would facilitate the optimal coordination of the customer-owned RES [10] and for improving the efficiency of the power system operation [12]. As a result, the adoption of the digital transformation along with the inherent controllability of RES, if properly managed, is expected to maximise the cost-effectiveness of incorporating RES into the grid while maintaining system reliability. In this respect, managing the network requires a new paradigm of RES control strategies, whose overview is presented in this chapter. For this paradigm, it is crucial to leverage ICT, data-driven and machine learning-based methods given the increasing availability of the data measurement. In this context, a so-called grid-edge control refers to the control of RES at the grid edges, which uses various data resources from the digital transformation. Fig. 2.1 illustrates the concept of grid-edge monitoring and control.

This chapter provides an overview of the grid-edge monitoring and control of RES in LV distribution networks. As a part of this overview, the challenges of operating LV distri-

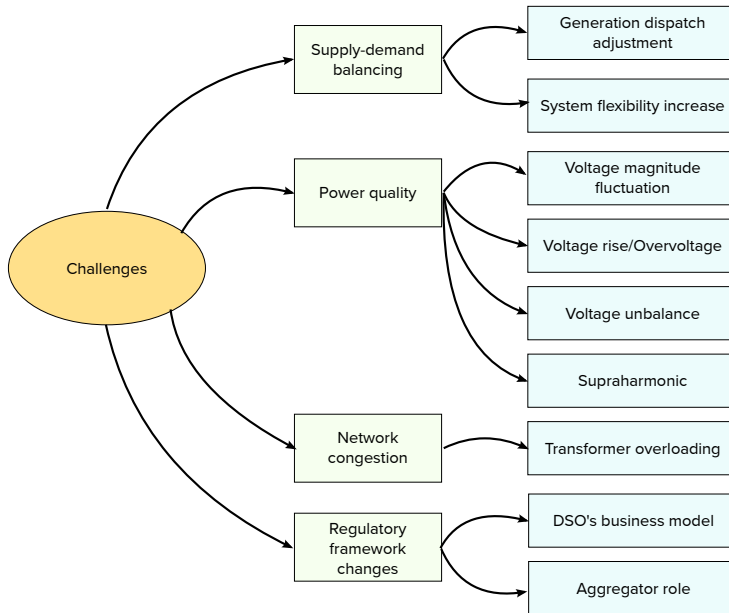


Figure 2.2: *Main challenges for grid operation and planning due to high RES penetration.*

bution networks due to the increasing RES integration are presented. Next, the grid-edge monitoring is discussed, followed by the modelling and simulation of the grid-edge control. Then, a thorough discussion of the structures, layers and strategies for the grid-edge control is provided. The last section shows particular use-cases for the grid-edge control.

2.1.2 Challenges from high RES penetration

With the inherent intermittency and randomness, the rapid proliferation of RES, especially PV systems, in LV distribution networks causes several challenges for grid operation and planning as shown in Fig. 2.2. In this section, such challenges is discussed to provide a sound foundation for determining proper control solutions.

Supply-demand balancing

PV technologies have uncertain characteristics by nature, such as intermittency, randomness and variability [13]. As the primary renewable energy cannot be stored, PV power output is discontinuously usable to supply the electricity demand. Moreover, fluctuation of PV power

outputs with fast and frequent fashion adds more stress on network and market operation. To ensure a reliable electricity supply, the adjustments of power generation dispatches must be carried out quickly and more frequently. In this regard, the system flexibility to efficiently operating the entire system needs to increase.

At the system level, the flexibility can be arranged by an adequate level of reserved power from generation-side resources. Because of the operational constraints, e.g., minimum permissible power and standby duration time, are fundamental for power plants, this flexibility provision capacity level can be difficult to be achieved.

Thanks to the large-scale deployment of RES, the demand-side flexibility can be considered as an alternative resource to contribute to the system balancing task, especially at the local and regional level [14]. The potential can be even enlarged by leveraging a synergy from coupling sectors, including electrification in the transportation and building sectors, i.e., EVs and HPs, respectively.

Power quality

With the increasing share of RES in a particular geographical area, the generated power can vary fast and considerably in magnitude. This can be due to sudden changes in solar irradiance (i.e., cloud passing) [15], subsequently provoking voltage magnitude fluctuation. In some cases, the voltage fluctuation can be significant that interfere with the operation of voltage regulation equipment, such as load tap changer of distribution transformers, line voltage regulators and capacitor banks [16].

A large scale of PV systems eventually causes voltage magnitude to rise along the distribution feeders, resulting from significant reverse power flows into the upstream networks when the load is low. Many European DSOs have reported the frequent occurrence of voltage rise problems due to the implementation of RES in their LV networks [17]. This undesired voltage rise potentially damages the customers' electrical appliances. Furthermore, the voltage rise can lead to the generator tripping activated by internal protection. This subsequently induces the loss of the owners' revenue as they are not able to sell the surplus power generation. The level and widespread of voltage rise depend on the PV penetration level in the grid.

Besides, uneven distribution of single-phase PV systems and unbalance PV power generation can lead to voltage unbalance. Voltage unbalance is quantified by a percentage term, called Voltage Unbalance Factor (VUF), in which the 10-min average value should be within 2% for 95% of the time. Voltage unbalance increases at the end of the feeder. High level of voltage unbalance causes all induction motor type and distribution transformer to be overheated and derated. Subsequently, the lifetime of the equipment will be reduced.

PV inverters with high-frequency switching techniques are the major sources of high-frequency

currents injection into distribution networks [18], subsequently, creating high-frequency voltage and Total Harmonic Distortion (THD) [19]. These supraharmonics potentially become contributing factors for increased heating in the equipment and conductors, and then power loss increase in distribution networks [19]. Widespread adoption of RES at the grid edges with power electronic interfaces results in a growing level of supraharmonics in power systems [20].

Network congestion

One of the operational difficulties created from the rapid proliferation of RES is the issue of congestion or thermal overloading of the network assets, e.g., lines, cables, and transformers [21]. The reverse power flowing through the distribution transformer from RES located in its secondary side can exceed the rated power. The network congestion likely occurs in the urban power networks with high population density [22]. As reported in [23], nearly 90% of distribution transformers in the Netherlands will become more prone to the overloading in 2040 due to the new generation technologies (such as PVs), as well as new load types (such as electrified HPs and EVs). The congestion issues can become a significant barrier to further deployments of RES in LV networks. In practice, the limits on penetration level or peak power generation have been imposed on the PV integration in LV networks [15]. These approaches are, obviously, not desirable and should be replaced by alternative solutions, which are discussed in the next sections.

Changes in regulatory framework

The integration of RES, as well as EVs and HPs, is radically altering the performance of the power distribution systems because these systems were not originally designed to accommodate such technologies. To facilitate this alteration while still effectively managing the network performance, DSOs must adjust the planning and operational procedures for distribution networks. Additionally, the active, decentralised features of the future power distribution systems resulted from RES integration are not originally considered in the design of the business model of DSOs. Currently, DSOs are operating, maintaining and upgrading the distribution systems mostly in the passive fashion with fix remuneration specified annually by the regulators [4]. Hence, DSOs' business model also needs to be modified to actively manage the grid [4].

Besides, RES can support the grid operation as their production profiles can be controlled directly or indirectly by the owner/network operators. This support, subsequently, can be utilised to handle the local issues, e.g., congestion/voltage violation. Using the support from RES, however, is currently limited due to the wide geographical distribution of RES [4]. Therefore, to effectively mobilise the support of RES, a new role in the form of the aggrega-

tors is essential to be introduced [4]. These aggregators should be empowered to have direct or indirect control over the RES, then offering a supporting tool for DSOs to address technical problems. To enable the introduction of the aggregator, a radical change in the regulatory frameworks is required.

It is worth to mention that other issues are emerging due to increasing integration of RES, such as low initial and frequency stability as indicated in [6, 19, 24–27]. However, these issues are more concerned in the transmission networks. The deployment of ICT at the grid edges imposes the challenges from the viewpoint of control and performance of the power systems by introducing cybersecurity and privacy threats [6, 11].

2.2 Grid-edge monitoring

To address the operational difficulties for LV distribution networks resulting from the increasing integration of RES, a proper monitoring of the network performance is critical. However, several burdens hinder the DSOs from adequately monitoring and managing the operational difficulties in their networks. The DSOs have to install the measurement systems and develop an extensive communication infrastructure between their systems and customers' premises. Additionally, building the data management systems is required to handle the gathered data [28]. These developments are deemed costly and not easily implemented, given the sheer scale of LV networks.

A recent implementation of the LECs, along with an increasing availability of residential SMs, can offer a solution to the monitoring and management in LV networks. The LECs intend to actively participate in RES projects in their regions [29]. If the LECs can read SM data of the end-users and control the RES, the controllability and energy efficiency of the local networks can be improved [30]. Trading energy within the LECs is also possible; thus, use of locally generated and shared energy from RES can be stimulated [31]. However, while the LECs can access customers' SMs, they generally do not have the information on the network topology. Therefore, if cooperating actively with the DSOs, the LECs can provide essential operational supports to the utility grids [30]. In contrast, if the collection and management of all customers' SM data, as well as later the control of customers' RES, are performed by the DSOs, this can impose additional burden to their works, especially when considering the high volume of SMs and the wide geographical distribution of RES [4]. All these in turn can negatively affect the monitoring and management of the network operation. In this regard, using data-driven approaches (i.e., using the residential SM data and implemented by the LECs) is considered promising while supporting the network operation and preserving customers' rights.

While recognising added-values of SM data from residential houses for LV network monitoring, most previous works focused on the physics-based approaches that limit their appli-

cability in the diversified, complex LV networks [32–39]. For instance, the dedicated monitoring systems are still required at the substation secondary side. Besides, the aggregated SM readings from LV end-users are required to implement the state estimation methods for LV systems [35]. The distribution system state estimation enables the DSOs to monitor their grid variables, i.e., voltages, currents, and power, allowing the network congestion monitoring. However, the volume of SM data aggregation grows exponentially given the increasing number of the customers, which likely creates difficulties in collecting and processing the data [40]. Therefore, selection of representative meters is desired for the particular monitoring applications in LV networks. Furthermore, active and reactive power data from residential SMs are used in some studies. Since the consumption data contains highly private information about the households, their privacy and security are subjected to violation [41]. The privacy concerns cause the customers in certain countries to raise the objections to use of SM readings.

Among the machine learning techniques for power systems, regression models are commonly used because of its easy-to-implement and -interpret features [41]. Regression models mathematically formulate the correlation between one output variable and one or multiple input variables, afterwards allowing to estimate the output variable from the input variables. Regression models are widely employed for load forecasting [41–43], RES generation forecasting [44, 45], power system state estimation [46, 47], and network operation supporting [48, 49].

2.3 Modelling and simulations of grid-edge control

Proper development of the grid-edge control has necessitated the modelling and simulations of RES (focusing on PVs), which are firstly listed in Fig. 2.3 and subsequently presented in detail in this section.

2.3.1 From physics-based to data-driven models

The physics-based models, also regarded as white-box, include the physics of the object to be modelled, providing reliable and accurate modelling tools [50]. However, adequate knowledge of the system characteristics is required and then needs to be modelled in a detailed manner. The model execution, consequently, shows the computational burden and is time-consuming. Typically, the physics-based models are applied for component levels up to device levels [50]. For instance, the examples at device-level details, e.g., inverter modelling, are introduced in [51], and for component levels in [52].

Data-driven models represent the statistical relationship between input and output data of a given system without presenting the underlying physics. Data-driven models can use sta-

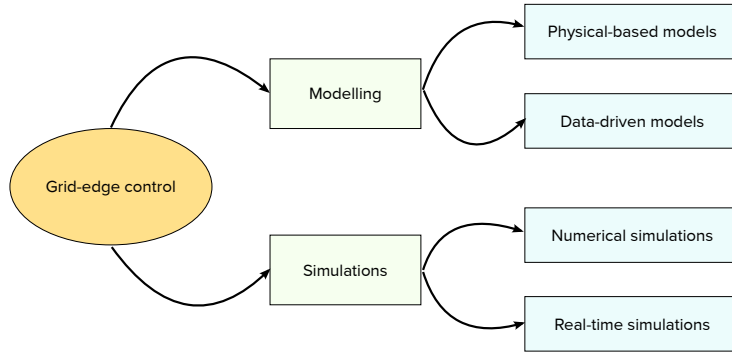


Figure 2.3: *Types of modelling and simulations of the grid-edge control.*

tistical and machine learning approaches. Thus, data-driven model execution is less computationally demanding compared to physical-based models [50]. Considering the increasing availability of data measurement, data-driven models are being employed more frequently, especially for system-level modelling. For instance, applying data-driven models at the system levels is presented in [53], and at device-level details in [50]. However, the accuracy of the data-driven models is strictly related to the amount of training data available [54].

2.3.2 From numerical to real-time simulation

A simulation platform to enable the grid-edge control solutions can be implemented using either numerical simulation or real-time (RT) simulation approaches. The first approach, i.e., non-RT, is widely used in the early stage, e.g., design, due to ease of implementation, low cost and safety reasons, using simulation software. Several common simulation software includes MATLAB/Simulink, PSCAD, GAMS, and HOMER [55]. Subsequently, the second approach is used in the next stages, e.g., validation, to further test the proposed works beyond the numerical simulation for solutions before real deployment. In this platform, the RT simulator machine takes the central role as its powerful simulation capability enables the modelled network to operate closely to realistic manner [56]. RT simulators can be of great help for designers and researches to better understand the main problems and to identify the more appropriate solutions. The commonly used RT simulators include RTDS and Opal-RT. Some laboratory-based setup and test-beds for RT simulation platforms have been developed in various countries, e.g., Austria, Germany, France, and the UK, as discussed in [56, 57]. However, it is worth noting that these simulators may not be accurate enough because the models on which they are based are not always capable of replicating the realistic behaviour of the physical system [58]. As a consequence, the solutions identified by

these simulators may be inefficient when applied to the actual system.

2.4 Grid-edge control architecture, layers and strategies

This section describes different architecture, layers and strategies for the grid-edge control. Possible grid-edge control solutions are also presented.

2.4.1 Control architecture

Based on the communication network, the grid-edge control strategies can be categorised into centralised, distributed, and decentralised control, as shown in Fig. 2.4.

Centralised control

This control method (illustrated in Fig. 2.4 (a)) is considered as a conventional approach, constituted of a central controller and bi-directional communication links between this unit to every single component of the networks. Theoretically, the central controller needs to receive and process the messages exchanged from all units, causing a large number of message exchanges within the grid. All control decisions are made by the central controller. This control architecture makes the system development expensive [57] while weakening the system reliability due to a single-point-of-failure of the central controller or the malfunction of any communication links [59]. Scalability is another shortcoming of the centralised control, resulted from the additional complexity to the communication network and required setting update of the central controller. With the high integration of RES, centralised control is potentially impractical [60]. Instead, the adoption of centralised control is appropriate for a

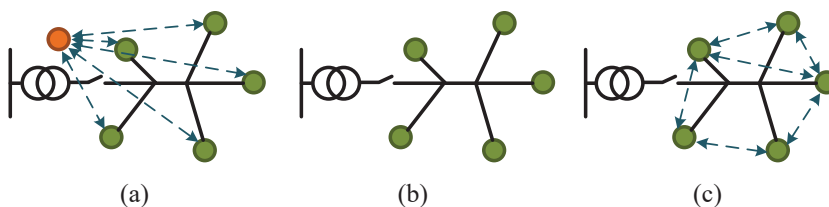


Figure 2.4: Classification of grid-edge control strategies based on their communication network: (a) Centralised control, (b) Decentralised control, (c) Distributed control. The green circles represent RES, while the orange circle represent a central controller. The dashed blue lines represent two-way communication links.

small-scale grid that includes a small number of nodes and does not require frequent system expansion [61]. Using the Energy Management System (EMS) is a promising solution to the implementation of centralised control.

Decentralised control

The decentralised control (shown in Fig. 2.4 (b)) dismisses the duties of a central controller nor one-to-all communication system; thus, allowing simplicity and relatively low cost of implementation, and obtaining higher reliability. As no extensive communication infrastructure is required, the required investment decreases as compared to the centralised control. The control decisions are made individually at each RES by its local controller using the local information [62]. This method makes ICT performance robust against the failures. However, RES lack the awareness of system-wide performance as well as other units' status [63]. Moreover, these methods usually apply the same control settings for all RES, which have different types and operating conditions [64]. This approach can lead to uncooperative operation of RES, subsequently unexpected problems [64].

Distributed control

In the distributed control (illustrated in Fig. 2.4 (c)), a central controller is excluded, but communication is needed, which is in the form of sparse communication links between some adjacent RES with low bandwidth. This kind of communication allows developing the distributed control with lower cost compared with the centralised control. By using the sparse communication, all RES take the responsibilities for the network optimisation and stability via coordinating each other. In case of a new RES installed, only the configuration for the communication links between this unit and the neighbouring ones is required [16]. Distributed control is suitable for a system that has a large number of nodes, high complexity of system structure, and more frequent expansion of the system [61].

2.4.2 Hierarchical control

Because distribution networks compose different power generation systems based on different technologies and power ratings, it is necessary to implement a hierarchical control to maximise the controllability, reliability, efficiency while minimising the operation cost [65]. The hierarchical control, thus, can assist the robust operation of the networks. Determination of optimum operation for the grid takes into account various factors, for example, rated and available capacity of generation systems, distribution of loads and generation systems, electrical market prices, generation costs. In that sense, neither fully centralised nor fully decentralised control can accomplish the proper control of the system. A compromise

between fully centralised and decentralised control can be obtained employing a hierarchical control [62]. The hierarchical control can be formulated by three main layers: primary, secondary, and tertiary control. These control layers are different in their: time frame and response speed when they are operating, and the supporting infrastructure requirement [62].

Primary control

Primary control is the first level of hierarchical control. It is implemented by local controllers, which is embedded in each component, such as RES, ESS and loads. This control layer is capable of acting fast (on the order of milliseconds) in a pre-determined way without needs for communication with neighbouring units [66], contributing to the enhancement of network stability [67]. The functions of the primary control are islanding detection, output control of individual RES and power-sharing among RES [59, 62]. This control layer, consequently, enables the inverters to autonomously operate at each unit, resulting in the improvement of power stability.

Secondary control

Secondary control is upstream control layer of the primary control that is responsible for the reliable, secure and economical operation of the grid [62]. This control layer provides the reference parameters for the primary control, e.g., output power or voltage at the POC [59, 68, 69]. Therefore, the secondary control eliminates the steady-state error caused by primary control [62, 70]. For example, secondary control restores grid frequency, and voltage amplitude within the accepted range, e.g., by ± 0.1 Hz in Nordel (North of Europe) or ± 0.2 Hz in UCTE (Continental Europe) [71], as well as voltage unbalance and harmonic compensation. Besides, it is in charge of synchronisation and power exchange with the main grid [14]. The response speed of the secondary control is slower than the primary due to some limitations, such as availability and capacity of primary sources.

The approach to design secondary control can be classified as centralised, decentralised, and distributed control architecture [72] as discussed in Sec. 2.4.1. The centralised one is suitable for the network operating in an islanded mode in which supply-demand balance is a critical issue [62]. The decentralised and distributed ones are suitable for the network operating in a grid-connected mode in which multiple objectives exist. Communication network plays a crucial role as secondary control gathers information from a primary control within each RES and in return, dispatches control signal to the primary control [59].

Tertiary control

Tertiary control is the top control layer which optimises the power flow in the grid once the grid already operates at its rated frequency and acceptable voltage range [70]. Awareness of operation conditions of neighbouring and upstream distribution networks is essential to execute the optimisation functions, in which ICT is a key enabling technology. This optimisation considers the relationship between the demand and the energy supply balance, and the marginal generation cost of each generation unit. The tertiary control regulates the power flows between the main grid and the controlled grid. Additionally, such control level also takes charge of restoring the secondary control reserve and supporting the secondary control is necessary [69]. Tertiary control works in the time frame of several minutes, issuing the control command to secondary controls within a grid [62].

2.4.3 Grid-edge control strategies

To enable potential from the grid-edge control, it is important to consider the coexistence of the control structures from distribution networks down to available local control functions of individual RES. This synergy from all control layers can be realised from either corrective or predictive control approach, which will be discussed in the followings.

Corrective control

Corrective controls refer to control actions to mitigate or reduce the potential impacts of the undesirable operational situations when they occur, aiming to maintain the system with normal operation. Within the context of distribution networks, the undesirable operational situations include voltage limit violation, power quality issues, congestion and faults in the network. Implementation of corrective controls can be based on rule-based methods, model predictive control (MPC) and statistical/machine learning techniques. Examples of corrective controls for RES consists of control of power outputs of PVs and EVs for voltage regulation [73, 74]; reduce in HPs' power consumption for congestion management [22]; fault-tolerant control of wind generators to achieve ride through capability [75].

Preventative control

Preventative controls are designed to carry out before corrective controls, i.e., when the threat events have not occurred. The purpose of preventative controls is to prevent the likelihood of such threat events or non-conformities in the system, then avoiding their potential impacts. To this end, preventative controls typically adopt the forecast/prediction techniques and risk

analysis for a specific time horizon in the future. MPC can also be used to realise the preventative control algorithm. Examples of the applications in LV networks with the high integration of EVs using preventative controls include optimal operational planning/scheduling of EVs [76]; power ramp-rate control of PV systems using forecasting methods [77]; and MPC-based control of ESS to reduce the fluctuating power outputs of PV systems [78].

2.5 Particular use-cases for grid-edge control

In this section, the review of some particular use-cases for the grid-edge control, focusing on PVs are described as they are the main pillars of the grid-edge control.

2.5.1 Autonomous control

Autonomous control for RES, also called local control, provides voltage and frequency control of the regional LV network in the islanded operation mode, and the support services for the regional LV network in the grid-connected mode (e.g., voltage regulation support) [79]. Furthermore, this control supports the elimination of voltage and frequency deviation during the transition from the grid-connected operation mode to the islanded operation mode and vice versa [79]. The control actions are implemented at the electronic inverters interfacing the sources with the grid and involves the local measurement of frequency and voltage only, no information exchange with surrounding sources needed.

Active power control

Controlling active power injection from RES is perceived as the most effective solution to address their negative effects on the grid operation due to the fluctuating power production. This means that RES must be capable of controlling its active power output upon the request, e.g., to respond to voltage rise problems, instead of solely maximising the energy harvesting. The active power control of RES can be categorised into two main groups: power reduction control (PRC) and power ramp-rate control (PRRC). In the PRC, the actual power output of RES is reduced from the instantaneous available power to a specified level, which can be fixed or variable during the operation period [80]. In the PRRC, the rate of change of RES power output is limited to a certain value during the fluctuation of the primary renewable resources (e.g., passing clouds) [80]. This control decreases the power fluctuation of RES, subsequently stimulating the reduction in the network voltage fluctuation. Possible approaches to fulfil these active power control functionalities can be based on ESS, control of PV inverters, and local controllable loads [81]. Meanwhile, provision of the power reference

values and supervision of the active power control for RES can be made by using the droop control, or auto-adaptive control, or data-driven methods.

- **Control of ESS:** In [82–87], ESS is combined with the PV system in distribution networks to realise the PRC for mitigating the voltage fluctuation problems due to high penetration of PVs. Furthermore, during the unavailability of power generated from PVs (e.g., during the nights), the ESS can inject active power into the grid, contributing to the voltage support and congestion management during peak load periods. Authors in [88, 89] proposed the integration of ESS into PV systems to implement the PRRC for the PV power fluctuation reduction. The combination of ESS and RES offers a promising solution to effectively control RES power because of its high flexibility. Meanwhile, maximising the energy harvesting of RES will be imperious. However, the cost associated with the installation, operation and maintenance of that system is the main concern. Authors in [74] proposed the use of EV batteries as ESS to deliver the PRC for residential PV units.
- **Control of PV inverters:** Without ESS, active power control of PVs can be carried out to address the technical issues arisen by their significant development. In [73, 74], the maximum power point tracking (MPPT) algorithm embedded in the power converter of PV systems is modified to realise the PRC supporting the voltage rise alleviation. Authors in [77] introduced the modification of MPPT in PV inverters to provide the PRRC without energy storage. Controlling PV power converters requires no additional hardware component, making it cost-effective to regulate PV power. The main drawback of this method is the loss of energy yield due to the power curtailment, and the impossibility of injecting extra power to the network [81].
- **$P - f$ and $P - V$ droop control:** $P - f$ droop control, also known as conventional droop control, mimics the behaviour of synchronous generators, which reduces the frequency when active power increases [25, 66]. This behaviour can be stimulated by the following formula:

$$(f - f^*) = -K_{Pf}(P - P^*) \quad (2.1)$$

where f and P correspond to the measured output frequency and active power of the DG system, respectively, and f^* and P^* correspond to the reference values for frequency and active power of the DG system, respectively. The coefficients K_{Pf} denotes the active droop slope. Thus, $(f - f^*)$ represents the frequency deviation from its reference value and $(P - P^*)$ represents the variation of output active power delivered by the DG system to proportionally compensate such deviation. Fig. 2.5 (a) illustrates the $P - f$ droop control. Such $P - f$ droop control is suitable for the inductive grid, such as high voltage and medium voltage network.

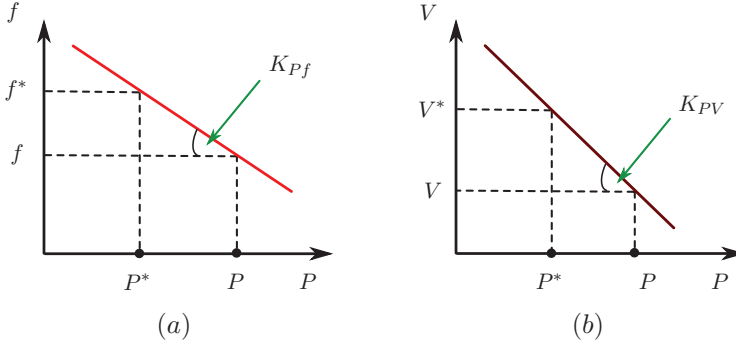


Figure 2.5: Active power control based on (a) - $P - f$ droop control and (b) - $P - V$ droop control.

The $P - V$ droop control, on the other hand, is widely used to provide the power reference values and supervise the PRC of RES in LV networks as presented in [22, 66, 71, 80, 90–94]. The control principle can be represented as,

$$(V - V^*) = -K_{PV}(P - P^*) \quad (2.2)$$

where V and V^* correspond to the measured output voltage magnitude and its reference value of the DG system, respectively. The coefficients K_{PV} denotes the active droop slope. Therefore, $(V - V^*)$ represents the voltage magnitude deviation from its reference value. Characteristics of $P - V$ droop control are shown in Fig. 2.5 (b).

Reactive power control

With high penetration of RES, there is growing interest in using these technologies as distributed reactive power resources for voltage/VAr support. It is technical viable since the RES use the advanced power electronic interfaces, where active and reactive power exchange to the grid can be adjusted separately. Hence, the reactive power support can be provided from ESS and PV systems. Controlling the reactive power of PV inverters for VAr support has been proposed in [95–97]. Approaches to coordinate ESS and reactive power control of PV systems are proposed in [87, 98]. There are various strategies to generate the reactive power output references, including fixed power factor (FPF), varying power factor in terms of active power generation (VPF(P)), and reactive power responding to the voltage level (Q-V droop control) [99].

- **Fixed power factor (FPF):** This method regulates the reactive power output of the RES system (Q) as a fixed proportion of active power outputs (P) as described by:

$$Q = \tan[\arccos(\text{PF})]P \quad (2.3)$$

where PF is the power factor, i.e., $\text{PF} = \cos\varphi$, which is predefined as a fixed parameter. As shown in Fig. 2.6 (a), given predefined PF the operating points for Q stays along the red diagonal line and rely upon only P of the RES system in a linear manner. In [98, 100], PV inverters operate with FPF to provide reactive power support, while ESS stores active power generation from PV systems during voltage rise conditions. This combination aims to avoid active power curtailment of PV systems.

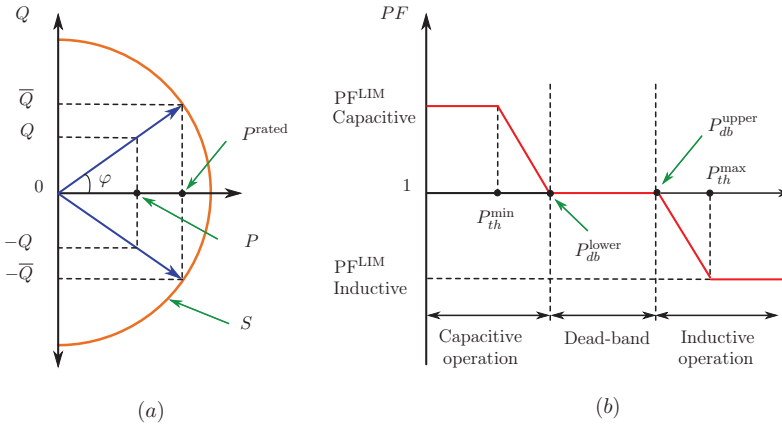


Figure 2.6: (a) - FPF method for reactive power control of a RES system: the orange curve represents the apparent power S , P^{rated} and P denotes the rated and injected active power, respectively, and \bar{Q} denotes maximum reactive power. (b) - VPF(P) method for reactive power control of a RES system: PF^{LIM} Capacitive and Inductive represent PF limit values in capacitive and inductive operation, P_{th}^{min} and P_{th}^{max} denote threshold active power for PF^{LIM} Capacitive and Inductive, respectively. P_{db}^{lower} and P_{db}^{upper} denote lower and upper values of the dead-band interval.

Although this method is simple and reliable, it has a major drawback. In case of a low level of P of the inverter, the probability of voltage rises and low voltage at POC of the inverters is low. Consequently, the reactive power output of the inverters is not desired because it leads to additional losses in the network. Applying the FPF method in such condition, therefore, will be not beneficial [99]. This negative consequence can be avoided by applying the VPF(P) method as discussed below.

- **Varying power factor (VPF(P)):** In the VPF(P) method, the PF is varying according to the value of P of the RES system. Consequently, the reactive power output Q can be defined using the modified equation below:

$$Q = \tan[\arccos(\text{PF}_t)]P \quad (2.4)$$

where PF_t is the power factor set point in correspondence with P at time instant t . Fig. 2.6 (b) presents the VPF(P) method. When P is still in the dead-band interval, the inverter operates with unity power factor ($\text{PF} = 1.0$) and no reactive power injection or absorption is required. The capacitive part is used when voltage drop problems occur, which requires reactive power generation. In contrast, the inductive part is used when over voltage rise problems occur, which requests reactive power absorption.

- **$Q - V$ Droop control:** Compared to the FPF and VPF(P) method, the $Q - V$ droop control method provides more flexibility when controlling reactive power for supporting the voltage regulation [95]. The $Q - V$ droop control directly utilises the voltage measurements for regulating reactive power output of the inverter as demonstrated in Fig. 12. Reactive power capacity of the inverters is restricted by the apparent power rating of the inverter and P generating at a given irradiance. Also, reactive power capacity will be further defined if the requirement of the minimum allowed PF is applied. To illustrate this, the operating region for reactive power in the $Q - V$ droop control method is shown in Fig. 2.7 for two cases of operation region without and with the minimum allowed PF requirements.

In [74, 77, 81, 85, 101, 102], PV inverters operate with the $Q - V$ droop control to reduce voltage rise problems due to surplus PV power generation. Nevertheless, reactive power control by itself can be inefficient to solve the voltage rise problems due to the high R/X ratios in LV distribution networks, and the limited reactive power capacity of the PV inverters [103]. Thus, the combination of reactive and active power control is applied as discussed in [72, 94, 100, 104, 105].

Data-driven approaches

The digital transformation at the grid edge provokes the development of data-driven/machine learning approaches using real data measurements to support the network operation. The

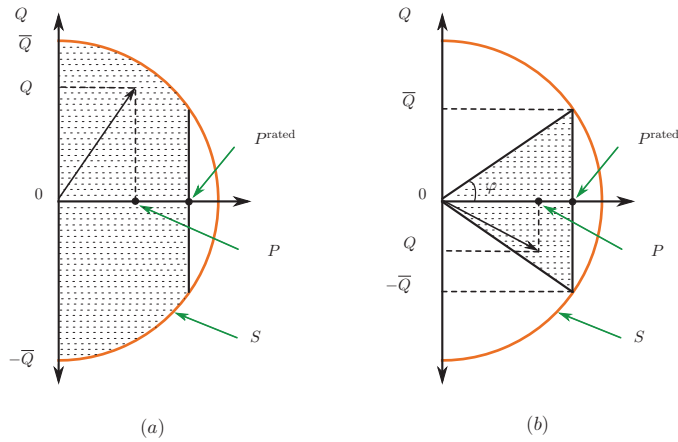


Figure 2.7: Operation regions of RES power outputs demonstrated by the dash-line regions for two control strategies: (a) - without minimum allowed PF requirement and (b) - with the minimum allowed PF requirement.

authors in [64] introduces a machine learning approaches based on support vector machines to optimise the local control design of DGs, loads and ESS. The optimised local control performs reactive power control, active power curtailment without the needs for communications. In [77], data measured by the sensors in a PV system is used to forecast the output power, which is then used as an input for the PRRC of PV systems to reduce voltage fluctuation due to could passing. A data-driven method presented in [106] adopts non-linear control techniques to determine the reference values for real-time reactive power outputs of inverter-based DGs. The machine learning methods proposed in [107, 108] employ multi-learning regression to calculate the optimal reactive power outputs of DGs. In [109], a voltage control approach at the grid edges is proposed using an artificial neuron network (ANN) for RES inverters.

2.5.2 Coordinated control

Since RES are increasingly connected to distribution networks, the coordinated control is important to effectively exploit these resources for the system operation support. The coordinated control can be considered as an upper layer of autonomous control with the use of

the ICT infrastructure and coordinated control algorithms.

Optimisation method

The optimisation method tunes the autonomous control of RES by periodically providing the set points of active and reactive power of RES for the optimal uses. For this method, the operational information of all RES unit must be collected. The non-linear optimisation is discussed in [95] to solve multi-objective functions of minimising network losses, voltage level deviation, and transformer tap changing. Linear programming is used in [86] to optimise the power threshold levels, which trigger the ESS charging to enable PRC of PV systems during their peak generation. In [110], cost-optimal control is proposed to maximize PV self-consumption by operating HPs. In [95] centralised optimisation approach is employed to optimally coordinate reactive and active power of PV systems for voltage rise mitigation with reduced active power curtailment. Similarly, the centralised optimisation method is used in [22] to coordinate HPs for congestion management in LV networks. Authors in [104] formulated the optimal tuning of autonomous control, including active and reactive power, of PV units as a convex optimisation problem solved by a central controller. In [111], the optimisation of PV systems and EVs is also formulated as a convex optimisation problem but solved in a distributed manner.

Consensus method

Consensus algorithms have been widely used as a basis for distributed control. In this concept, each RES system communicates and shares its local information as the variable of interest with adjacent ones using a distributed procedure [55]. The objective function of the consensus algorithm is to converge all RES to a common agreement after an iterative process. The variable of interest can be regarded as a quantity that is agreed by all RES systems. The coordinated charging/discharging control of EVs for voltage regulation based on the consensus method is presented in [74]. In [111], the consensus method is employed to coordinate the active and reactive power output of renewable-based DGs and EVs. The method in [112] utilises consensus-based distributed control to obtain fair generation curtailment of PV systems. In [113], consensus protocols is used in combination with fuzzy logic to tackle voltage regulation problems.

Agent-based method

Another method to coordinate various RES for their control and management in distribution networks is to use the MAS approach [63]. In the networks, RES can be represented by individual agents, that has a certain level of autonomy and communication capability.

Authors in [22] developed a MAS-based control strategy to coordinate the process of a unified approach for managing thermal and voltage violation problems. Compared with the centralised scheme, the proposed MAS approach requires decreased communication and computational power due to the lower amount of exchanged information. In [114, 115], peer-to-peer control in LV networks based on MAS technique have been proposed. The control architecture is distributed and contains three control layers (i.e., primary, secondary and tertiary). MAS market-based control for charging fleets of EVs is proposed in [116] with transformer congestion and voltage violation issues being considered.

MPC-based method

As described in previous sections, the MPC-based method can be utilised to implement the corrective and preventative control. MPC method is a discrete-time control scheme, in which at each time step, the future control sequence is determined for a finite time-horizon. In [51], MPC-based techniques are used to realise the basic control functionalities of PV power converters, such as MPPT, current and voltage control. MPC-based control of ESS to reduce the PV power fluctuation of PVs is discussed in [78]. The authors in [117] adopted MPC approach to define optimal set points for active and reactive power of DGs and transformer load tap changer for voltage regulation. In [118], MPC is used to schedule HPs aiming to reduce its operation cost by preheating the houses during peak hours with low TOU electricity price or high PV power outputs.

2.6 Discussion

2.6.1 Advanced functionalities of RES

With more installation in distribution networks, RES are increasingly expected to provide more support with the network control and operation using advanced functionalities. The expected functionalities include virtual inertia [27], Volt/VAR support, frequency regulation, harmonic compensation, and dynamic grid support (fault-ride-through capability) [119]. To realise these functionalities, the existing network operating standards for RES systems is suggested to be re-investigated and appropriately adjusted.

2.6.2 Distribution network monitoring improvement

The presence of RES increases the complexity of distribution network control and performance. Therefore, it is important to properly control these resources as well as the network

to ensure the reliability of the power supply. On the other hand, the digital transformation at the grid edge brings opportunities to increase the observability of the grids by using data measurement. These two aspects highlight the needs to improve the network monitoring leveraged by the digital transformation at the grid edges.

2.6.3 Cybersecurity consideration

The digital transformation at the grid edges expands ICT system and increases the information exchange, which imposes the challenges from the viewpoint of control and performance of the power systems by introducing cybersecurity and privacy threats. The cyber-attacks can be carried out by a living person, or malicious software, or the systems' resources [11], inducing the interruption of the communication services and then the electricity provision and also harm to end-users privacy. Hence, it is suggested to investigate the impact of cyber-attack on the operation of RES and the networks.

2.6.4 Regulatory/Framework consideration

It is increasingly important to not only promote RES integration in the grid but also effectively exploit their controllability to support grid performance. Apart from technical aspects, attention is required for reconsidering the existing regulatory/framework about the DSOs' business model as well as new roles in the form of the aggregators [4]. The local flexibility market, moreover, is suggested to be implemented to enable the efficient procurement of flexibility available from RES [4].

2.6.5 Uses of Data-driven/Machine learning approaches

The increasing availability of data from the digital transformation at the grid edges has motivated the application of data-driven/machine learning approaches. These applications can be associated with network planning, monitoring, controlling and operation. Besides, the data-driven/machine learning approaches can be used as tools for data governance. With the widespread digital transformation at the grid edges, it is expected that data measurement in distribution networks will be growing spectacularly. This calls for new processes of managing and exploiting the data effectively. Furthermore, as data-driven/machine learning approaches can be applied without the system modelling, the applications of these approaches can be replicated in a better and easier way compared to the conventional control methods, such as master-slave or cloud-edge structure.

2.7 Summary

A comprehensive overview of the grid-edge control, i.e., the control of RES leveraged by the digital transformation at the grid edges, is presented in this chapter. Despite of many benefits, the increasing integration of RES with its intermittent and unpredictable nature and uses of power electronic interface creates challenges in maintaining the network power quality and stability. Hence, a new paradigm of RES control and operation strategy is required to effectively manage the LV distribution networks. This new paradigm calls for data-driven methods to capture uncertainty and complexity of RES while the coexistence between the grid and RES control strategies are important to be adopted. If properly implemented, this new paradigm can effectively leverage the inherent controllability of RES and the availability of the digital transformation at the grid edges.

3

Transformer loading monitoring

In this chapter, a data-driven approach to enable self-management capability of the local energy communities (LECs) via transformer congestion monitoring in LV distribution networks is proposed. The proposed approach adopts the machine learning-based regression models and uses the data from residential smart meters. A thorough analysis is conducted to discover the relationships between the transformer loading and residential smart meter readings. A comprehensive framework is provided to implement, validate and compare different machine learning algorithms for the transformer loading estimation from the LECs' perspective. The efficiency of the proposed approach is investigated through simulations in the unbalanced IEEE European LV test network. Simulation results highlight that the proposed approach can effectively determine the transformer loading using only a limited set of smart meter measurements provided by the LECs while preserving customers' privacy rights.¹

3.1 Introduction

With the inherent intermittency and randomness, the rapid proliferation of RES, especially PV systems, in LV distribution networks creates operational difficulties to the DSOs [122].

¹This chapter is based on [120] and [121].

One of these difficulties is the issue of congestion or thermal overloading of the network assets, e.g., lines, cables, and transformers [21], which likely occurs in the urban power networks with high population density [22]. The congestion issues can become a significant barrier to further deployments of RES in LV networks. Hence, the proper monitoring of such congestion is critical for the DSOs to manage new load connections and network asset upgrading [28]. The DSOs and the end-users should be aware of the congestion to make informed decisions on controlling their equipment to resolve the problems, ensuring safe operation of the network. This chapter focuses on the congestion of the MV/LV distribution transformers.

As discussed in Chapter 2, several issues hinder the DSOs from adequately monitoring and managing the congestion in their LV networks. An alternative approach is to cooperate actively with the LECs, where end-user's SM data can be gathered and RES can be remotely controlled. Within the LECs, locally-produced RES energy can be traded [31]; therefore not only energy efficiency but also the controllability the local networks can be enhanced [30].

While using SM data for LV network monitoring, most of the existing works adopted the physics-based approaches that have restriction itself to be applicable in the diversified, complex LV networks. In this chapter, a data-driven approach is discussed that will be implemented by the LECs to monitor the transformer congestion in LV distribution networks. Use of the data-driven approach by the LECs is considered promising to support the network operation while preserving customers' rights. The proposed approach involves adopting the machine learning-based regression models and using data measured from residential SMs. The problems of transformer congestion monitoring is elaborated first. The procedure of pre-processing data is subsequently discussed along with the procedure of training and evaluating various learning algorithms for estimating transformer loading. The simulation results of the proposed approach are discussed and relevant conclusions are finally drawn.

3.2 Problem definition

3.2.1 Transformer congestion monitoring

Transformer congestion occur when the loading of the transformer exceeds the thermal capacity due to high power consumption or reverse power flows from residential RES units [22]. The loading of the transformer is defined as the instantaneous apparent power of the transformer, S_{trans} , which can be calculated from the voltage levels at the LV bus, V_s and the total current flowing in the bus, I_s using Eq. (3.1),

$$S_{trans} = V_s I_s \quad (3.1)$$

Despite the ability of the transformer to withstand loads beyond a specified limit, prolonged overloading impairs the insulation of transformer windings [123], subsequently degrading the transformer lifetime. The congestion monitoring, therefore, is essential for a coordinated control to be activated to restrict residential consumption or curtail RES generation. In this work, a procedure to monitor the congestion due to reverse power flows is introduced. For this procedure, the transformers loading S_{trans} is estimated, then enabling the monitoring of the transformer congestion or thermal overloading.

3.2.2 Residential smart meter data

Beyond the consumption measurement for billing, SMs can record voltage, current, and power quality information [124]. The information can be recorded at preset time intervals (typically 15, 30 or 60 minutes) and with high accuracy. These advanced features allow residential SMs to be already employed for management and planning in distribution networks, such as detecting energy theft, forecasting load, and verifying network topology. A detailed analysis of SM application in distribution networks can be found in [41, 125]. For determining the transformer loading discussed in this work, the voltage magnitude measured by residential SMs is used as an input variable. For the sake of simplicity, residential SMs will be termed as SMs in the rest of this chapter.

3.2.3 Data-driven monitoring framework

A framework is introduced in this study to realise the data-driven approach for the transformer congestion monitoring, which can be schematically presented in Fig. 3.1. This framework includes two main building blocks as follows:

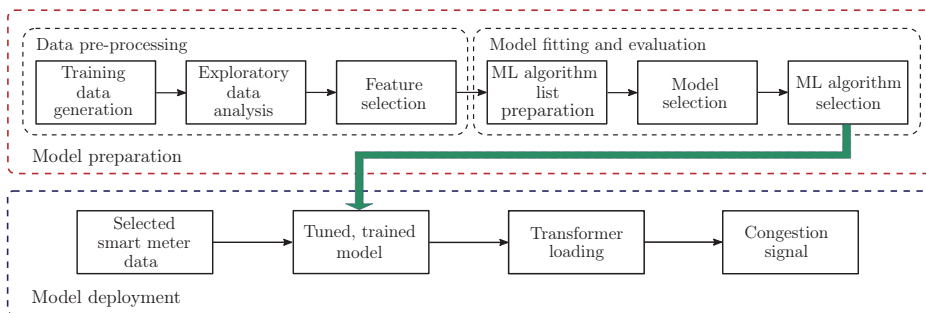


Figure 3.1: Methodological framework.

- **Model preparation:** a comprehensive procedure for transformer loading estimation is executed involving data pre-processing, and ML model fitting and evaluation. Main outputs of the procedure are a reduced set of SMs identified as input data sources and the best-performing ML algorithm for the regression model. Individual steps in the procedure are elaborated in Sec. 3.3 and Sec. 3.4.
- **Model deployment:** data from the selected SMs is collected and fit into the tuned, trained model given by the model preparation stage to estimate the transformer loading. The transformer congestion, subsequently, can be identified. The model performance is tested with the results being discussed in Sec. 3.5.

3.3 Data pre-processing procedure

This section explains the procedure adopted to pre-process data in the framework depicted in Fig. 3.1. Implementing the procedure for a specific test case is also described.

3.3.1 Training data generation

An equitable training dataset plays a decisive role in obtaining promising results when utilizing any data-driven technique. In this chapter, to prepare the reasonable training dataset, stochastic samples are generated by solving a substantial number of power flows and logging the corresponding results. For a given LV network and PV penetration levels, the variations in household load consumption and PV production need to be considered.

Simulation approach

A simulation approach to generate stochastic training dataset is developed using Python and OpenDSS [126]. In the following, the main stages are briefly described.

- Firstly, for \mathcal{N} households, a set of profiles \mathcal{P} , with size $|\mathcal{P}|$ of one year and a time resolution of 15 minutes (i.e., $|\mathcal{P}| = 35040$), of load consumption and PV generation are built following the modelling approach presented in the next sections. Consequently, the obtained profiles are randomly distributed to the houses in the test network. For simplicity, it is assumed that PV units have same phase connection as the houses.
- Secondly, one-year time-series power flows with size $|\mathcal{P}| = 35040$ are solved iteratively. A data sample (X, Y) is recorded at each execution. For this, X is a set of input variables, which is regarded as the SM data, including voltage magnitudes, and net

active and reactive power measured at the POC of all houses, i.e., V_i , P_i^{net} , and Q_i^{net} with $\forall i \in \mathcal{N}$, respectively. Meanwhile, Y is the output variable, i.e., the transformer loading, S_{trans} .

- Thirdly, the obtained dataset is split into two parts: 80% of the dataset is used to simulate the historical data for model preparation, and the remaining dataset simulates future data for model deployment. These sets are then stored for later processing steps.

Test network description

The test network is based on the IEEE European LV distribution network [127]. This three-phase, radial LV network is energized from a 250 kVA, 11/0.4 kV distribution transformer with the secondary side voltage level settings of 1.03 p.u. The remaining features are retained as the origin in the IEEE European LV distribution network. A geographical single-line diagram of the IEEE European LV test network is displayed in Fig. 3.2. The test network serves as an unbalanced grid supplying 55 residential users with single-phase connections, of which 21 users on phase A (i.e., $\mathcal{N}^A = 21$), 19 users on phase B, and 15 users on phase C. Every household is assumed to own a PV system. The rated capacities of PV systems in the test network are randomly chosen between 4.06 and 6.27 kWp [126], which is derived from the information on the real residential PV installations in the Netherlands. The test network is assumed to have a LEC, that can access the residential SM data and control RES at the customer premises. For the demonstration purpose, an overview of household load characteristics and installed PV capacities for phase A is shown in Table 3.1. Furthermore, in this study it is assumed that the topology of the test network remains constant. The properties of load and PV systems for phase B and C are described in Appendix A.

Table 3.1: Summary of household load characteristics and PV installations in phase A

House No.	Node No.	Peak load (kW)	Installed PV capacity (kWp)	House No.	Node No.	Peak load (kW)	Installed PV capacity (kWp)
H1	34	3.9	6.1	H30	563	3.6	4.1
H3	70	3.1	4.7	H31	611	2.5	4.5
H4	73	2.9	4.3	H34	629	3.4	4.5
H5	74	2.8	4.7	H46	817	4.0	4.6
H9	225	4.1	4.9	H48	860	2.7	5.5
H14	289	3.6	4.1	H49	861	3.5	5.5
H20	349	3.5	4.7	H51	896	2.8	4.3
H21	387	3.0	5.0	H52	898	3.6	4.9
H22	388	4.2	5.2	H54	900	4.1	5.0
H25	502	4.8	5.0	H55	906	2.7	5.1
H29	562	3.4	6.2				

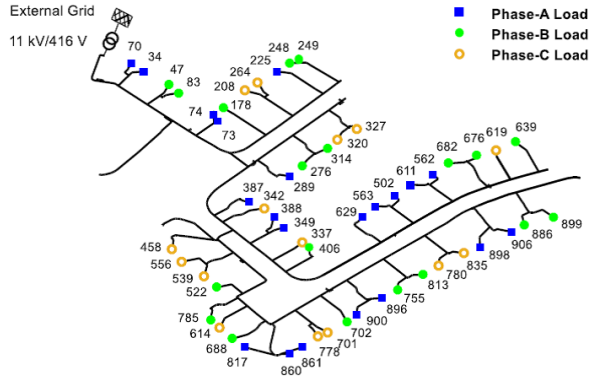


Figure 3.2: Single-line diagram of the IEEE European LV test network. The numerical value denotes the number of the node where the load is connected [127].

Load consumption and PV generation profiles

The household load consumption used in the training data generation is modelled based on real one-year 15-min historical SM measurements in terms of active power from residential consumers in the Netherlands. To consider reactive power consumption, all loads have a power factor, that is assumed to be 0.97 (inductive).

The synthetic PV generation profiles are built on a PV model, which utilises meteorological data and specified PV installations to calculate the active power output (P_{PV}) as in Eq. (3.2) [128],

$$P_{PV} = \frac{I_{tr}}{I_r} P_0 [1 + \gamma(T_c - T_r)] \quad (3.2)$$

where P_{PV} is the active power output (kW), I_{tr} is the irradiance incident transmitted to the PV module (W/m^2), I_r is the reference irradiance at test condition, i.e., $1000 \text{ W}/\text{m}^2$, P_0 is the rated power of PV unit (kW), γ is the temperature coefficient provided by the PV panel manufacturers ($\%/^{\circ}\text{C}$), T_c is the actual cell temperature ($^{\circ}\text{C}$), and T_r is the reference temperature at test condition, i.e., 25°C .

In this work, the value of γ is selected to be $0.35 \%/^{\circ}\text{C}$ corresponding to a premium type of PV module [128]. Moreover, a set of real historical meteorological data of I_{tr} and T_c with a 15-min resolution, provided by the Royal Netherlands Meteorological Institute, is adopted [129]. Because of short geographical distances between the houses within the test network, the exposure to irradiance and ambient temperature is assumed to be similar for all

PV systems. However, to justify the modest variations of the meteorological data and other uncertainties, the computed active power output for individual PV units is multiplied by a random sample drawn from a uniform distribution between 0.95 and 1.05 [130].

The proposed process for training data generation has been implemented in Python programming language and OpenDSS software. Simulations using a computer (3.4 GHz Intel CPU and 28 GB RAM) were executed in around 27 minutes in total to solve a large number of power flows and process the input and output data.

Having the generated training data, the remaining steps in the methodological framework are implemented using Python. It should be noted that because the test network is an unbalanced three-phase LV grid with all single-phase connected loads, the data-driven monitoring is developed for each phase of the transformer. For clarity, only the monitoring for phase A of the transformer is presented for illustration in the rest of the chapter. The proposed method, nevertheless, can be readily applied to the other phases.

3.3.2 Exploratory data analysis

After obtaining the input data, Exploratory Data Analysis (EDA) is of a crucial implementation in the deployment of any data-driven technique. EDA is a process of initial investigation of the data from various angles to discover interesting features [131]. The discovered features are related to existing patterns, relationships among input variables, relationships between input and output variables, and anomalies [132]. Such gained insights from the data assist in check of initial assumptions and preliminary choosing of applicable models [132].

In this work, EDA process is performed on the training data achieved from Sec. 3.3.1 utilising two methods: summary statistic and graphical visualisation. Fig. 3.3, Fig. B.1, and Fig. B.2 show pair plots computed for the transformer loading on phase A (S_{trans}^A) and voltage magnitudes at the POC of all houses connected to the same phase (V_i with $\forall i \in \mathcal{N}^A$) in the dataset. A pair plot is comprised of histogram plots along the diagonal, Pearson correlation coefficients below the diagonal, and scatter plots above it [42], which constitute a matrix of relationship between each variable. The resulting Pearson correlation coefficients illustrate the extent of linear dependence either between S_{trans}^A and V_i with $\forall i \in \mathcal{N}^A$ or among V_i with $\forall i \in \mathcal{N}^A$, which are calculated utilising Eq. (3.3),

$$R(v, u) = \frac{\mathbb{E}[(v - \mu_v)(u - \mu_u)]}{\sigma_v \sigma_u} \quad (3.3)$$

where R denotes the Pearson correlation coefficient between two variables v and u , and \mathbb{E} represents the expectation with standard deviations σ_v and σ_u , and means μ_v and μ_u . As can be seen from the subplots below the diagonal in Fig. 3.3 and Appendix B, the resulting coefficients R between S_{trans}^A and V_i with $\forall i \in \mathcal{N}^A$ are with significant positive values

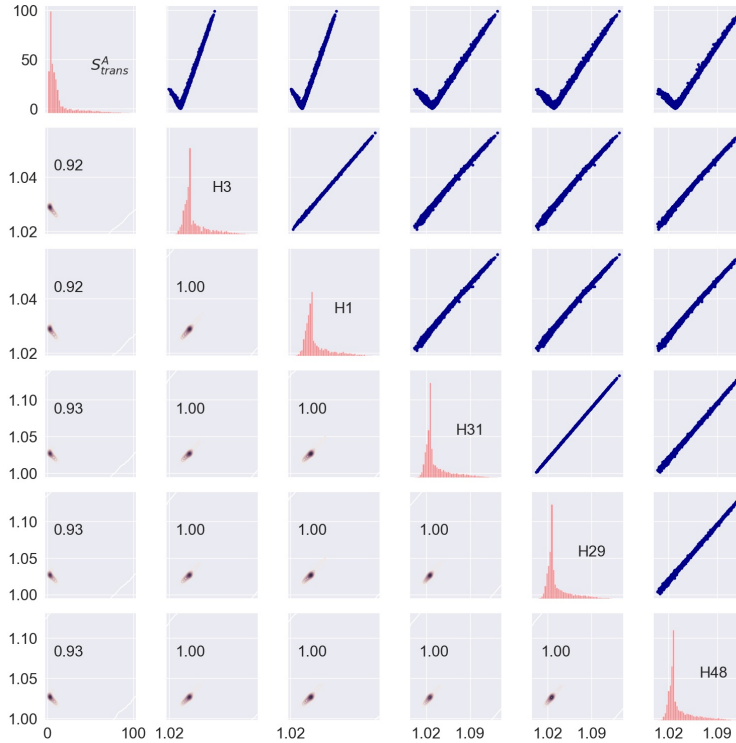


Figure 3.3: A pair plot for the transformer phase A loading (S_{trans}^A) and voltage magnitudes (V) at the POC of the houses H3, H1, H31, H29, and H48 connecting to the same phase. This pair plot consists of histogram plots along the diagonal, Pearson correlation coefficients below the diagonal, and scatter plots above it.

above 0.9, indicating strong correlation between them. It means that increasing voltage magnitudes correlate with higher transformer loading. The voltage levels, therefore, can serve as explanatory variables for calculating transformer loading (i.e., response variable).

The relationship between S_{trans}^A and V_i with $\forall i \in \mathcal{N}^A$ can also be validated by the computed scatter plots in Fig. 3.3 and Appendix B. In these figures, pairs of numerical data are plotted to visualise the relationship of the variables. Interestingly, the scatter plots indicate clear V-shaped patterns, highlighting a potential for applying regression models to compute power flow through the transformer from the nodal voltage magnitudes. Thus, the statistic and graphical analysis prove that combining voltage measurements from SMs within a particular LEC and regression models provides a possible solution to the transformer loading estimation.

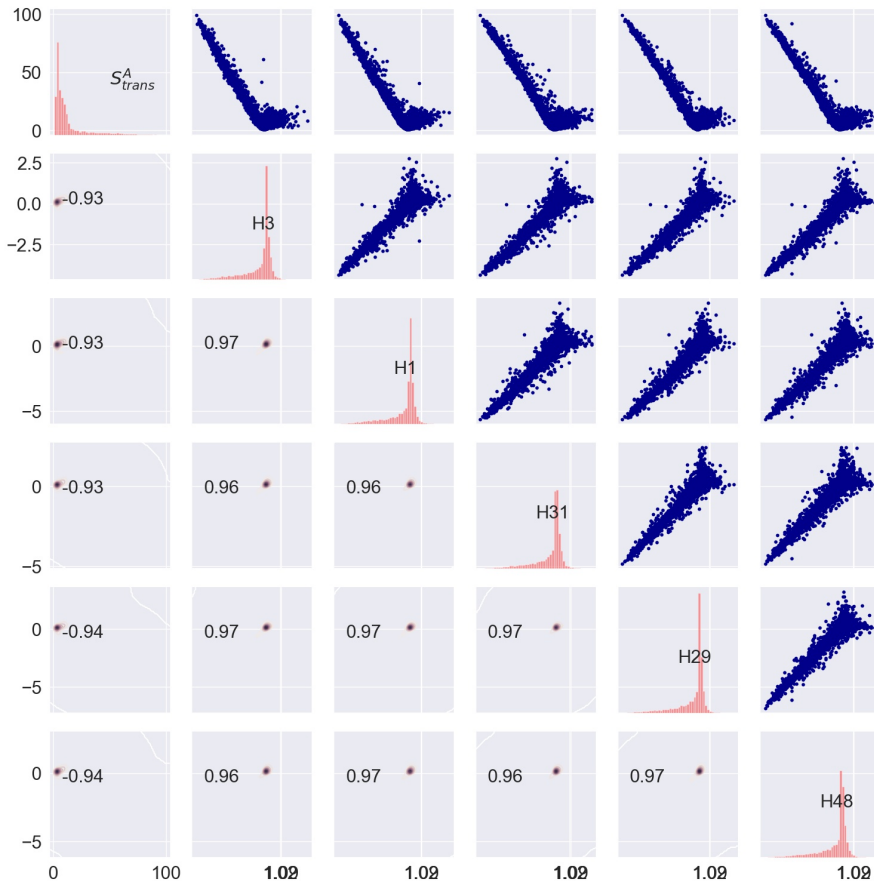


Figure 3.4: A pair plot for the transformer phase A loading (S_{trans}^A) and net active power (P^{net}) of houses H3, H1, H31, H29, and H48 connecting to the same phase. This pair plot consists of histogram plots along the diagonal, Pearson correlation coefficients below the diagonal, and scatter plots above it.

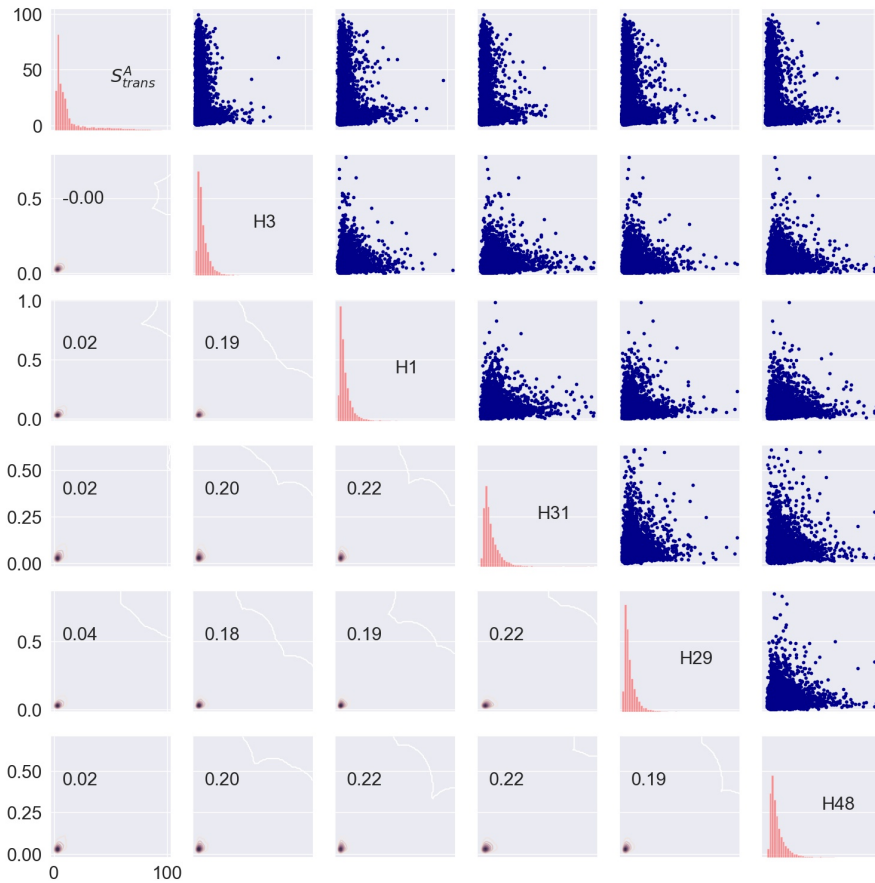


Figure 3.5: A pair plot for the transformer phase A loading (S_{trans}^A) and net reactive power (Q_{net}) of houses H3, H1, H31, H29, and H48 connecting to the same phase. This pair plot consists of histogram plots along the diagonal, Pearson correlation coefficients below the diagonal, and scatter plots above it.

Because net power measurements are also available from household SMs, EDA is implemented for the training data of S_{trans}^A and net active power measured at the houses connected to phase A (P_i^{net} with $\forall i \in \mathcal{N}^A$) as demonstrated in Fig. 3.4 and Appendix B. Similarly, EDA is implemented for the training data of S_{trans}^A and net reactive power measured at the houses connected to phase A (Q_i^{net} with $\forall i \in \mathcal{N}^A$) as illustrated in Fig. 3.5 and Appendix B. A common issue from these figures is that the scatter plots have data points spreading out widely and more outliers, while the shape of the patterns is less clear compared to these scatter plots between S_{trans}^A and V_i with $\forall i \in \mathcal{N}^A$ in Fig. 3.3 and Appendix B. On the other hand, the pair plots for S_{trans}^A and Q_i^{net} with $\forall i \in \mathcal{N}^A$ shows very low correlation coefficients between these variables, i.e., with the absolute values ranging from 0.0 to 0.05. Although the correlation coefficients between S_{trans}^A and P_i^{net} with $\forall i \in \mathcal{N}^A$ have high values, i.e., with the absolute values ranging from 0.83 to 0.94, using active power measurements from SMs to estimate transformer loading will violate the privacy right of customers. Hence, active and reactive power data from SMs are deemed unsuitable input candidates for the data-driven monitoring of transformer loading.

3.3.3 Feature selection

Since the dataset contains a high number of features (variables), feature selection (variable elimination) is of importance to select a subset of relevant features directly from the original set [133]. Reason for this is that some features are irrelevant, redundant, or noisy for model construction, which likely degrades the performance of the model [134]. Additionally, high-dimensional data results in more computational burden and increased execution time for model training; thus, reducing computational efficiency [135]. Feature selection aims to reduce the dimensionality of the data, subsequently decreasing computational requirements, accelerating the learning process, and enhancing the model performance [134, 135].

Feature selection methods can be categorised as supervised, semi-supervised and unsupervised according to the label information [133]. Solving regression problems generally involves applying supervised feature selection, that measures the importance of an individual feature via its correlation with the regression output [91]. On the other hand, methods of feature selection can be broadly classified into 3 groups: filter, wrapper and embedded according to searching strategy [133]. Owing to having the merits of both filter and wrapper methods, the embedded method is preferable to realise feature selection [91]. The embedded method employs the inherent structure of a learning algorithm to incorporate feature selection into the learning process [91]. Among available models for embedded method-based feature selection, regularisation models, e.g., Least Absolute Shrinkage and Selection Operator (LASSO), are most widely utilised [91].

In this chapter, the LASSO approach is adopted to perform supervised feature selection on the training dataset. This adoption allows preventing bias in comparing ML algorithms used

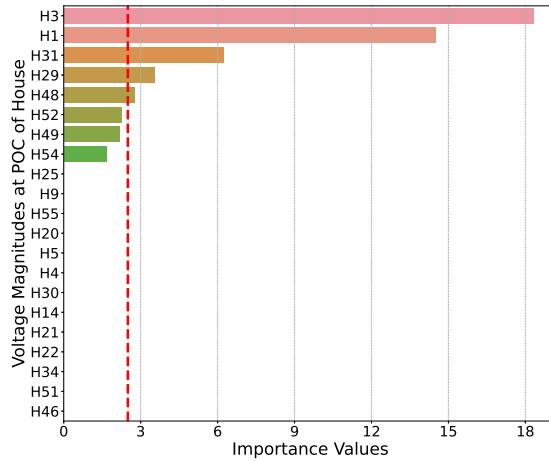


Figure 3.6: Feature importance and selection with the LASSO approach. H_i with $\forall i \in \mathcal{N}^A$ denotes the house number as listed in Table 3.1. The vertical red dashed line represents the importance threshold with $\omega = 2.5$.

for the regression problem (as discussed in the next steps) as the LASSO model is not in the algorithm list. The supervised feature selection based on LASSO is conducted separately in a task before the training process. Thus, the same subset of features will be selected for every algorithm fitting, consequently facilitating the fair comparison of the algorithms. The importance values of a single feature (i.e., V_i with $\forall i \in \mathcal{N}^A$) to the regression output (i.e., S_{trans}^A) calculated on the training dataset by using LASSO is illustrated in Fig. 3.6. It is observed that the houses are ranked in order of importance with their values varying largely. Several houses have small or even zero importance values, while others have high values. This is derived from the working principle of LASSO that minimises the fitting errors whilst shrinking the magnitude of feature coefficients [91]. An importance threshold ω is then required to define the relevant features with their importance values greater than the threshold. Therefore, with $\omega = 2.5$, the voltage levels at the POC of 5 houses, including H3, H1, H31, H29, and H48, are selected from a total of 21 houses on phase A to be the explanatory variables of the regression model. Choosing this value of ω for feature selection has no loss of generality because the main focus of this study is to compare the relative performance of various ML algorithms. The feature selection based on LASSO is conducted separately in a task before the training process; thus, the same subset of features will be selected for every algorithm fitting. Using the same feature subset (i.e., same inputs) for the algorithms, along with tuning its hyperparameters and comparing the generalisation and stability of its performance (as discussed in the next section), facilitate the fair comparison of the algorithms. In addition, selecting the feature based on this ω value is adequate to

exemplify the model fitting and validation procedure. Hence, the dataset corresponding to the selected features can be formed from the training set for constructing the regression model in a later stage.

3.4 Model fitting and evaluation

Given the provided input data, this section focuses on the procedure of training and evaluating several ML algorithms for calculating transformer loading, as depicted in Fig. 3.1. It is important to note that properly evaluating and comparing different ML algorithms necessitates addressing two matters. Firstly, tuning the hyperparameters of the algorithm should be performed before the evaluation stages as its values will highly impact the algorithm performance. Secondly, the comparison of various algorithms should be based on generalisation [28] and the stability of their estimated performance [136]. In this section, these two essential concerns are thoroughly considered using Nested Cross-Validation, aiming to facilitate the fair comparison between the studied ML algorithms. Specifically, the hyperparameter tuning task is presented in Sec. 3.4.2, and the algorithm comparing task is elaborated in Sec. 3.4.3.

3.4.1 ML algorithm list preparation

As there are several different ML algorithms for the regression problem, this section aims to prepare a list of various ML algorithms selected to compare their performance for transformer loading estimation. There are 4 ML algorithms added in the list as follows,

- Ridge Regression (RR): This regression model can be formulated in matrix form as [137],

$$\hat{\beta}(\alpha) = (\mathbf{X}^T \mathbf{X} + \alpha \mathbf{I})^{-1} \mathbf{X}^T \mathbf{Y} \quad (3.4)$$

where $\hat{\beta}(\alpha)$ is the ridge regression estimator, α is the penalty parameter, \mathbf{X} and \mathbf{Y} are explanatory and response variables, respectively, and \mathbf{I} is the identity matrix.

- Support Vector Regression (SVR): SVR attempts to find the coefficients that minimise the function given by [138],

$$\varepsilon \sum_{i=1}^N (\lambda_i + \lambda_i^*) - \sum_{i=1}^N (\lambda_i^* - \lambda_i) y_i + \frac{1}{2} \sum_{i=1}^N \sum_{j=1}^N (\lambda_i^* - \lambda_i) (\lambda_j^* - \lambda_j) \kappa(x_i, x_j) \quad (3.5)$$

subject to

$$\sum_{i=1}^N (\lambda_i^* - \lambda_i) = 0 \quad \forall \lambda_i^*, \lambda_i \in [0, C] \quad (3.6)$$

while, the function approximation for SVR is written as,

$$\hat{f}(x) = \sum_{i=1}^N (\lambda_i^* - \lambda_i) \kappa(x_i, x) \quad (3.7)$$

where ε denotes the epsilon parameter, i.e., the tolerance for error, N denotes the size of data, $\lambda_i, \lambda_i^*, \lambda_j, \lambda_j^*$ denote the Lagrange multipliers with non-negative values, $\kappa(\cdot, \cdot)$ denotes the kernel coefficient, C denotes the regularisation strength, and x and y denote explanatory and response variables, respectively.

- Random Forest Regression (RFR): As a tree-based ensemble algorithm, the function approximation of RFR (i.e., a collection of Tr randomised regression trees) for a training sample $D_N = (\mathbf{X}, \mathbf{Y})$ can be formulated as [139],

$$\hat{f}_{Tr,N}(x, \Theta_1, \dots, \Theta_{Tr}) = \frac{1}{Tr} \sum_{i=1}^{Tr} \hat{f}_N(x, \Theta_i) \quad (3.8)$$

where Tr is the number of randomised regression trees in the forest, N is the size of data, $\Theta_1, \dots, \Theta_{Tr}$ are random variables (i.e., independent of the sample D_N), $\hat{f}_N(x, \Theta_i)$ denotes the predicted value of point x for a single i -th tree (i.e., constructed using the bootstrapped samples [140]), and \mathbf{X} and \mathbf{Y} are explanatory and response variables, respectively.

- eXtreme Gradient Boosting Regression (XGBR). XGBR is an ensemble tree algorithm with the aim of minimising the objective function given as [141],

$$\sum_{i=1}^N l(y_i, \hat{y}_i^{(t-1)} + f_t(x_i)) + \Omega(f_t) \quad (3.9)$$

where N is the size of data, $\hat{y}_i^{(t-1)}$ denotes the prediction output at the $(t-1)$ -th (i.e., previous) iteration of the i -th instance, y_i denotes the observation, f_t denotes the independent tree structure at the t -th iteration, l denotes the loss function measuring the difference between $y_i, \hat{y}_i^{(t-1)}$, and f_t , and $\Omega(f_t)$ denotes the penalty term for the model complexity. The term $\Omega(f)$ can be calculated as,

$$\Omega(f) = \gamma L + \frac{1}{2} \alpha \|\omega^2\| \quad (3.10)$$

where L is the number of leaves in the tree, ω is the score of leaves, and γ and α are regularisation coefficients [142].

The motivation behind the preliminary use of these 4 algorithms is the capability to handle the non-linear regression problem and continuous variables, i.e., by using SVR [43] and RFR [143]. Besides, the algorithm capability for analysing data suffering from the multicollinearity problem, which refers to the linear relationship among explanatory variables, is considered, i.e., by using RFR [143] and RR [144]. This is derived from the fact that non-linearity and multicollinearity exist in the obtained training data, as can be seen in Fig. 3.3, Fig. B.1, and Fig. B.2. Additionally, the algorithm having state-of-the-art advantages in ML research and recently being increasingly used in power engineering is included, i.e., XGBR [48]. Simulation set-up of the listed ML algorithms for the next steps is implemented using Scikit-learn package in Python [145]. For this, the principles of the ML algorithms represented by Eq. (3.4) - Eq. (3.10) are considered. Simulation set-up of the listed ML algorithms is discussed in the next section.

3.4.2 Model evaluation and selection

Model evaluation aims to estimate how well the performance of the specified model generalises to unseen data, so-called the generalisation error [136]. To this end, it is required that model fitting and evaluation are executed on the independent datasets, i.e., training and validation data. Otherwise, the performance estimation can be biased due to overfitting [136].

Model selection refers to a process for tuning the hyperparameters of a specific ML algorithm to the best settings corresponding to the best-performing model [146]. A ML algorithm is generally designed with several hyperparameters; those are tuning parameters with adjustable values and have the decisive effects on the performance of the algorithm [136]. Given a specific ML approach, applying different hyperparameters will lead to different models. Thus, it is desired to select the model with the best estimation accuracy by tweaking the optimal hyperparameters [136].

To perform model evaluation and selection (as well as the algorithm evaluation and selection), Nested Cross-Validation (CV) is well-suited as it demonstrates several advantages [136]. This advanced method is a nesting of two k -fold CV loops: the inner and the outer, which form a $k \times k$ set-up. The k -fold CV of the outer loop splits the entire historical dataset into k random, non-overlapping subsets: one subset serves as the testing data for the algorithm selection and the remaining $(k - 1)$ subsets are merged to form the training data used in the inner loop [147]. The inner loop based on the k -fold CV implements model evaluation and selection by crossing over the training and validation steps in an iteration manner, i.e., over the original training data derived from the outer loop k times. For model evaluation purpose, the k -fold CV of the inner loop further splits the provided training data into k ran-

dom, independent subsets. The k subsets are then interchangeably used so that one subset serves as the validation data and the remaining $(k - 1)$ subsets are merged and serve as the training data [147]. This split prevents the leaking of test data during the training process, thus avoiding overfitting and reducing the bias of models' performance estimates [146]. For model selection purpose, the inner loop runs a specific ML algorithm with each fixed hyperparameter configuration over the training data k times in a loop. Each iteration of the loop uses a distinct subset of training and validation data; therefore, when that loop finishes, each hyperparameter configuration is associated with k different models and k different performance estimates [136]. Afterwards, the multiple resulting estimates of every model are averaged to produce the ultimate generalisation error, ranked against each other to select the best model, i.e., with the lowest error. This loop is essential because the algorithm cannot learn the hyperparameter settings by itself during the fitting process, meaning these settings need to be specified a priori and then evaluated separately [136]. More details of Nested CV method can be found in [136, 146].

Table 3.2: *Pre-defined hyperparameters of the compared ML algorithms*

ML algorithms	Hyperparameters	Bounded domain
RR	Maximum number of iterations (IT_{max}) i.e., an integer	Uniform distribution over [1000, 10000]
	Regularization strength (α), i.e., a float	Log-uniform distribution over $[10^{-5}, 100]$
SVR	Kernel coefficient (κ), i.e., a float	Log-uniform distribution over [1, 200]
	Regularization strength (C), i.e., a float	Log-uniform distribution over $[10^{-5}, 100]$
	Epsilon parameter (ϵ), i.e., a float	Log-uniform distribution over $[10^{-5}, 100]$
	Maximum number of iterations (IT_{max}), i.e., an integer	Uniform distribution over [1000, 10000]
RFR	Number of trees in the forest (Tr), i.e., an integer	Uniform distribution over [100, 1000]
	Maximum depth of the tree (D_{max}), i.e., an integer	Uniform distribution over [10, 500]
	Minimum number of samples required to split an internal node (S_{min}), i.e., an integer	Uniform distribution over [1, 20]
	Minimum number of samples required to be at a leaf node (L_{min}), i.e., an integer	Uniform distribution over [1, 20]
XGBR	Subsample ratio of columns when constructing each tree (η), i.e., a float	Uniform distribution over [0, 1]
	Regularization strength (α), i.e., a float	Log-uniform distribution over $[10^{-5}, 100]$
	Parameter to shrink the contribution of each tree (P), i.e., a float	Uniform distribution over [0, 1]
	Maximum depth of the individual regression estimators (D_{max}), i.e., an integer	Uniform distribution over [100, 1000]
	Number of gradient boosted trees (Tr), i.e., an integer	Uniform distribution over [100, 1000]

This study involves adopting Nested CV with a 10×10 set-up for the model evaluation and selection for the ML algorithm list (prepared in Sec. 3.4.1). The k -fold CV outer loop with $k = 10$ partitions the whole dataset into 10 parts utilised for the inner loop. For an algorithm, a range of settings is initially specified as the bounded domain of hyperparameters. Then, from that domain, a set \mathcal{H} , with size $|\mathcal{H}| = 15$, of the combinations of hyperparameter settings are randomly sampled using randomised search technique [136]. To facilitate the random sampling, the hyperparameters settings are defined as the uniform distributions of values as shown in Table 3.2. Afterwards, the k -fold CV inner loop with $k = 10$ in the initiated Nested CV is applied for each combination of hyperparameter values $h \in |\mathcal{H}|$. The goal is to find the hyperparameter combination achieving the lowest generalisation error among all the investigated combinations in $|\mathcal{H}|$. For this, a set \mathcal{S} with $|\mathcal{S}| = 10$ of various subsets of training and validation data is generated. In total, 6000 simulations are required for a list of 4 ML algorithms. A performance metric used for the model evaluation and selection is Root Mean Square Error (RMSE), which quantifies the average magnitude of the error between the real values (y) and the computed values (\hat{y}), as calculated by [148],

$$RMSE = \sqrt{\frac{1}{T} \sum_{t=1}^T (y_t - \hat{y}_t)^2} \quad (3.11)$$

where y and \hat{y} denote the real and computed values, respectively, T denotes the total number of steps of the time-series validation data, t denotes the time-step in T . The best hyperparameters are chosen with the lowest RMSE. The process can be schematically presented, as shown in Fig. 3.7. For the demonstration purpose, the numerical results in terms of the optimal hyperparameter configurations associated with the averaged RMSE as a generalisation error for SVR algorithm are summarised in Table 3.3. It is worth mentioning that since the inner loop operates over 10 distinct subsets of the simulated historical data, which are formed due to the outer loop, 10 combinations of best hyperparameters along with their estimated performance are also achieved. It is observed that the hyperparameters are properly customised with varying levels of settings among the subsets. With the optimal hyperparameters from the inner loop, the algorithm will be trained and evaluated in the outer loop, presented in the next section.

3.4.3 ML algorithm selection

The ML algorithm selection involves finding the algorithm having the lowest generalisation error and the best stability capability among all the compared algorithms. The generalisation error represents the performance estimates of the algorithm in new, unseen data, i.e., not in the training set. Meanwhile, the stability capability quantifies how well the algorithm performs on multiple, different test datasets [136]. The k -fold CV enables both estimating of the generalisation performance and testing of the stability of the algorithm. The rationale

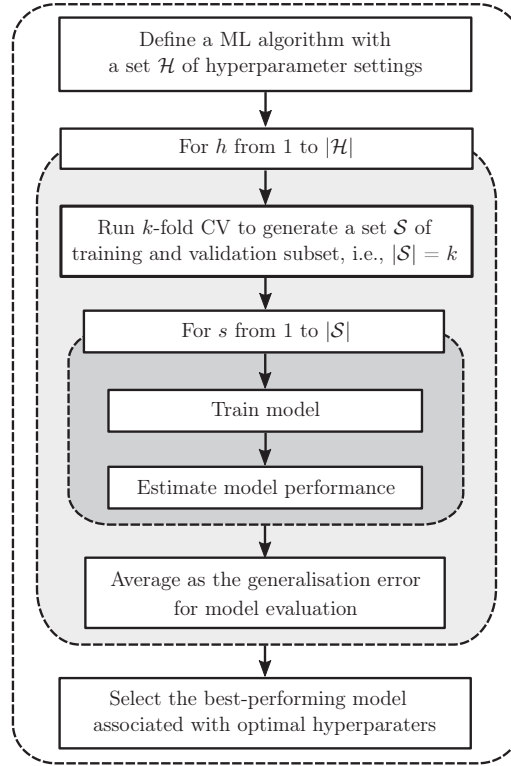


Figure 3.7: Methodology of model evaluation and selection for a ML algorithm based on the k -fold CV inner loop of Nested CV.

Table 3.3: Summarised results for model evaluation and selection of SVR

Data subset	Optimal hyperparameters				Mean RMSE
	κ	C	ε	IT_{max}	
1	6.44	30.57	1.71	9122	3.04
2	15.7	1.16	4.44	3440	3.66
3	6.92	6.26	1.7×10^{-4}	6959	3.77
4	54.5	0.096	0.74	7879	3.2
5	5.26	38.08	0.37	3976	3.72
6	65.8	0.28	0.66	3599	2.92
7	95.4	2.02	5.86	2571	2.84
8	79.6	84.6	4.05	9608	1.95
9	38.1	63.9	0.84	8015	2.48
10	7.07	1.32	3.3×10^{-4}	5547	4.87

is that this method retains the independent test dataset for the performance estimate, and it iterates the performance testing k times in different datasets. These features make the k -fold CV a common approach to complete the algorithm selection [136].

Owing to the k -fold CV in the outer loop, Nested CV is applicable to the ML algorithm selection. Accordingly, Nested CV with a 10×10 set-up established in Sec. 3.4.2 is employed in this section. Specifically, in every iteration k of the outer loops, every algorithm fits the model along with its optimal hyperparameters determined from the inner loop on the training data and then evaluates the model performance on the withholding test data. For this regards, the performance metrics are based on RMSE using Eq. (3.11). Similar to the inner loop, 10 resulting generalisation errors of each algorithm, subsequently, are averaged as the ultimate generalisation error for comparing the algorithms.

The RMSE results across each fold of the outer loop for individual ML algorithm are displayed in the box plot, as shown in Fig. 3.8. The numerical values of RMSE and the computational time are listed in Table 3.4. In this table RMSE results are the mean values from the CV outer loop. The computational time is measured for the entire procedure of model evaluation and selection, and ML algorithm selection using Nested CVs. As can be observed from both the figure and the table that, RFR and XGBR clearly outperform SVR and RR as the first two algorithms have lower mean RMSE values from around 3.5 to 4.5 times than that of the last two algorithms. Moreover, it can be seen from the figure that, the error spreading of RFR and XGBR, significantly decreases compared to SVR and RR. Between RFR and XGBR, the RMSE results are relatively comparable as both these models are based on the ensemble tree algorithm. In view of the computational time, SVR has the longest time, followed by RFR and XGBR, and RR is the fastest algorithm. This is due to the fact that SVR model is built by solving a quadratic programming problem and selecting the best support vectors from the dataset, which typically lead to computationally expensive [149]. RFR consists of a large number of regression trees, in which each tree is grown by drawing a set of bootstrapped samples. This makes the training of RFR relatively time-consuming, nevertheless faster than SVR as a result of growing in parallel the trees [140]. XGBR has significant lower computational time than RFR because XGBR adopts an improved tree learning algorithm (for managing sparse data) and quantile sketch scheme (for considering weights) [141]. With only solving the linear equations and sorting, RR requires the lowest simulation time [150], but at the expense of significantly reduced accuracy. Hence, these findings suggest that RFR and XGBR algorithms are worth to further study on the defined regression problem.

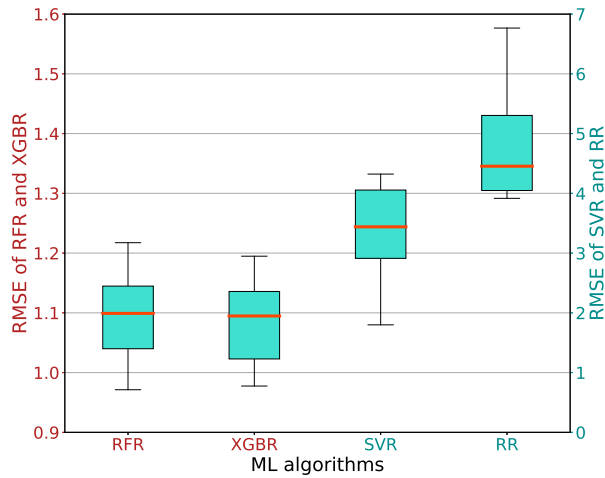


Figure 3.8: Spread of RMSE results across each fold of the CV outer loop for ML algorithms.

Table 3.4: Summary of RMSE results and computational time for individual ML algorithm

ML algorithms	Mean RMSE	Computational time (mm:ss)
RFR	1.095	34:48
XGBR	1.085	11:42
SVR	3.373	55:40
RR	4.762	00:14

3.5 Model deployment

Given the selected ML algorithms from the previous section, this section focuses on the procedure of deploying the algorithms to estimate the transformer loading, as depicted in Fig. 3.1. Evaluating the algorithm performance is also analysed. It is worth to mention that the algorithm evaluation completed in Sec. 3.4.3 involves the small sets of test data, and only RMSE served as the performance metric. Therefore, it is desired to carry out further tests on a larger dataset and several performance metrics for the selected algorithms.

Table 3.5: Summarised results for model set-up of RFR and XGBR

ML algorithms	Hyperparameters	Optimal values	Mean RMSE
RFR	Tr	955	0.96
	D_{max}	357	
	S_{min}	12	
	L_{min}	2	
XGBR	η	0.73	0.97
	α	1.75	
	P	0.8	
	D_{max}	158	
	Tr	574	

3.5.1 Model set-up

The model set-up stage prepares the input data for ML algorithms and implements the model evaluation and selection. Firstly, the input data preparation requires gathering the voltage measurements of the selected household SMs as specified in Sec. 3.3.2 and Sec. 3.3.3 from the operational network data. In this study, the operational data during the model deployment is simulated by using 20% of the stochastic training dataset withheld from the data generation in Sec. 3.3.1. As a result, a set of 7008 time-series voltage measurements with 15 minute time resolution at the POC of 5 houses, including H3, H1, H31, H29, and H48, are obtained. Secondly, implementing the model evaluation and selection adopts the k -fold CV with $k = 10$, that is similar to the inner loops of Nested CV as explained in Sec. 3.4.2, to optimise the model hyperparameters. To this end, the randomised search technique is also utilised to randomly sample a set \mathcal{H} , with size $|\mathcal{H}| = 15$, of the hyperparameter combinations from the pre-defined ranges listed in Table 3.2.

A difference from Sec. 3.4.2, however, is that the model selection process in this section excludes the k -fold CV outer loop with $k = 10$ of Nested CV. It means that the model hyperparameters are tuned based on the entire set of the simulated historical data at once instead of being iterated several times in various folds. A total of 300 simulations, thus, are required for two ML algorithms of RFR and XGBR. The results of optimal hyperparameters, along with the estimated model performance based on RMSE, are summarised in Table 3.5. With these optimal hyperparameters, RFR and XGBR models are trained on the entire historical data for the later performance estimates.

3.5.2 Model performance analysis

After being trained with the optimised hyperparameters, RFR and XGBR algorithms use the gathered input data of household voltage measurements to calculate the transformer loading. Aiming to analyse the model performance, 3 performance metrics are computed. First, by

using RMSE as determined by Eq. (3.3), the quantitative insights into the generalisation performance of the model are yield [148]. Secondly, Pearson correlation coefficients R , as defined by Eq. (3.11), is used to gain the insights into the degree of linear dependence between the real value and the estimated value. Thirdly, the Kolmogorov-Smirnov (KS) statistical test is performed to provide insights into the statistical significance of the model results [151]. The KS statistical test is adopted in this study because it sufficiently operates with non-normally distributed data. Meanwhile, the non-normally distributed data of V_i with $\forall i \in \mathcal{N}^A$ is shown in the histogram plots in Fig. 3.3, Fig. B.1, and Fig. B.2. In the KS statistical test, the K statistic indicates how close the proximity of the compared distributions of data will be. Hence, lower K statistic will be expected for higher estimation accuracy. Moreover, for a comparison of RFR and XGBR models to non ML models, the ordinary least squares linear regression (LR) model is applied as a bench-marking for transformer loading calculation using the same input data and performance metrics.

The results of the performance metrics are listed in Table 3.6. As can be seen, the ML models (i.e, RFR and XGBR) significantly outperform the non-ML model (i.e., LR). The ML models have the coefficients R and RMSE around 5.2 and 7.8 times, respectively, higher than the non-ML model, while the K statistic from KS test around 3.4 times lower. Owing to the features of the tree-based ensemble algorithm, RFR and XGBR are comparable in the estimation accuracy as their differences in the calculated 3 performance metrics are insignificant. These results shows the efficacy of the regression-based methods for estimating the transformer loading.

Furthermore, the Probability Density Function (PDF) based on Kernel Density Estimate is adopted to visualise the performance of regression models based on RFR, XGBR, and LR algorithms on the transformer loading calculation. A comparison of PDF of the database of transformer loading measurements (i.e., true values) and the values calculated by RFR, XGBR, and LR models is shown in Fig. 3.9. Meanwhile, a comparison of PDF of the errors between the measured and calculated values is demonstrated in Fig. 3.10.

It is observed from Fig. 3.9 that the RFR and XGBR profiles have similar patterns and statistical properties (i.e., the peak of the tail of Kernel Density Estimate) with the true data. In contrast, LR profiles show a large difference with the true data. As can be noticed from Fig. 3.10, RFR and XGBR profiles have comparable statistical properties, e.g., the peak at 0 kVA and the short tails between approximately -9 kVA and 5 kVA. All these indicate that

Table 3.6: *Summary of model performance*

ML algorithms	RMSE	Coefficients R	K statistic from KS test
RFR	0.8782	0.9828	0.0499
XGBR	0.8767	0.9829	0.0515
LR	6.8771	0.1884	0.1752

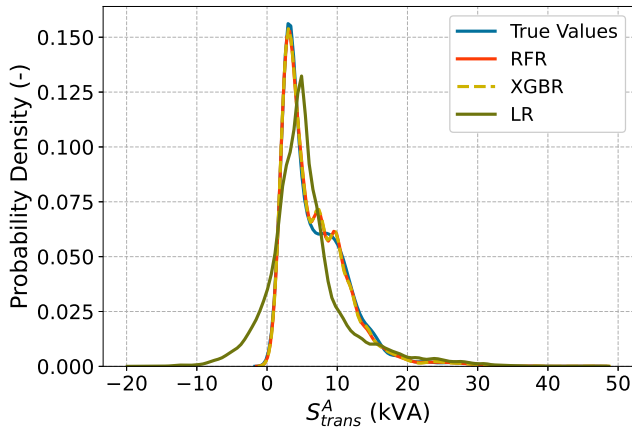


Figure 3.9: *PDF of the absolute values of transformer loading.*

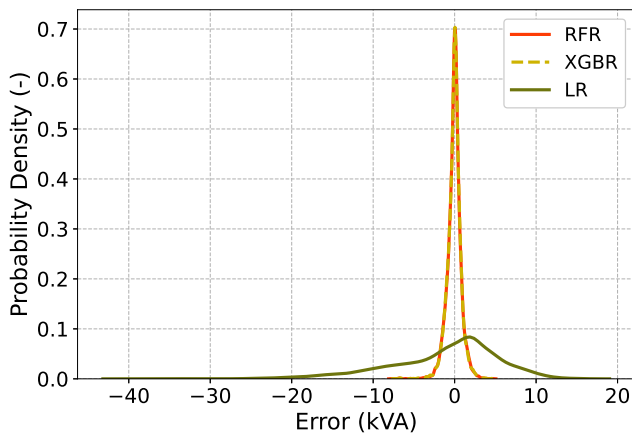


Figure 3.10: *PDF of the errors between the measurements and the estimations by the models.*

regression modes based on RFR and XGBR appear equally effective in accurately estimating the transformer loading when using the voltage measurements from SMs. The main driver of these similarities is that RFR and XGBR are both originated from the ensemble tree algorithm.

Aiming to compare these two models further, in addition to the computation time during the model fitting and evaluation, the computation time during the deployment phase is

Table 3.7: *Measurements of simulation time (mm:ss)*

ML algorithms	Model preparation	Model deployment	Total
RFR	34:48	03:08	37:56
XGBR	11:42	00:57	12:39

measured and displayed in Table 3.7. In this phase, the computation time is for re-tuning the model parameters and re-evaluating the model performance (as explained in Sec. 3.5.1). This table points out that the XGBR-based regression model runs considerably faster than the RFR one as the former takes only one-third of the latter's simulation time. Hence, considering the high effectiveness and lower execution time, it is evident that XGBR algorithm provides the best solution to the regression problem of transformer loading calculation.

3.6 Summary

Data-driven approaches are being employed more frequently to support the power system operation, resulted from the increasing availability of data measurements. The data-driven approach for the LV distribution transformer monitoring has been investigated in this chapter. The approach adopts the machine learning-based regression models and uses the data from residential smart meters in terms of voltage magnitudes, for the transformer loading estimation. A thorough analysis is conducted to discover the relationships between the transformer loading and residential smart meter readings. A comprehensive framework is provided to implement, validate and compare 4 different machine learning algorithms for the transformer loading estimation from the LECs' perspective. The compared algorithms include Ridge Regression (RR), Support Vector Regression (SVR), Random Forest Regression (RFR), and eXtreme Gradient Boosting Regression (XGBR). The presented procedure covers all the essential stages in deploying a data-driven technique, consisting of training data generation, exploratory data analysis, feature selection, model selection and algorithm selection. With this respect, state-of-the-art advances in machine learning research have been integrated, such as XGBR algorithm and Nested CV technique.

The obtained simulation results indicate that combining the machine learning-based regression model with voltage magnitude measurements from residential smart meters can effectively estimate the transformer loading, i.e., with the Pearson correlation coefficient R and RMSE calculated for the real values and the estimated values of around 0.98 and 0.87, respectively, by using only a reduced set of smart meter data (5 out of 21 smart meters used). Simultaneously, the proposed approach can preserve customers' privacy rights. Among 4 learning algorithm examined, XGBR appears the best method as it achieves adequate accuracy on estimating the transformer loading but spends significantly less time for the execution, (e.g., in total, a one-third of the execution time of RFR). Hence, the introduced

approach provides an innovative alternative to implementing transformer congestion monitoring in LV distribution networks. The approach can eliminate the need for sensors and communications dedicated to transformer congestion management due to the uses of available residential smart meters. Furthermore, the approach enables the congestion monitoring capability of the LECs. Thus, the LECs can control their consumption or generation profiles to solve congestion problems, enhancing their self-management in the regional network for the safe operation. However, applying the proposed approach heavily hinges on the accessibility of residential smart meters to the LECs since their readings will be required as historical and real-time operational data for the regression model preparation and deployment. In this respect, modifications of the existing regulatory framework about the LECs' business model need to be implemented.

Although successful, the data-driven approach comes with their own limitations. Applying the proposed approach hinges on the existence of the LECs and their ability to access the residential SMs. The LECs will use the SM readings as historical and real-time operational data for the regression model preparation and deployment. In this respect, modifications of the existing regulatory framework about the LECs' business model and the accessibility to the residential SMs will be required. In addition, the proposed approach is not adaptive with grid topology changes or increasing PV installation, which is inherent in the grid operation and evolution. These changes will induce variations in the correlation between the transformer power and nodal voltage levels, which needs to be re-captured by the regression model. Periodically assessing the regression model performance and afterwards re-training the model are essential. To facilitate these activities, the laboratory experiments can be performed for the proposed approach before the field applications.

In this research, a typical LV distribution network with a radial configuration is considered. For LV distribution networks with mesh topology, the application of the proposed approach can face challenges. The relationships between the transformer power and the nodal voltage magnitude can be complicated for regression models. Thus, further research is required to consider the mesh networks more efficiently.

4

Local control for voltage regulation

The sequential droop control (SDC) for reactive and active power outputs by the PV inverters is being widely considered to allow high PV penetration and to alleviate voltage rise problems in LV distribution networks. In this chapter, a comprehensive impact assessment, both long-term technical and economical aspects of PV units operating with the SDC mechanisms, are discussed by employing a Monte Carlo-based stochastic approach. A large set of simulations with various threshold values of the SDC mechanism are performed for different PV penetration levels and a large number of scenarios. For these simulations, a test network based on the well-known IEEE European LV distribution network is used. The obtained results point out that the technical and economical impact of the PV inverter control on the network and the PV owners relies on how fast the SDC mechanism regulate reactive power absorption (RPA) and active power curtailment (APC) in response to voltage rise in different PV penetration levels. The case with more reactive power absorption (by setting a lower threshold level) enlarges reactive and active power exchange in the network, then increasing the transformer loading and the system power losses. On the other hand, a smaller PV energy curtailment is attributed to such case with a lower level of voltage threshold, corresponding to a higher export of PV energy and then more PV owners' revenue from selling the surplus PV energy.

4.1 Introduction

The growing penetration of residential-scale PV systems in LV distribution networks presents a series of operational and power quality challenges. Besides the congestion issues (as discussed in Chapter 3), voltage limit violations have been also observed by several distribution system operators (DSOs), such as in Italy, Spain, Ireland, and Germany [29]. If voltage level exceeds the maximum limit, i.e., 1.1 p.u., the customers' electrical appliances can suffer damages and PV systems will be switched off due to their internal protection [152], which causes the loss of energy yields of PV systems. It is, thus, essential to properly address voltage rise issues. To address voltage rise problems, a number of solutions can be found in the literature, including network reinforcement, capacitor bank installations, transformer tap changer adjustment, electrical energy storage-based methods, and PV inverter control [99, 153].

Among the above-mentioned solutions, controlling the PV inverters for reactive power absorption (RPA) and active power curtailment (APC) is emerging as a promising one. By using the droop control mechanism, these PV control functions can be locally performed by the PV inverters using local measurement; meaning that neither communications among PV units nor control signals from DSOs are needed. Additionally, as these approaches employ the controllability of the existing PV inverters, this can be implemented with an affordable cost and limited grid modifications for DSOs. Performing these PV control functions in a sequence, i.e., RPA prior to APC, are deemed effective in mitigating voltage rise problems while reducing the curtailed active power of PV systems, resulting from the absorbed reactive power by these systems. In this respect, operating the PV inverters with the droop control mechanism has both the technical and economical impact on LV distribution networks as well as the PV owners.

However, the assessment of these impacts of PV systems operating with the sequential droop-based RPA and APC schemes to solve voltage rise problems on LV distribution networks and the PV owners are limited. The existing works mostly focus on the technical impact for a short-time period without considering the uncertainty from PV power generation as well as the customers' power consumption. A recent work in [126] presents a Monte Carlo stochastic assessment for both technical and economical impact of PV droop control functions for voltage rise mitigation. All these works, however, consider only one value of the droop control parameter, so-called threshold level. This threshold level plays a decisive role in the performance of the PV droop control mechanisms, which is important to undertake a more comprehensive assessment of operating PV systems with different threshold levels.

In this chapter, a procedure of assessing the impact of PV droop control with different threshold levels on LV distribution networks and the PV owners for voltage rise alleviation are presented. This comprehensive impact assessment aims for both long-term technical and economical aspects by employing a Monte Carlo-based stochastic approach and several impact metrics. To realise this stochastic approach, a conditional Copula method in [154] is

adopted to generate a large set of time series data of PV power generation and the customers' power consumption. The proposed assessment procedure applies for the sequential droop control for the RPA and APC schemes of the PV inverters. Additionally, various threshold values for the droop control mechanisms are pre-defined. The operation of the PV inverters with various droop control parameters can be, thus, assessed efficiently. First, the problems of voltage rise is analysed, followed by the droop control schemes. Next, the stochastic impact assessment is presented. Then, the modelling and simulation set up are described. Finally, the simulation results and discussion are given and concluding remarks are drawn.

4.2 Voltage rise issues

Due to the increasing level of PV integration in LV distribution networks, voltage rise has become a more frequent issue. Voltage difference (ΔV) between the sending and receiving end voltage of a typical LV distribution line section with an impedance of $(R + jX)$ can be expressed as,

$$\Delta V = \left(\frac{P^{tr} - jQ^{tr}}{V_R^*} \right) (R + jX) \quad (4.1)$$

where V_R^* denotes the conjugate of the receiving end voltage, P^{tr} and Q^{tr} denote the active and reactive power transferred through the line, respectively.

Further consider the receiving end bus supplies local power consumption of P_L and Q_L of loads, and receives local power generation of P_G and Q_G from PV systems. By ignoring the imaginary part, Eq. (4.1) can be rewritten as,

$$|\Delta V| \approx \frac{(|P_L| - |P_G|)R + (|Q_L| - |Q_G|)X}{|V_R^*|} \quad (4.2)$$

where $P^{tr} = |P_L| - |P_G|$ and $Q^{tr} = |Q_L| - |Q_G|$.

It can be inferred from Eq. (4.2) that when a high level of P_G coincides with a low P_L , $|\Delta V|$ is negative, indicating that voltage level rises towards the end of the line. In practice, if the voltage level measured at the POC exceeds 1.1 p.u., PV systems are disconnected from the network and are reconnected after some delay [155]. If the solar irradiance varies insignificantly, the PV systems continue switching off and on with the network. To solve voltage rise issue, the reverse power flow needs to be limited by reducing P_G and Q_G from PV systems.

An important notice from Eq. (4.2) is that for a typical LV network with high R/X ratio, changes in active power strongly impact the voltage magnitude variation. However, the reac-

tive power control of the PV inverters is, therefore, still beneficial for voltage control. If the PV inverters can operate with power factor (PF) of ± 0.9 , it can absorb reactive power with an amount of approximately 50% of the rated active power for grid ancillary services [156], which reduces the curtailment of active power injection. Some of the commercial PV inverters are capable of providing such reactive power absorption as discussed in [122]. In this chapter, the reactive power control strategy is further studied to mitigate voltage rise problems in LV distribution networks.

4.3 Droop control for voltage regulation

4.3.1 Active power curtailment (APC)

APC scheme can be based on $P - V$ droop control or voltage/active power sensitivity [22]. Among these, the $P - V$ droop control is most widely utilized [157]. This method applies control rules based on the network state, e.g., voltage magnitude, to regulate the amount of generated active power by the PV inverters. The voltage magnitude at the point of connection (POC) of the inverter, subsequently, is reduced.

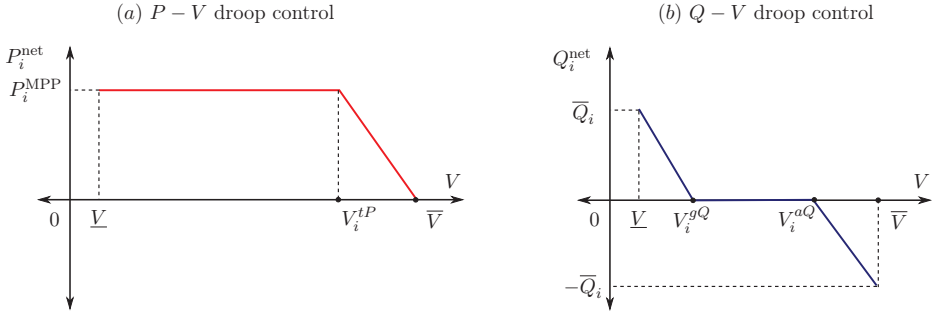


Figure 4.1: Droop characteristics for local voltage control of PV systems. (a) $P - V$ droop control, (b) $Q - V$ droop control.

In this chapter, the $P - V$ droop control, as shown in Fig. 4.1 (a), has been integrated to realise the APC scheme. During normal operations, i.e., no voltage violations, the active power output of the PV inverter i^1 (P_i^{net}) is set to the maximum power point, P_i^{MPP} . If voltage level at the connection point, V_i of the inverter reaches the threshold level for active power curtailment (V_i^{tP}), the PV inverter starts APC mode using $P - V$ droop control with P_i^{net} being reduced following a linear function of V_i as expressed in Eq. (4.3).

¹In this study, it is assumed that the PV system i is connected to the node i of the distribution network.

$$P_i^{\text{net}} = \begin{cases} P_i^{\text{MPP}}, & \text{if } \underline{V} < V_i \leq V_i^{tP} \\ P_i^{\text{MPP}} - P_i^{\text{MPP}} \frac{(V_i - V_i^{tP})}{(\bar{V} - V_i^{tP})}, & \text{if } V_i^{tP} < V_i < \bar{V} \\ 0, & \text{if } V_i \geq \bar{V} \end{cases} \quad (4.3)$$

where $[\underline{V} \ \bar{V}] = [0.9 \ 1.1]$, as specified in the European Standard EN 50160.

4.3.2 Reactive power absorption (RPA)

RPA scheme applies control rules based on the network state, e.g., voltage magnitude or power quality indices, to regulate the amount of absorbed reactive power by the inverters, aiming to reduce the voltage magnitude at the POC of the inverter. The RPA scheme can be implemented using $\cos\phi(P)$, $\cos\phi(P, V)$, or $Q - V$ droop control, of which $Q - V$ droop control is widely used [97]. The $Q - V$ droop control has been integrated in this work.

Without voltage violations, the reactive power output of the PV inverter (Q_i^{net}) is set to zero. If the voltage level at the POC (V_i) exceeds the threshold level for reactive power absorption (V_i^{aQ}), RPA is activated according to the $Q - V$ droop control mechanism. As can be seen in Eq. (4.4), Q_i^{net} is set following a linear function of V_i .

$$Q_i^{\text{net}} = \begin{cases} \bar{Q}_i \frac{(V_i^{gQ} - V_i)}{(V_i^{gQ} - \underline{V})}, & \text{if } \underline{V} \leq V_i < V_i^{gQ} \\ 0, & \text{if } V_i^{gQ} \leq V_i \leq V_i^{aQ} \\ -\bar{Q}_i \frac{(V_i - V_i^{aQ})}{(\bar{V} - V_i^{aQ})}, & \text{if } V_i^{aQ} < V_i \leq \bar{V} \end{cases} \quad (4.4)$$

where \bar{Q}_i is the maximum reactive power output and V_i^{gQ} is the threshold level for reactive power injection.

4.3.3 Proposed sequential droop control

Applying the APC scheme directly leads to losses of PV owners' revenue due to generation reductions. Meanwhile, the RPA scheme by itself is unable to sufficiently solve voltage rise problems due to the high R/X ratios in LV distribution networks, and the limited reactive power capacity of the PV inverters [153]. A combination of RPA and APC has been reported in [158, 159] to be more promising for voltage rise mitigation. This type of combined method helps to mitigate voltage rise problems with a decreased amount of curtailed

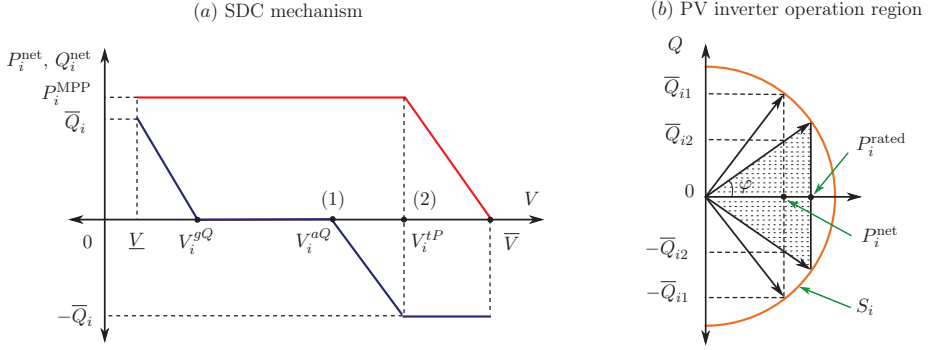


Figure 4.2: (a) The SDC mechanism applied for PV unit i consisting of $Q - V$ droop control (dark blue curve) and $P - V$ droop control (red curve). (b) The operation region (shaded triangle) of the PV inverter i determined by the apparent power S_i (orange curve), rated active power P_i^{rated} , maximum reactive power \bar{Q}_i , and PF requirement ($\cos \varphi = PF$).

active power. In this chapter, the combination of the RPA and APC schemes has been considered to form the sequential droop control (SDC), as illustrated in Fig. 4.2 (a).

The proposed SDC allows the PV inverters to operate in reactive power priority mode, implying that voltage regulation is first attempted through the RPA scheme (i.e., based on the $Q - V$ droop control, as discussed in Sec. 4.3.2) with a modification. If V_i exceeds V_i^{gQ} , i.e., at point (1), the RPA scheme is activated. The APC scheme (i.e., based on the $P - V$ droop control, as discussed in Sec. 4.3.1) is triggered only if the voltage levels can not be maintained below the threshold value using the RPA scheme. If V_i reaches V_i^{tP} , i.e., at point (2), Q_i^{net} is set to $-\bar{Q}_i$, i.e., maximum amount, with the aim at reducing the curtailed active power for voltage rise mitigation. Concurrently, the PV inverter starts APC mode using $P - V$ droop control. The APC scheme uses the linear function shown in Eq. (4.3), while the modified RPA scheme can be mathematically presented as:

$$Q_i^{\text{net}} = \begin{cases} \bar{Q}_i \frac{(V_i^{gQ} - V_i)}{(V_i^{gQ} - \underline{V})}, & \text{if } \underline{V} \leq V_i < V_i^{gQ} \\ 0, & \text{if } V_i^{gQ} \leq V_i \leq V_i^{aQ} \\ -\bar{Q}_i \frac{(V_i - V_i^{aQ})}{(V_i^{tP} - V_i^{aQ})}, & \text{if } V_i^{aQ} < V_i \leq V_i^{tP} \\ -\bar{Q}_i, & \text{if } V_i^{tP} < V_i \leq \bar{V} \end{cases} \quad (4.5)$$

Note that, the maximum reactive power output \bar{Q}_i varies with P_i^{net} and it is calculated in

compliance with the European Standard EN 50438, which stipulates that all distributed generation units connected to LV distribution networks must operate with PF ranging from 0.9 lagging to 0.9 leading [160]. Fig. 4.2 (b) shows the operation region of a PV inverter, which is within the shaded triangle, along with the apparent power S , rated active power P_i^{rated} , maximum reactive power \bar{Q}_i specified by the PF requirement ($\cos \varphi = \text{PF}$). The above-mentioned constraints of \bar{Q}_i has been integrated into the proposed SDC in this work as expressed below,

$$\bar{Q}_{i1} = \sqrt{(S_i)^2 - (P_i^{\text{net}})^2} \quad (4.6)$$

$$\bar{Q}_{i2} = (\tan[\arccos(\text{PF})])P_i^{\text{net}} \quad (4.7)$$

$$\bar{Q}_i = \min(\bar{Q}_{i1}, \bar{Q}_{i2}) \quad (4.8)$$

4.4 Stochastic impact assessment

4.4.1 Assessment procedure

A procedure for the stochastic impact assessment is comprised of several main stages, which are briefly described below.

- A set of one-year data profiles \mathcal{P} with a time resolution of 15 minutes (i.e., size $|\mathcal{P}| = 35040$) of PV generation and load consumption are firstly prepared for a set of \mathcal{N} households in the different scenarios. Sec. 4.5 describes this preparation in more details.
- Next, with given a PV penetration level ranging from 0% to 100%, the households equipped with PV systems are randomly selected. Consequently, the prepared data profiles (including PV generation and load consumption) is randomly distributed to the houses in the test network. For a sake of simplicity, it is assumed that PV units have same phase connection as the houses.
- Then, one-year time-series power flows are solved in an iterative manner, per PV penetration level as well as the data scenario. A data sample is recorded at each execution, containing voltage magnitudes, net active and reactive power measured at the POC of the PV units, and powers flowing in the network. These sets are then stored for later processing steps.

4.4.2 Metrics for impact assessment

Metrics presented in this section are used for assessing the impacts of the PV inverter controlling functions on LV distribution networks and the PV owners. These metrics are adopted from [126].

Impacts on LV Distribution Networks

Metrics for quantifying the technical impacts on LV distribution networks are comprised of the following indexes.

- *Maximum voltage deviation index (MVDI)*: This index (in percentage) quantifies how far the network voltage deviates from the nominal value, V^{nom} , which is given by Eq. (4.9). For a network with \mathcal{N} nodes, MVDI is calculated at each time step t , in which the maximum voltage level in the network, i.e., $\max\{V_i^t\}$ with $\forall i \in \mathcal{N}$, needs to be obtained.

$$MVDI^t = \frac{(\max\{V_i^t\} - V^{nom})}{V^{nom}} \cdot 100 \quad [\%] \quad (4.9)$$

- *Transformer loading index (TLI)*: This index (in percentage) is determined in timely basis as a ratio of maximum apparent power at time t , S_{trans}^t , to the transformer rated power, S_{trans}^R . This is an important metric because the PV inverters operating with the SDC mechanism affects both active and reactive power exchange in the network.
- *System power losses*: Since the SDC mechanism in the PV inverters performs both RPA and APC schemes to support voltage regulation, the assessment of the system power losses is essential (as similar to TLI). Thus, the total active power losses of the network (in kW) is calculated at each time step t .

Impacts on the PV Owners

The impacts on the PV owners are technically and economically quantified utilising the indexes below.

- *Curtailed energy index (CEI)*: As given by Eq. (4.10), this index is determined as a ratio (in percentage) of the total curtailed energy generation of PV systems with droop

control (i.e., sequential RPA and APC scheme) in the network over the total energy generation from PV systems without droop control.

$$CEI = \frac{\sum_{t=1}^{\mathcal{T}} \sum_{i=1}^{\mathcal{N}} \Delta P_i^t \Delta t}{\sum_{t=1}^{\mathcal{T}} \sum_{i=1}^{\mathcal{N}} P_i^t \Delta t} \cdot 100 \quad [\%] \quad (4.10)$$

where ΔP_i^t is the curtailed active power of PV unit i at time t due to droop control activated, P_i^t is PV active power generation without droop control, and \mathcal{T} is the total number of time steps.

- *Exported energy index (EEI)*: Similar to CEI, the EEI is specified as a ratio (in percentage) of the total exported energy generation from the PV inverters with droop control in the network over the total exported PV energy generation without droop control, as expressed in Eq. (4.11).

$$EEI = \frac{\sum_{t=1}^{\mathcal{T}} \sum_{i=1}^{\mathcal{N}} P_i^{E,t} \Delta t}{\sum_{t=1}^{\mathcal{T}} \sum_{i=1}^{\mathcal{N}} P_i'^{E,t} \Delta t} \cdot 100 \quad [\%] \quad (4.11)$$

where $P_i^{E,t}$ denotes the exported active power of the PV inverter i (PV generation minus load consumption) at time t with droop control applied, and $P_i'^{E,t}$ denotes the exported PV active power without droop control. It is worth noting that the *CEI* represents purely the changes in the amount of PV energy generation when droop control is implemented in comparison with the case without droop control.

- *System Annual Billing (SAB)*: This index represents the total annual billing (in €) for all the PV owners in the network. For each individual PV system, the annual billing is calculated using Eq. (4.12).

$$\sum_{t \in \mathcal{T} | P^{N,t} > 0} P^{N,t} \rho^c \Delta t + \sum_{t \in \mathcal{T} | P^{N,t} < 0} P^{N,t} \rho^f \Delta t, \quad (4.12)$$

where $P^{N,t}$ is the net active power (load consumption minus PV generation) of the PV owner at time step t , while ρ^c and ρ^f are the energy consumption and the feed-in tariff, respectively. Since the *SAB* includes the energy price and tariffs, it indicates a higher accuracy than the *EEI* with regard to the effects of the different control strategies on the PV owners [161].

4.5 Simulation setup

A modified well-known IEEE European LV distribution network is used as the test network [162]. In this network there are 55 households, which are all assumed to have three-phase connections. The test network is supplied by a substation consisting of a 250 kVA, 11/0.4 kV transformer with a $\Delta - Y_n$ connection and the secondary side voltage level settings assumed to be 1.03 p.u. The remaining characteristics of the test network are retained as the origin in the IEEE European LV distribution network.

The residential PV systems and household load consumption for this study represent a real case in the Netherlands. The installed PV capacities are randomly chosen between 4.06 and 6.27 kWp [126]. For PV generation modelling, the solar irradiation profiles adopted from [126] are used, which are built following a random sampling procedure based on a Gaussian Mixture Model and the real meteorological measurements from by the Royal Netherlands Meteorological Institute (KNMI), is adopted [129]. For household power consumption modelling, the daily load profiles adopted from [126] are utilised, which are generated using a probabilistic method based on conditional Copula model and the real smart meter readings from Dutch end-users. These methods allow preserving the statistical correlation among the time steps and properly taking into account the the seasonality fluctuations during the year. To carry out the stochastic assessment, all the obtained data contains a set of different scenarios, in which each scenario is one-year time-series data with a resolution of 15 minutes (i.e., with size $|\mathcal{P}| = 35040$ per scenario).

The proposed stochastic assessment approach is simulated in Python programming language and OpenDSS software. Aiming for a comprehensive assessment, the simulations involve examining various cases with different threshold levels of the SDC mechanism (V_i^{tP} and V_i^{aQ}) for PV systems as tabulated in Table 4.1. These simulation cases are categorised into 3 groups with each group having the same value of V_i^{tP} and the varying values of V_i^{aQ} . In addition, the simulation case without voltage control is also performed to gain the insights into the network voltage profiles.

Because of considerable computation time required to execute one-year time-series power flows, 20 scenarios (i.e., each scenario is one-year time-series data with size $|\mathcal{P}| = 35040$) are implemented for each PV penetration level. To complete all the simulations, 5 computers have been utilised for 7 days.

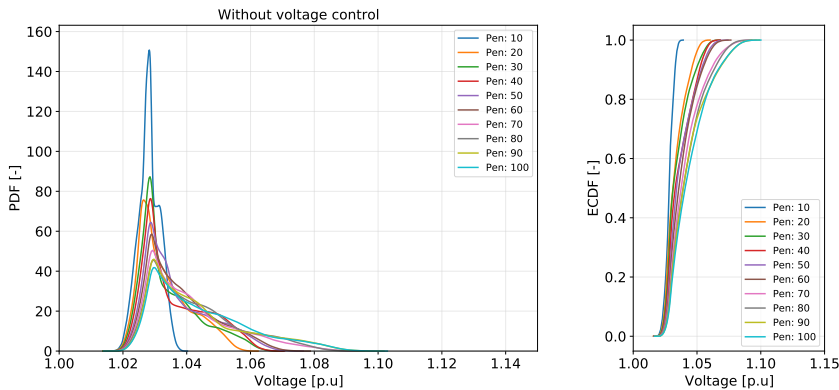
4.6 Numerical results

The outputs of all the scenarios considered in the stochastic assessment process is averaged to generate the final results of all the simulation cases. For the case without voltage control,

Table 4.1: *Simulation cases for the impact assessment*

Group	Cases	Threshold levels of SDC mechanism	
		V_i^{aQ} (p.u.)	V_i^{IP} (p.u.)
Group A	Case 1	1.03	1.06
	Case 2	1.04	1.06
	Case 3	1.05	1.06
Group B	Case 4	1.04	1.07
	Case 5	1.05	1.07
	Case 6	1.06	1.07
Group C	Case 7	1.05	1.08
	Case 8	1.06	1.08
	Case 9	1.07	1.08

the voltage levels at all the POCs of the PV systems in the network are visualised in Fig. 4.3 using Probability Density Function (PDF) and Empirical Cumulative Distribution Function (ECDF). It is observed that the voltage levels increase with the growing PV penetration and reach the violation limit 1.1 p.u. (so called overvoltage) with the PV penetration level above 70%. This indicates that the PV penetration level between 60% and 70% is the maximum level that the network can host without voltage violation caused (also known as PV hosting capacity).

**Figure 4.3:** *PDF and ECDF of the voltage levels in the network without any control mechanism.*

Since the simulation results is in the form of one-year time-series data, the second quartile (Q2) i^2 is, subsequently, considered to analyse the results. The simulation results are divided into 3 groups according to the threshold level variations, including Group A, B and C with

²Note that, Q2 is 50th percentile of the data set, i.e., 50% of the data is below this point.

its diverse settings as defined in Sec. 4.5. As can be seen from Fig. 4.3, the voltage level of 1.06 p.u. appears in most of the PV penetration levels (i.e., 20% and above). Hence, to provide an extensive discussion on different PV penetration cases, the simulation results for the cases in Group A (with V_i^{tP} of 1.06 p.u. and V_i^{aQ} from 1.03 to 1.05 p.u.) are discussed in details in following subsections. For the cases in Group B and C, the simulation results are given in Appendix C.

4.6.1 Impacts on LV distribution networks

The maximum voltage deviation at the POCs of the PV units with Group A SDC mechanism is illustrated in Fig. 4.4 using the MVDI as defined in Sec. 4.4.2. All 3 control cases are effective to prevent the overvoltage problem as no the MVDI above 10% is recorded. This promising effectiveness can also be observed in Fig. 4.5. Among those 3 cases (with the same V_i^{tP} value), Case 1 (with the lowest V_i^{aQ} value) results in the smallest MVDI while Case 3 (with the highest V_i^{aQ} value) results in the largest MVDI in all the PV penetration level. Such voltage regulation impact of those 3 cases are derived from the control they take of the PV power output, which is further elaborated below.

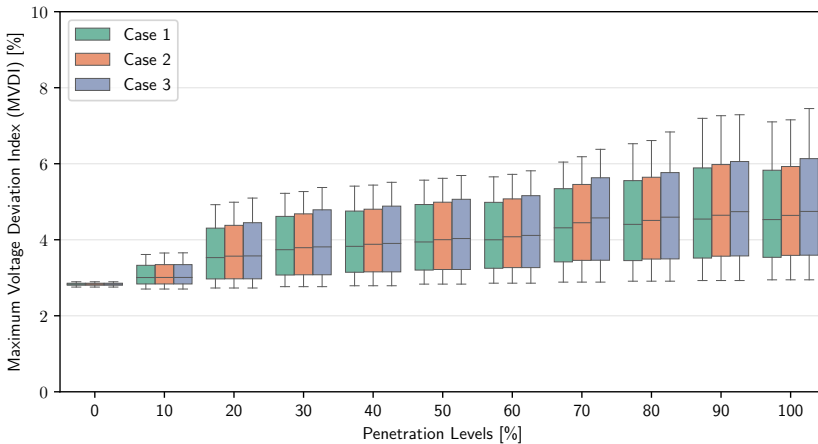


Figure 4.4: Maximum voltage deviation index at the POCs of the PV units with Group A cases.

Fig. 4.6 displays the resultant transformer loading index (TLI as defined in Sec. 4.4.2) for 3 control cases in Group A per PV penetration level. The TLI with the PV penetration levels ranging from 10% to 20% is lower than that in case of no PV installed as the total PV generation can partly supply the total load consumption in the network. For this PV penetration

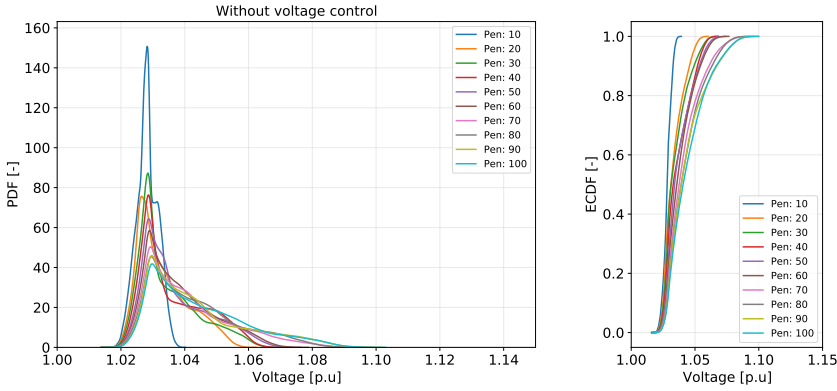


Figure 4.5: PDF and ECDF of the voltage levels in the network with Group A cases.

range, the impact of the 3 control cases on the transformer loading is almost the same. From the PV penetration level above 30%, the difference between the 3 control cases is more observable with Case 1 causing the greatest loading and Case 3 causing the lowest loading of the transformer. A smaller value of V_i^{aQ} leads to a larger amount of reactive power absorbed by the PV inverters to support voltage rise mitigation, enabling a smaller amount of active power curtailed from the PV units (which can also be seen in next subsection). This enlarges the reactive and active power exchange in the network, then causing a faster transformer loading increase. In contrast, a higher value of V_i^{aQ} results in a slower transformer loading increase. It can be seen that the transformer capacity is capable of operating the network hosting up to 100% PV penetration level with the RPA scheme operating with a PF of 0.9. However, if a lower PF is applied for the PV units, the overloading of the transformer can occur, which must be considered by the DSOs to properly select the transformer capacity and the threshold levels of the SDC mechanism for PV units.

The resultant system power losses (in kW) for Group A cases per PV penetration level is shown in Fig. 4.7. As the system power losses are correlated with the TLI, a similar conclusion for the TLI can be drawn for the system power losses. In general, the SDC mechanism with a lower V_i^{aQ} level provokes the increased system power losses, resulted from the higher reactive power absorbed by the PV systems.

4.6.2 Impacts on the PV owners

The impact of the SDC mechanism with different threshold settings on the PV owners is evaluated in the technical aspect (i.e., using the CEI and the EEI metrics) and in the eco-

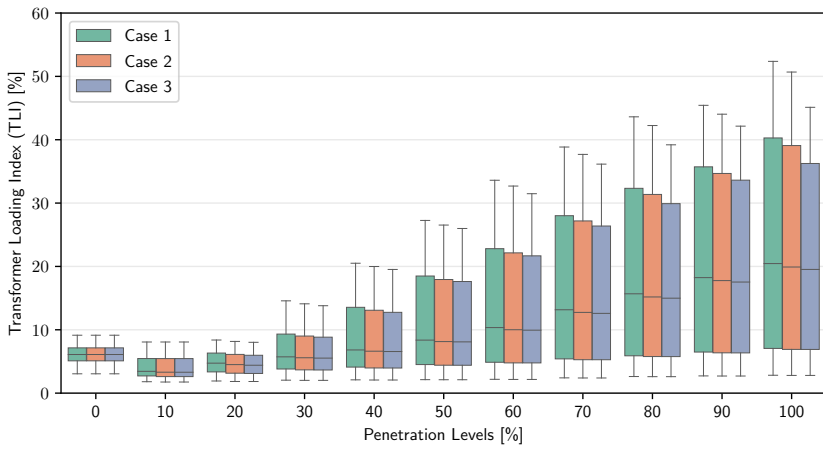


Figure 4.6: Transformer loading index with Group A cases.

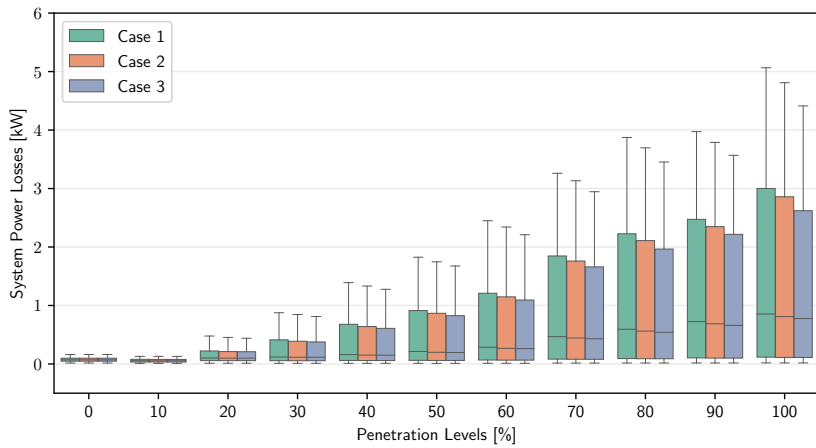


Figure 4.7: System power losses with Group A cases.

nomic aspect (i.e., using the SAB metric) as defined in Sec. 4.4.2.

The amount of total curtailed energy of the PV units is shown in Fig. 4.8 as percentage using the CEI. The resultant CEI increases for the growing PV penetration levels due to

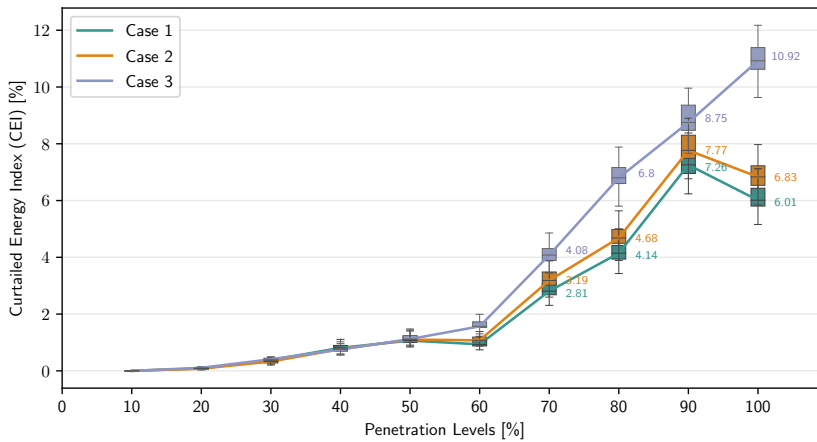


Figure 4.8: Curtailed energy index with Group A cases.

more severe voltage rise issues (as shown in Fig. 4.3 and Fig. 4.4). This points out a strong correlation between the voltage and PV generation curtailment. Consequently, the exported energy from the PV units decreases as depicted in Fig. 4.9 using the EEI.

As can be seen from Fig. 4.8, for the PV penetration levels of 50% and below, the CEI in 3 control cases (Group A) have similar values. The CEI values gradually, besides, increase from around 0.08% (Q2) for 20% PV penetration level to around 1.06% (Q2) for 50% level. Such similar impact of 3 control cases on PV energy for the PV penetration levels of 50% and below can be recognised from Fig. 4.9. Also, there exists a gradual change in the EEI (i.e., reducing from 99.8% (Q2) for 20% PV penetration level to around 98.7% (Q2) for 50% level) as a consequence of the gradual change in the CEI. These outcomes reveal that, for the PV penetration levels of 50% and below, the SDC mechanisms with 3 different sets of threshold levels do not have significant impact on the PV generated energy. Additionally, the difference in the performances of these 3 control cases is negligible. These characteristics are derived from the slow voltage rise for the PV penetration level growing to 50%. From the PV penetration level of 60% and above, 3 control cases are more different in its impact on PV energy generation. Case 1 and Case 2 have an equivalent impact as the EEI and CEI curves follow the same pattern with a relatively close proximity. Compared to these cases, Case 3 is different dramatically as shown in Fig. 4.8 and Fig. 4.9.

Both the CEI and EEI results in 3 control cases shows more rapid changes for the PV penetration levels above 70% (corresponding to the PV hosting capacity as discussed earlier) than the ones for the lower PV penetration levels. These are caused by the fact that the voltage

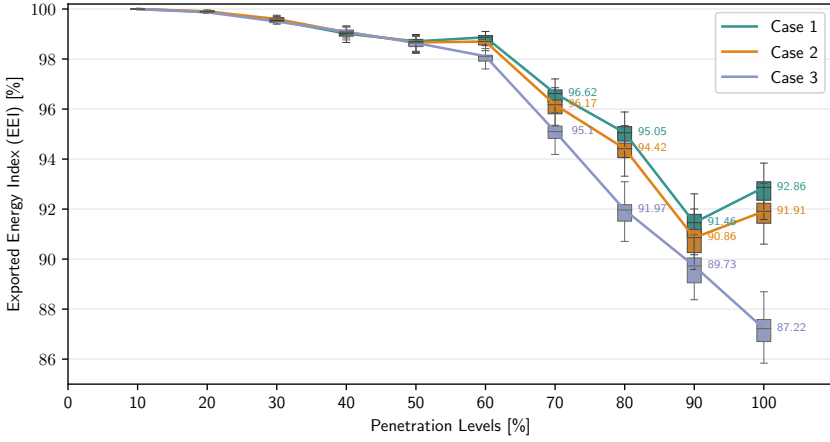


Figure 4.9: Exported energy index with Group A cases.

rise conditions in the last 4 levels of PV penetration is higher than that in the first 6 levels (as demonstrated in Fig. 4.3 and Fig. 4.4).

Furthermore, the notable difference between 3 control cases arises when the PV penetration level equals to 70% and above. The amount of curtailed energy in Case 1 is lowest, followed by Case 2, and that in Case 3 is highest. For instance, for 100% PV penetration level, the CEI is estimated in 6.01% (Q2) with Case 1, 6.83% (Q2) with Case 2, and 10.92% (Q2) with Case 3. Subsequently, Case 1 enables the highest exported energy while Case 3 represents the lowest, i.e., the maximum EEI being estimated in 92.86% (Q2) and 87.22% (Q2), respectively, also for the level of 100% PV penetration. These outcomes demonstrate the benefit of employing a faster RPA scheme (by setting a lower V_i^{aQ} values, e.g., in Case 1), when compared with a slower RPA scheme (by setting a higher V_i^{aQ} values, e.g., in Case 3), to reduce the PV generation curtailment. By doing this, the adverse impact of the SDC mechanism on the PV owners can be limited.

The benefit of the faster RPA scheme can also be seen in Q2 results of the SAB (in €) as listed in Table 4.2. Following Eq. (4.12), the positive SAB values correspond to the energy fees owned to the DSO, i.e., paid by the PV owners, and vice versa, the negative SAB values correspond to the energy revenue to the PV owners, i.e., paid by the DSO. Similar to the CEI and the EEI results, the major impact of the SDC mechanism is observed at the PV penetration level of 70% and above. For instance, at 70% PV penetration level, the SAB in Case 1 is 1.4% and 4.3% lower than that in Case 2 and Case 3, respectively. This means that the total energy fees paid by the PV owners to the DSO decreases from Case 1 to Case

Table 4.2: Q2 results of the system annual billing with Group A cases

PV penetration levels (%)	System Annual Billing (SAB) (€)		
	Case 1	Case 2	Case 3
Pen: 0	30966.8	30966.8	30966.8
Pen: 10	27134.6	27134.6	27134.6
Pen: 20	23863.0	23862.7	23864.1
Pen: 30	19851.6	19848.1	19854.9
Pen: 40	16485.6	16479.3	16469.5
Pen: 50	12478.9	12482.0	12478.9
Pen: 60	9056.4	9077.2	9102.1
Pen: 70	5388.4	5464.5	5629.4
Pen: 80	2196.8	2315.0	2387.9
Pen: 90	-471.4	-352.4	-432.99
Pen: 100	-3900.3	-3705.2	-3493.9

3. At 100% PV penetration level, the SAB in Case 1 is 5.3% and 11.7% higher than that in Case 2 and Case 3, respectively, which means that the total energy revenue of the PV owners increase. These outcomes, therefore, clearly demonstrate the beneficial effect of the SDC mechanism with increased reactive power absorption on the PV owners' economic operation.

However, these promising results for the PV owners come at the expense of the increase in the transformer loading and the system power losses for DSOs as elaborated in Sec. 4.6.1. On the other hand, the impact on each individual PV owner is unobserved yet as the above assessment is performed for the network as a whole. A more comparative analysis between the technical and economic impact, as well as the impact assessment on the individual PV units are required.

4.7 Summary

The use of the droop-based control for RPA and APC by the PV inverters is being considered to support the voltage rise alleviation in LV distribution networks. However, the long-term impact assessment of these PV control functions, including the technical and economical aspect, on LV distribution networks as well as the PV owners, are relatively limited.

This chapter discusses a procedure of comprehensively assessing the technical and economical impact of PV SDC mechanisms, consisting of RPA and APC scheme, on LV distribution networks and the PV owners for voltage rise alleviation. A Monte Carlo-based stochastic approach and several impact metrics (both technically and economically) are adopted, along with the latest conditional Copula method used for generating a large set of time series input data. The impact metrics for the network includes the MVDI, the TLI, and the system

power losses. The impact metrics for the PV owners are the CEI, EEI, and the SAB. Then, 9 simulation cases of the SDC mechanism with various threshold values are built, in which, each case for 11 PV penetration levels (ranging from 0% to 100%) in 20 scenarios (one-year time-series data with size $|\mathcal{P}| = 35040$ per scenario). These simulations are performed in a test network based on the IEEE European LV distribution network.

The obtained results points out that the technical and economical impact of the PV inverter control on the network and the PV owners relies on how fast the SDC mechanism regulate RPA and APC in response to voltage rise in different PV penetration levels. With the PV penetration level below 30%, the impact of the simulation cases on the TLI are equivalent. With the higher PV penetratio levels, their impacts on TLI are more recognisable, in which the case with more reactive power absorption causes the increase in TLI to be faster due to an enlarged exchange of reactive and active power in the network. Such power exchange enlargement also corresponds with an increased system power losses. Overall, all the control cases are effective to solve voltage rise issues as the MVDI are efficiently maintained below the limit.

On the other hand, the control cases have insignificant impact on the PV generated energy and have negligible difference in their performance, for the PV penetration levels of 60% and below, derived from the slow voltage rise. The difference between the control cases are more noticeable when the PV penetration level exceeds 70%. Smaller values of CEI are found in the case where a lower level of V_i^{aQ} is set. This corresponds to higher values of EEI, which turn to a lower value of SAB (meaning more PV owners' revenue from selling the surplus PV energy). These outcomes show the efficacy of coordinating more reactive power absorption before active power curtailment to solve voltage rise issues, allowing an decrease in the adverse impact on the PV owners.

As noted, the advantages in using more reactive power absorption for the PV owners is made at the expense of a higher transformer loading and the system power losses, which are major concerns of DSOs. Besides, the influence of the SDC mechanism on individual PV owner is not assessed. At this stage, the procedure of stochastic impact assessment discussed in this study can provide DSOs with more insights. Further research can be conducted to develop a more comparative analysis between the technical and economic impact, as well as the impact assessment on the individual PV units.

5

Centralised control for voltage regulation

*The centralised control has been studied widely to coordinate residential-scale photovoltaic (PV) inverters as well as other power network components to achieve the optimal operation of the system. This chapter presents the centralised control to coordinate PV inverters for voltage rise mitigation. The local control and centralised control algorithms are used and integrated following a hierarchical control architecture. The local control algorithm adopts the sequential $Q - V$ and $P - V$ droop control scheme discussed in Chapter 4. This droop-based local control is embedded in each inverter for continuously monitoring and addressing voltage rise problems. Meanwhile, the centralised control algorithm is executed by a central controller aiming to optimally regulate PV power outputs by using the linear programming technique. The feasibility of the proposed control approach is successfully verified through simulations on a typical Dutch LV network.*¹

5.1 Introduction

The integration of residential-scale PV units is accelerating in LV distribution networks, which poses technical challenges regarding power quality and reliability [164]. One of the foremost issues is the voltage rise, which become a major limiting factor for further PV

¹This chapter is based on [163].

deployment [165]. Therefore, adequately solving the voltage rise problems and avoiding lost of PV energy production are both essential.

As mentioned in Chapter 4, among the available methods, using PV inverter to control PV power outputs, including active and reactive power, is widely considered as the most effective one. For this local control, the sequential $P-V$ and $Q-V$ droop control mechanism shows promising perspective for voltage rise mitigation. This droop-based local control leverages the reactive power absorption capability of the inverter to support the voltage regulation. Subsequently, the active power control of the inverter will be used if voltage rise issues still occur; thus, allowing to reduce the curtailed amount of PV active power. Main shortcomings of the droop-based local control, however, is the deficient employment of reactive power absorption of the inverter. This issue refers to the situation when the capacities of some inverters are not being employed to support voltage regulation, while some other inverters have to curtail the active power generation. Further discussion on this is presented in the next section.

The centralised control has been widely studied to coordinate PV inverters as well as other power network components to obtain the optimal operation of the system. In this chapter, the development of the centralised control to coordinate PV inverters for voltage rise mitigation is presented. This proposed control approach is based on the hierarchical control to integrate the local control and centralised control algorithms. The local control algorithm adopts the sequential $Q-V$ and $P-V$ droop control scheme, as discussed in Chapter 4, which is performed at every inverter to continuously monitor and address voltage rise problems. The centralised control algorithm is performed only by a central controller with the aim to optimally manage the PV power outputs by using an optimisation technique. The coordination between the centralised and local control is obtained when the former updates the latter with new control parameter values. First, the proposed control approach is described in details. Thereafter, the simulation set up for a typical Dutch LV distribution network is elaborated. The simulation results are then shown and discussed thoroughly, followed by the conclusion being drawn.

5.2 Centralised coordination control

The centralised control is formulated with the aim of effectively coordinating the reactive power absorption and reducing active power curtailment of residential PV systems for voltage rise mitigation. For this, a hierarchical control framework (described in Chapter 2) is employed, as schematically presented in Fig. 5.1. The proposed control strategy is composed of local control and centralised control algorithms given the communications are available. The local control algorithms are performed at each of PV inverters to solve voltage level violations by introducing the set points of PV power outputs (P^{net} , Q^{net}). The centralised

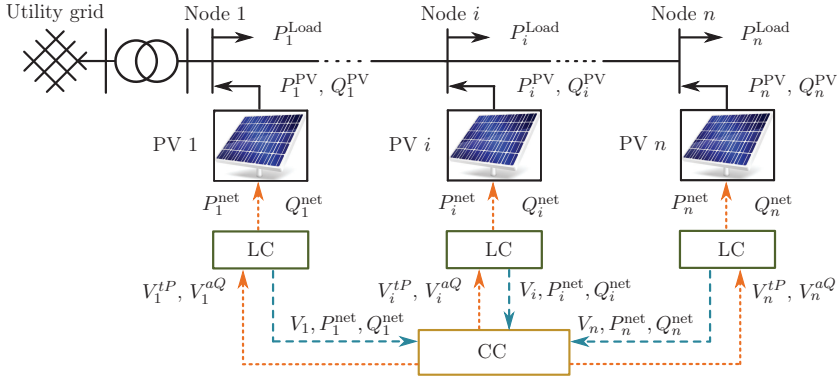


Figure 5.1: Schematic representation of a LV distribution network with the proposed control strategy, consisting of local control (LC) and centralised control (CC). The orange dotted lines represent the control signals, while the blue dashed lines represent the information exchange.

control algorithm steers all PV systems by periodically updating the local control algorithms with new parameter settings (V^{tP} , V^{aQ}), based on the operational data sent from all the inverters.

5.2.1 Local control algorithm

A local control algorithm is integrated into every PV inverter, aiming to continuously monitor and alleviate violations of voltage limits at the POCs. To this end, the SDC mechanism, as explained in Chapter 4, is adopted to regulate the power injection of the PV systems at the POCs. In the SDC mechanism, $Q - V$ droop control to realise the RPA scheme is modified that has a higher slope to reach its maximum rate at the voltage value that triggers the APC scheme. The APC scheme based on $P - V$ droop control is only activated when RPA scheme reaches the reactive power capacity and voltage at the connection point, V_i of PV system i^2 exceeds the threshold voltage level of V_i^{tP} . The injected active power, P_i^{net} and absorbed reactive power, Q_i^{net} are regulated following linear functions depicted by Eq. (4.3), and Eq. (4.5), respectively. The method disconnects the PV unit when the voltage at the connection point exceeds the maximum allowable limit, which is typically set at 1.1 p.u. in the distribution network.

²In this study, it is assumed that the PV system i is connected to the bus i of the distribution network.

Deficient employment of PV reactive power capability

Applying the SDC mechanism with the same, static threshold values in voltage rise conditions causes the deficient employment of reactive power capability of PV inverters. Fig. 5.2 shows the SDC mechanism applied to two PV units in a radial LV feeder: PV a at the beginning and PV b at the end. These two units are assumed to have the same installed capacity and expose to the same solar irradiation. Because of the radial characteristic, voltage level V_a of PV a is lower than voltage level V_b of PV b . Consequently, the inverter b absorbs increased amount of reactive power, while the inverter a has no absorption. This can be regarded as an improper utilisation of PV reactive power capability to the voltage regulation, which necessities developing a coordination control for enhancing the contribution of PV systems during voltage rise conditions.

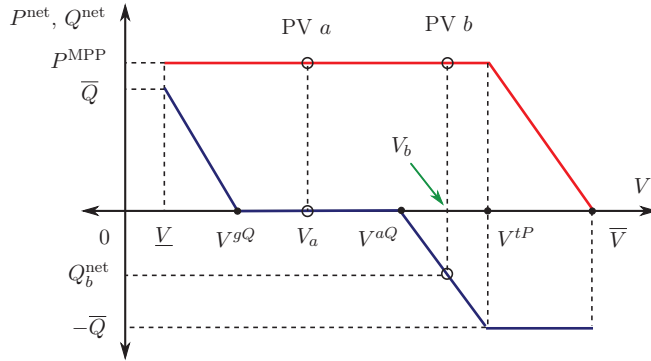


Figure 5.2: SDC mechanism applied for two PV inverters in different locations of a radial LV feeder.

5.2.2 Centralised control algorithm

The deficient employment of PV reactive power capability can be solved by using the centralised control. Unlike the local control, the centralised control is performed only by a single device, so-called a central controller (as described in Chapter 2), in discrete time steps. In this chapter, the centralised control algorithm is developed with a view of coordinating the reactive and active power control of PV inverters while dealing with the voltage rise. Curtailments of active power outputs of PV systems are undesirable due to the loss of PV energy harvest. Absorption of reactive power from the network by PV inverters, on the other hand, can lower the voltage levels at the POCs, then lowering the curtailed volume of PV active power. Thus, the overall objective of the centralised control can be formulated as maximizing active power injection and reactive power absorption by PV inverters while maintaining

the voltage levels at all the POCs within the allowable range. This can be expressed by an optimisation problem as follows,

$$\min \sum_{i \in N, i=1}^N ((P_i^{\text{MPP}} - P_i^*) + (\bar{Q}_i - Q_i^*)) \quad (5.1)$$

where P_i^* and Q_i^* are the decision variables, which refers to active and reactive power outputs, respectively, of the PV unit i ,

subject to,

$$0 \leq P_i^* \leq P_i^{\text{MPP}} \quad (5.2)$$

$$0 \leq Q_i^* \leq \bar{Q}_i \quad (5.3)$$

$$\underline{V} \leq V_i \leq \bar{V} \quad (5.4)$$

The function in Eq. (5.1) is a linear optimisation problem; subsequently, this problem can be solved by Linear Programming technique. Moreover, Eq. (5.2) - (5.4) depicts the constraints, i.e., all inequality, of the defined optimisation problem. The constraints in Eq. (5.2) and Eq. (5.3) dictate that PV power outputs can not exceed the system capacity. On the other hand, the constraint described by Eq. (5.4) maintains the voltage levels at all the POCs within the allowable range. To solve the optimisation problem, the reformulation of the constraint of V_i to be the form of P_i^* and Q_i^* is vital. This reformulation necessitates finding the correlation between V_i , and P_i^* and Q_i^* .

Correlation between bus voltage and power injection

The variation in the bus voltage correlates in principle with the power injection behaviour at each of buses, in which the correlation can be determined using the concept of Jacobian matrix. The Jacobian matrix \mathbf{J} represents the linearised relationship between changes in active and reactive powers injection at bus (i.e., ΔP and ΔQ) with changes in bus voltage magnitude and angle (i.e., ΔV and $\Delta \delta$), as expressed in Eq. (5.5) [166],

$$\begin{bmatrix} \Delta \mathbf{P} \\ \Delta \mathbf{Q} \end{bmatrix} = \begin{bmatrix} \mathbf{J}_{P\delta} & \mathbf{J}_{PV} \\ \mathbf{J}_{Q\delta} & \mathbf{J}_{QV} \end{bmatrix} \begin{bmatrix} \Delta \boldsymbol{\delta} \\ \Delta \mathbf{V} \end{bmatrix} \quad (5.5)$$

where $\Delta \mathbf{P} = [\Delta P_1, \dots, \Delta P_i, \dots, \Delta P_N]^T$, $\Delta \mathbf{Q} = [\Delta Q_1, \dots, \Delta Q_i, \dots, \Delta Q_N]^T$, $\Delta \mathbf{V} = [\Delta V_1, \dots, \Delta V_i, \dots, \Delta V_N]^T$, $\Delta \boldsymbol{\delta} = [\Delta \delta_1, \dots, \Delta \delta_i, \dots, \Delta \delta_N]^T$ are the vectors of ΔP , ΔQ , ΔV , and $\Delta \delta$, respectively, and N denotes the set of buses in the network. The Jacobian matrix \mathbf{J} can be obtained by solving the nonlinear load flow using Newton-Raphson algorithm [166].

Based on Eq. (5.5), the effect of each of $\Delta \mathbf{P}$ and $\Delta \mathbf{Q}$ on $\Delta \mathbf{V}$ can be separately defined, by assuming that the remaining one approximates zero, as shown in Eq. (5.6) and Eq. (5.7), respectively.

$$\Delta \mathbf{V}^P = [\mathbf{J}_{PV} - \mathbf{J}_{P\delta} \mathbf{J}_{Q\delta}^{-1} \mathbf{J}_{QV}]^{-1} \cdot \Delta \mathbf{P} = \mathbf{S}^{VP} \cdot \Delta \mathbf{P} \quad (5.6)$$

$$\Delta \mathbf{V}^Q = [\mathbf{J}_{QV} - \mathbf{J}_{Q\delta} \mathbf{J}_{P\delta}^{-1} \mathbf{J}_{PV}]^{-1} \cdot \Delta \mathbf{Q} = \mathbf{S}^{VQ} \cdot \Delta \mathbf{Q} \quad (5.7)$$

where \mathbf{S}^{VP} is denoted as the voltage/active power sensitivity matrix and \mathbf{S}^{VQ} as the voltage/reactive power sensitivity matrix. As a result, $\Delta \mathbf{V}$ due to both $\Delta \mathbf{P}$ and $\Delta \mathbf{Q}$ is given by,

$$\Delta \mathbf{V} = \mathbf{S}^{VP} \cdot \Delta \mathbf{P} + \mathbf{S}^{VQ} \cdot \Delta \mathbf{Q} \quad (5.8)$$

The sensitivity matrix \mathbf{S}^{VP} and \mathbf{S}^{VQ} are similar in size of $N \times N$, in which its element, e.g., S_{ij}^{VP} or S_{ij}^{VQ} , quantifies the linear relation between voltage magnitude change at bus i and power injection change at bus j , $\forall i, j \in N$. The change in voltage magnitude at bus i , therefore, can be calculated by,

$$\Delta V_i = \sum_{j \in N, j=1}^N (S_{ij}^{VP} \times \Delta P_j + S_{ij}^{VQ} \times \Delta Q_j) \quad \forall i \in N \quad (5.9)$$

Gathering information on P , Q , V , and δ at all buses is requested for calculation of the sensitivity matrix \mathbf{S}^{VP} and \mathbf{S}^{VQ} . This information gathering heavily depends on the ICT infrastructure and the monitoring capability in the network. For application of the proposal central control, it is assumed that the considered network in this chapter is equipped with strong ICT infrastructure and monitoring systems, e.g. by using smart meters, as well as bi-directional communication links.

It is worth to note that power injection at a bus is given by,

$$P = P^{PV} - P^{\text{Load}} \quad (5.10)$$

$$Q = Q^{PV} - Q^{\text{Load}} \quad (5.11)$$

where P^{PV} and Q^{PV} denote power generation from PV unit, P^{Load} and Q^{Load} denote power consumption of loads at the same bus. Since demand response solutions are excluded from the proposed approach and P^{Load} is assumed to be retained within the time interval of the

optimisation process, power injection change at a bus can be simplified as,

$$\Delta P = P^* - P^{\text{PV}} \quad (5.12)$$

$$\Delta Q = Q^* - Q^{\text{PV}} \quad (5.13)$$

Hence, Eq. (5.5) - (5.13) enable the reformulation of the constraint of V_i in Eq. (5.4) to be the form of P_i^* and Q_i^* . This, subsequently, allows the constraint in Eq. (5.4) to be properly considered while solving the optimisation function in Eq. (5.1).

5.2.3 Integration of local control and centralised control

As discussed earlier, the local control and centralised control algorithms are executed in different time steps by different controllers (e.g., the PV inverters and the central controller). Thus, a complete integration of these two control algorithms is essential to actualising the proposed coordination approach. As illustrated in Fig. 5.3, the local control is integrated with the centralised control, which is activated in each Δt time interval. For the sake of explanation, the integration of these two control mechanisms is classified into 4 stages, as visualised in Fig. 5.4.

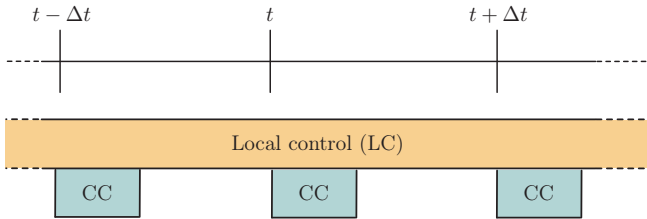


Figure 5.3: Integration of local control (LC) and centralised control (CC) (adjusted from [167]).

Stage 1 - Verification of PV active power curtailment due to voltage rise

For each time step Δt , the centralised control collects measurements ($V_i, P_i^{\text{PV}}, Q_i^{\text{PV}} \forall i \in N$) from all PV units in the network. If voltage rise occurs (i.e., V_i exceeds V_i^{tP}), that leads to active power curtailment for any PV inverters, the following stages will be executed.

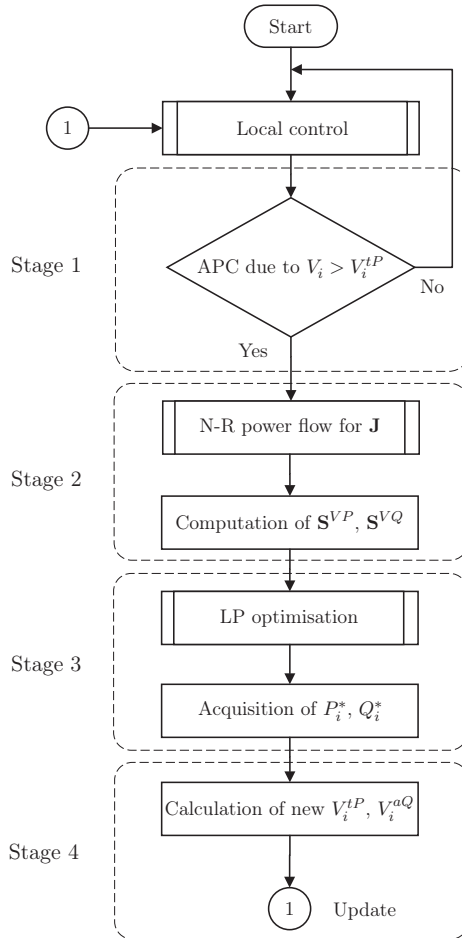


Figure 5.4: Methodology for integrating local control and centralised control. APC depicts active power curtailment of PV inverters. N-R denotes Newton-Raphson algorithm. LP represents Linear Programming technique.

Stage 2 - Computation of the voltage/power sensitivity matrix

In addition to PV operational data, the centralised control also receives measured data (P^{Load} , Q^{Load} , V , δ) from all loads, as discussed in Sec. 5.2.2. Applying these data to Eq. (5.5) - (5.7) along with the method as described in Sec. 5.2.2 yields the voltage/active power sensitivity matrix \mathbf{S}^{VP} and the voltage/reactive power sensitivity matrix \mathbf{S}^{VQ} .

Stage 3 - Solving the optimisation problem of PV power outputs

By using all received data and the computed voltage/power sensitivity matrix from the early stages, in this stage the centralised control aims to solve the optimisation problem expressed by Eq. (5.1) - (5.4). To this end, the functions in Eq. (5.8) - (5.13) and the Linear Programming technique are adopted, as discussed in Sec. 5.2.2. When the problem-solving is complete, the optimal values of PV active and reactive power, P^* and Q^* are determined for all the inverters. As the centralised control algorithm is executed every Δt time interval, the determined P_i^* and $Q_i^* \forall i \in N$ will be retained for the corresponding time interval.

Stage 4 - Calculation of new local control parameters

Based on the optimal power P_i^* and $Q_i^* \forall i \in N$ obtained from Stage 3, new droop control parameters (i.e., $(V_i^{tP}, V_i^{aQ} \forall i \in N)$ for each related PV unit can thus be calculated by the centralised control as shown in Eq. (5.14) and Eq. (5.15).

$$V_i^{tP*} = \frac{P_i^{\text{MPP}} \cdot V_i + (P_i^* - P^{\text{MPP}}) \cdot \bar{V}}{P_i^*} \quad \forall i \in N \quad (5.14)$$

$$V_i^{aQ*} = \frac{Q_i^* \cdot \bar{V} - \bar{Q}_i \cdot V_i}{Q_i^* - \bar{Q}_i} \quad \forall i \in N \quad (5.15)$$

These two equations are derived by modifying the droop control functions, which are earlier presented in Eq. (4.3) and Eq. (4.5). The local control in the inverters are subsequently updated with the new values of V_i^{tP} and V_i^{aQ} . Similar to P_i^* and Q_i^* , the new local control parameters also remain constant until next time steps. The whole procedure from Stage 1 to Stage 4 will repeats after every Δt time period.

5.3 Simulation setup

5.3.1 Case study

A simulation case study based on a residential Dutch LV network adopted from [22] is used to evaluate the efficacy of the proposed approach. As illustrated in Fig. 5.5, the test network consists of a MV/LV distribution transformer and 20 households with PV systems. The main properties of the transformer are shown in Table 5.1. All the power lines in the test network are underground cables with relatively high R/X ratio compared to the overhead lines. The

R , X characteristics of the underground cables are summarized in Table 5.2, which are based on [168].

Table 5.1: Properties of the MV/LV transformer used in the test network

Properties	Values
Transformer rating	100 kVA, 11/0.4 kV
Winding connection	D1Yg
Transformer full-load loss	1.4 kW
Transformer no-load loss	0.19 kW

Table 5.2: R , X characteristics of the power cables of the test network

Cable types	R (Ω/km)	X (Ω/km)	R/X
150 mm ² Al	0.228	0.0844	2.70
95 mm ² Al	0.353	0.0868	4.07
50 mm ² Al	0.706	0.0924	7.64
16 mm ² Al	2.10	0.106	19.81
10 mm ² Cu	1.837	0.088	20.88
6 mm ² Cu	3.061	0.1	30.61

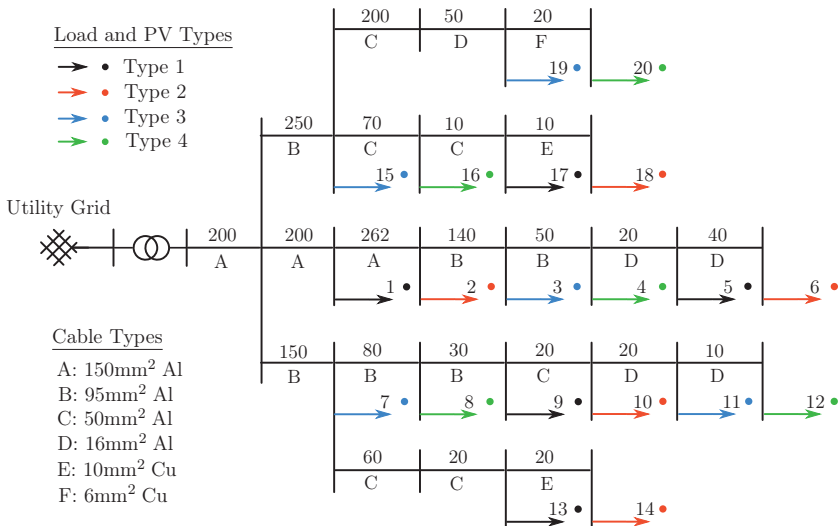


Figure 5.5: The test network based on a Dutch LV distribution network. The arrows and solid circles represent loads and PV units, respectively, along with their index. The numerical values along the power cable sections denote the cable length in meters, while the uppercase letters denote the cable types.

Each household is assumed to connect to the test network via a three-phase connection and be equipped with either of four types of uncontrollable residential loads and PV installed capacity. The main properties of these four types are tabulated in Table 5.3. The household load profiles are modelled using average normalized profiles of 400 residential customers in the Netherlands, which are derived from smart meters with 15-minute resolutions [22]. The meteorological data of the solar irradiation and the ambient temperature, which is obtained from the KNMI [129], is adopted to simulate PV power generation. Using the meteorological data, the amount of active power generated by PV systems has been modeled according to Eq. (3.2). Fig. 5.6 displays the solar irradiation and ambient temperature profiles used in the simulation. As the test network covers a small geographical area, all PV systems are assumed to expose to the same meteorological data profiles. Allowable power factor (PF) values of PV systems are considered to be ± 0.9 according to the Standard EN 50438 [160].

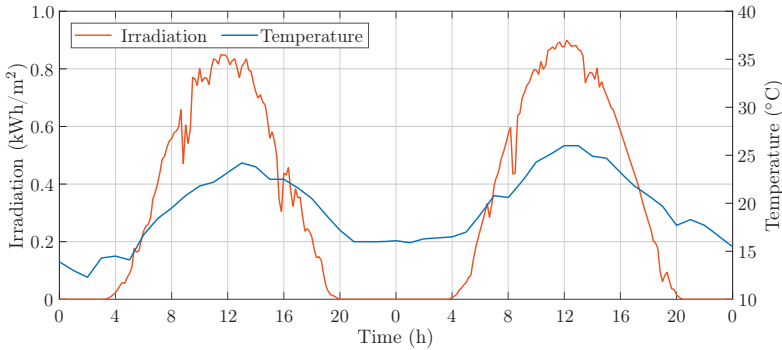


Figure 5.6: Solar irradiation and ambient temperature profiles used in the simulation.

Table 5.3: Properties of household loads and PV systems

Properties	Type 1	Type 2	Type 3	Type 4
Load demand range (kW)	0.54-2.37	0.94-3.67	0.64-2.7	0.68-2.53
PF of load demand (-)	0.98	0.98	0.98	0.98
Installed PV capacity (kWp)	5.62	6.37	6.75	7.12
Allowable PF of PV systems (-)	± 0.9	± 0.9	± 0.9	± 0.9

5.3.2 Simulation platform

The simulation case study is developed using Matlab/Simulink. In this environment, an advanced model with hierarchical control is required. The simulated model must be capable of implementing the SDC-based local voltage control, i.e., with 1-second resolution, and the centralised coordination control, i.e., with 15-minute resolution, according to the

integration framework as discussed in Sec. 5.2. The proposed optimisation problem for the centralised coordination control is solved using the MATLAB optimisation toolbox. The simulation is performed over two consecutive summer days and includes 3 control methods as follows,

- **Method 1:** This method utilises the $P - V$ droop control-based APC scheme (discussed in Chapter 4) for the local control at PV inverters and the centralised coordination control (mentioned in Sec. 5.2.1) for regulating PV systems in response to voltage rise issues. For this, the coordination control regularly updates the threshold value of the $P - V$ droop control.
- **Method 2:** This method purely employs the local voltage control based on the SDC mechanism (discussed in Sec. 5.2.1) to solve the voltage rise problems. The centralised coordination control is not considered, meaning that the threshold values of the SDC mechanism are fixed over simulation time.
- **Method 3:** This is the proposed approach, which integrates both the SDC-based local voltage control and the centralised coordination control for voltage rise mitigation. The threshold values for both $Q - V$ and $P - V$ droop control scheme, i.e., of the SDC mechanism, are periodically modified by the coordination control.

For the sake of comparison between the control approaches, the threshold value for $P - V$ droop control, i.e., $V_i^{tP} = 1.06$ p.u., are set identically to all PV inverters in Method 1 and 3 as the default setting, and in Method 2 as the fixed setting. Similarly, the threshold value for $Q - V$ droop control, i.e., $V_i^{aQ} = 1.05$ p.u., is set uniformly to every PV inverters in Method 3 as a default setting, and in Method 2 as the fixed setting. In this study, the default settings refer to the values assigned to the droop control parameters when the PV systems are not operational (e.g., during the night time) or no voltage rise is observed in the network.

5.4 Numerical results

5.4.1 Voltage control

Voltage levels measured at the POCs of all the houses in the test network during the simulated two days without any control algorithm are depicted in Fig. 5.7. Due to the radial topology, voltage levels in the network increase along the feeders. High voltage magnitudes are observed at the household POCs located to the end of the feeders, such as House index 6, 12 and 20. Meanwhile, the houses located closer to the transformer have lower voltage. The voltage control methods, listed in Sec. 5.3.1, are then applied for the test network.

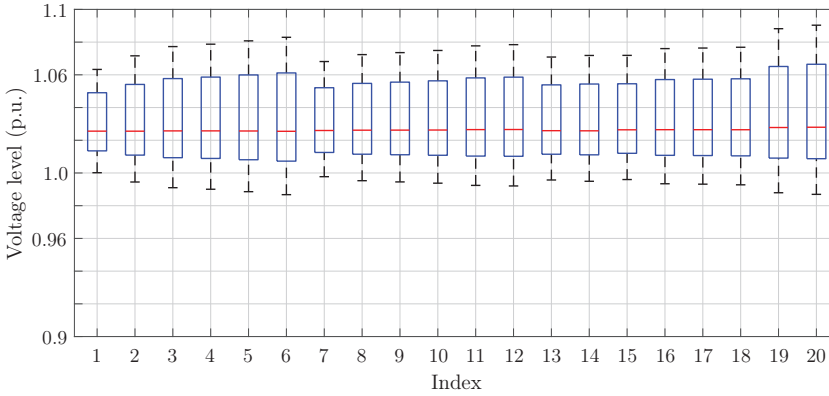


Figure 5.7: Measured voltage levels at the POCs of all the houses during the simulated two days without any control algorithms. Each index represents the corresponding individual house.

Fig. 5.8 displays the PDF and ECDF of voltage magnitudes in the network for 3 control methods over the simulated two days. This figure indicates that the voltage levels considerably increase (i.e., nearly 1.1 p.u.) without control and decrease for 3 methods. It is observed from the ECDF plot that the significant difference between Method 1 and each of the two methods, i.e., Method 2 and 3, occurs when the voltage magnitudes exceed the threshold of 1.05 p.u. This is due to the use of $Q - V$ droop control scheme, i.e., $V_i^{aQ} = 1.05$ p.u., for both Method 2 and 3, which combines with $P - V$ droop control scheme and results in a slower voltage rise. Owing to $P - V$ droop control scheme, Method 1 induces faster voltage rise than Method 2 and 3, although the centralised coordination control is employed. On the other hand, the PDF plot reveals that Method 2 appears to be slightly more conservative than Method 3. In Method 2, the probability density of the voltage levels equal to 1.06 is 23.03; while in Method 3 those quantities correspond to 19.48. Moreover, the maximum voltage in Method 2 is lowered than that in Method 3. This is derived from the adoption of the SDC mechanism with fixed settings for the local voltage control in Method 2.

Main results for 3 control methods, including maximum network voltage, total produced energy of PV systems, and total energy losses in the network, are listed in Table. 5.4. It is evident that Method 3 effectively limits the voltage rise and enables the highest amount of total energy generated from PV systems. This benefit of Method 3 comes from the combination of the SDC-based local voltage control and the centralised coordination control with optimisation objective of minimum PV power curtailment. In contrast, Method 1 has the lowest PV production value, although the maximum voltage is maintained below the allowable upper limit of 1.1 p.u. This is due to the fact that the voltage rise mitigation involves only curtailing active power of PV units, i.e., by activating $P - V$ droop control. The

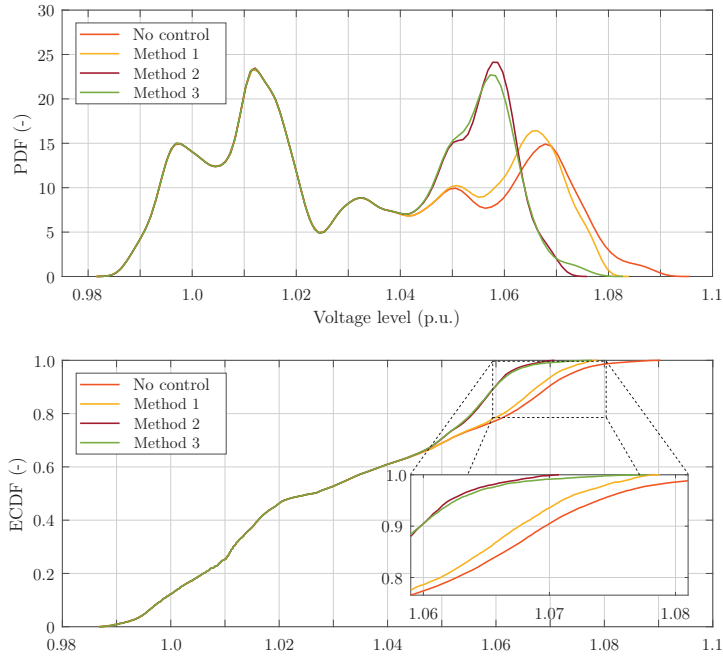


Figure 5.8: PDF and ECDF of the voltage levels for different control methods.

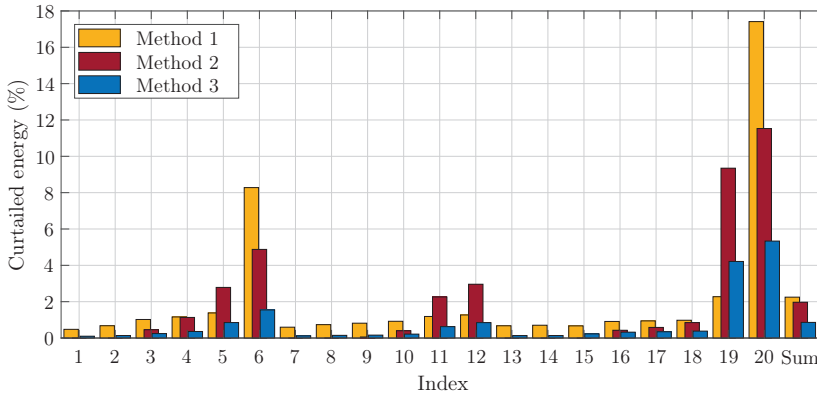
reactive power capacities of PV units, which can support the voltage rise mitigation, are left unused for Method 1. Nevertheless, the decreased active power production and unused reactive power absorption of PV systems reduces the power flows in the network, which in turns decreases the energy losses. Among 3 methods, Method 3 has the largest amount of total energy losses for the simulated two days (i.e., 80.46 kWh, representing 29.4% higher than Method 1). Unlike Method 1, Method 3 provokes the increased power flows in the network, caused by the limited active power curtailment and maximized reactive power absorption of PV units. For Method 2, the reactive power capacities of PV inverters are dispatched (i.e., by the SDC-based local control) but not maximized due to a lack of the the centralised coordination control. The total energy loss in the network for Method 2, consequently, is higher than that for Method 1 and smaller than that for Method 3. Since the voltage rise issues are effectively mitigated with all 3 control methods, evaluating other performance metrics is important to compare the methods further, which will be discussed in the next section.

Table 5.4: Results summary for all control methods

Properties	Method 1	Method 2	Method 3
Maximum network voltage level (p.u.)	1.0787	1.0708	1.0777
Total energy generated from PV systems (kWh)	2148.8	2155.0	2179.3
Total energy losses in the network (kWh)	62.15	75.33	80.46

5.4.2 Control of PV generation

In this section, the control of PV generation with 3 control methods is evaluated for further comparison of these methods. To this end, the curtailed energy generation of every PV inverters with different control methods are calculated as a percentage of the generated PV energy (kWh) in the case with no control. As depicted in Fig. 5.9, Method 3 (i.e., the proposed approach) outperforms all other ones as Method 3 leads to the smallest amount of total curtailed PV energy of 0.86%, decreasing by 56.3% and 61.8% compared to Method 1 and 2, respectively. This achievement demonstrates the effectiveness of combining the local control (based on SDC mechanism) and the centralised coordination control (based on the optimisation) to effectively reduce the PV generation curtailment when properly solving the voltage rise problems. Applying only either of each control approach as in Method 1 and Method 2 induces the increased amount of PV generation curtailments.

**Figure 5.9:** Percentage of curtailed energy of PV systems.

To verify the performance of Method 3 in terms of coordinating PV inverters, Fig. 5.10 shows the adaptation of the $P - V$ droop control parameters (V^{tP}) of PV inverter at House no. 1 and 6, which are located in the same feeder. As discussed in Sec. 5.2, such adaptation of the local control is steered by the centralised coordination control as the former is regularly updated with new set-points from the latter. As can be seen from Fig. 5.10, V_6^{tP} increases,

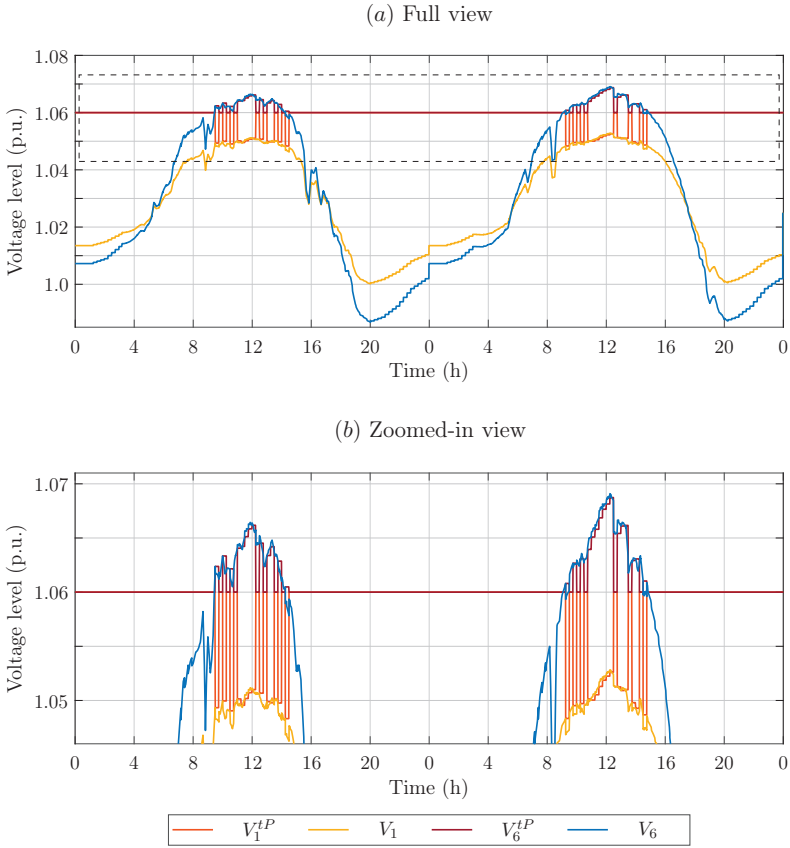


Figure 5.10: (a) Full view and (b) Zoomed-in view for the profiles of the measured voltage (V_i) and the adaptation of the droop control parameters (V_i^{tP}) of PV unit no. 1 and 6 when operating with Method 3. The dashed-line rectangular in Fig. (a) indicates the region of the zoomed-in view shown in Fig. (b).

while V_1^{tP} decreases during voltage rise conditions (i.e., above 1.06 p.u.). Subsequently, PV inverter no. 6 (i.e., located at the end of the feeder), curtail lower amount of PV generation when compared to the control scheme with the static V_i^{tP} , i.e., in Method 2 (as shown in Fig. 5.9). Simultaneously, PV inverter no. 1 located at the beginning of the same feeder (where voltage rise above 1.06 p.u. does not exist) starts absorbing reactive power (i.e., when $V_i^{aQ} < V_i \leq V_i^{tP}$) and reaches the maximum reactive power output (i.e., when $V_i > V_i^{tP}$) faster than that with the static V_i^{aQ} , i.e., in Method 2. The adaptation of

the droop control parameters allows to maximize utilisation of PV inverter reactive power capacity and decrease their active power curtailment for voltage rise alleviation. Hence, these results prove the adequate performance of the proposed coordination control to adapt the droop control parameters.

However, similar to Method 1 and 2, the proposed control strategy in Method 3 causes the unfair curtailment among the PV units as the ones connecting to the end of the feeder (e.g., PV unit no. 6, 12, and 20) curtail noticeably more active power than the others. An improvement for the centralised coordination control or an alternative approach is required to achieve a fair curtailment.

5.4.3 Summary

The centralised control has been studied widely to coordinate PV inverters as well as other power network components to achieve the optimal operation of the system. In this chapter, the development of the centralised control to coordinate PV inverters for voltage rise mitigation has been discussed. For this proposed control approach, the local control and centralised control algorithms are used and integrated following the hierarchical control architecture. The local control algorithm adopts the sequential $Q - V$ and $P - V$ droop control scheme discussed in Chapter 4. This droop-based local control is embedded in each inverter for continuously monitoring and addressing voltage rise problems. Meanwhile, the centralised control algorithm is executed by a central controller aiming to optimally steer the local control performance in terms of PV power outputs. To this end, the centralised control is equipped with the linear programming technique, that can solve the optimisation problems of PV power outputs.

A simulation case study considering a residential Dutch LV network with a real data set for household consumption and PV generation from the Netherlands has been conducted to evaluate the efficacy of the proposed approach. Two other control approaches have been also involved in the case study for the approach comparison. Simulation results show the effectiveness of the proposed control approach to mitigates the voltage rise problems and considerably decrease the total curtailed energy from PV systems, i.e., by 56.3% and 61.8% compared to the method including $P - V$ droop control and the centralised control, and the sequential droop control, respectively. This achievement derives from the combination of the local control (based on SDC mechanism) and the centralised coordination control (based on the optimisation). However, the benefits of the proposed method comes at the expense of increased total energy loss in the network and the unfair power curtailment among the PV systems. An improvement for the centralised coordination control or an alternative approach is recommended to achieve a fair PV power curtailment for voltage rise mitigation.

The proposed control approach uses extensive communications between the centralised controller and individual PV units without communication delay. However, communication

delays are inevitable, negatively impacting the real-time coordination control performance. Therefore, investigating such impact of communication delays on the proposed control performance can be a recommendation for future research.

6

Distributed control for voltage regulation

*In this chapter, a distributed coordination control strategy is proposed that adapts sequential ($Q - V$ and $P - V$) droop control for PV inverters to mitigate voltage rise problems in PV-rich LV distribution networks. The consensus algorithm is used to realise the distributed control, while the ε -decomposition technique is adopted to identify multiple control areas with the strong coupling nature of PV systems in order to facilitate the coordination of sequential droop control of PV inverters. The droop control parameters are tuned and adapted, based on a consensus among PV inverters within each control area. This proposed control strategy inherits the autonomous feature of the droop control for coping with voltage rise issues while avoiding curtailing a significant amount of PV production. The proposed control strategy is evaluated through simulations on a real European LV distribution network with high PV penetration. The simulation results highlight that the proposed control strategy can effectively mitigate voltage rise problems while significantly reducing the amount of curtailed PV generation and ensuring the effective contribution among all the PV systems towards voltage rise mitigation.*¹

¹This chapter is based on [169, 170].

6.1 Introduction

Voltage rise in LV distribution networks is one of the foremost issues associated with the high integration of residential-scale PV systems in LV networks [164]. Voltage rise problems occur along the distribution feeders due to the reverse power flows when the power generation of the feeder is higher than its power demand. Lack of proper solutions to this problem can result in loss of energy yields of PV systems [152] as well as causes damages to the electrical appliances. This problem can become a major limiting factor for further PV deployment [165]. As discussed earlier, controlling PV systems is of importance to address the voltage rise problems. With this respect, coordination control of PV systems can assist a proper utilisation of PV inverter capacity, i.e., in terms of active and reactive power outputs, for voltage rise alleviation.

While the centralised coordination control can effectively alleviate voltage rise problems with minimised PV power curtailment, as shown in Chapter 5, such centralised approach heavily depends upon extensive high-bandwidth communication networks along with a large number of interconnected devices making the system vulnerable to a single-point-of-failure and costly to be deployed [171]. In contrast, distributed control uses a sparse communication network with a significantly low bandwidth requirement, enabling this type of control architecture to be less costly and less complex. Considering the widespread integration of residential-scale PV units, distributed control is potentially practical to replace the centralised control.

In this chapter, a distributed coordination control strategy is proposed for PV inverters in combination with the ε -decomposition technique to alleviate voltage rise problems in PV-rich LV distribution networks. The proposed strategy makes use of a distributed coordination scheme based on the consensus algorithm to adapt the sequential ($Q - V$ and $P - V$) droop control of PV inverters, as discussed in Chapter 4. Additionally, the ε -decomposition technique is utilised to decompose the network into multiple control areas. The proposed strategy is, thus, implemented for PV units located in the same control area. The control objectives are to reduce the amount of curtailed generation and guarantee the effective contribution of all PV systems, while alleviating voltage rise problems. Compared to the centralised coordination control studied in Chapter 5, this chapter aims to obtain a reduced amount of required PV power reduction compared to the cases with the conventional, i.e, uncoordinated, droop control schemes and the adaptive active power droop control method for adequately solving the voltage rise problems, instead of obtaining an optimal minimum power curtailment. The variation in the impact of PV generation on voltage regulation is analysed first. Next, the proposed control strategy is presented along with the ε -decomposition technique. The related modelling and simulation on a real European LV distribution network with high PV penetration are then described. Finally, results and discussion presenting the efficacy of the proposed control strategy are given and concluding remarks are drawn.

6.2 Impact of PV generation on voltage regulation

The variation in the impact of active and reactive power injection from PV inverters on phasor bus voltages and voltage angle varies depending on the bus location, which can be observed by applying the concept of voltage sensitivity matrix. The voltage sensitivity matrix \mathbf{S} is derived by reversing the system Jacobian matrix \mathbf{J} , which is resulted from solving the nonlinear load flow using Newton-Raphson algorithm [166]. The matrix \mathbf{S} is given by,

$$\begin{bmatrix} \Delta\delta \\ \Delta\mathbf{V} \end{bmatrix} = \begin{bmatrix} \mathbf{S}_{\delta P} & \mathbf{S}_{\delta Q} \\ \mathbf{S}_{VP} & \mathbf{S}_{VQ} \end{bmatrix} \begin{bmatrix} \Delta\mathbf{P} \\ \Delta\mathbf{Q} \end{bmatrix} \quad (6.1)$$

where $\mathbf{S} = \mathbf{J}^{-1}$ and δ , V , P , and Q denote voltage angle, phasor bus voltage, active power and reactive power injection, respectively. $\Delta\mathbf{P}$, $\Delta\mathbf{Q}$, $\Delta\mathbf{V}$, and $\Delta\delta$ depict the changes of δ , V , P , and Q , respectively. The matrix \mathbf{S} changes with the power flow in the network and calculating \mathbf{S} requires to gather information about δ , V , P , and Q at all buses. This, therefore, makes the calculation of \mathbf{S} in an on-line manner highly demanding.

Owing to the radial feature, the critical voltage rise in the LV networks due to the surplus PV power generation predominantly occurs at the bus located at the end of the feeder. According to [172], in a radial LV feeder the voltage sensitivity at the critical bus to active power and reactive power injection from PV systems both increase as the distance to the transformer increases along the feeder. Then, controlling active power and reactive power injection from PV systems connected to the buses with the higher impact sensitivity becomes more effective on voltage rise mitigation. It is, therefore, necessary to group PV systems with strong coupling nature, e.g., voltage sensitivity, for solving the voltage violation problems.

6.3 Proposed control strategy

The proposed control strategy aims to mitigate voltage rise along the feeder while significantly reducing the amount of curtailed PV generation. To this end, the ε -decomposition technique is utilized to decompose the network into multiple control areas containing groups of PV systems. The distributed coordination control strategy is then applied in the decomposed control areas to alleviate voltage rise issues.

Fig. 6.1 presents the block diagram of the proposed control strategy, which is embedded in each PV inverter, consisting of two layers: a local control and a coordination control layer. The former is based on the SDC mechanism, and the latter is based on a consensus-based distributed control (CBDC) mechanism. The local control layer is responsible for continuously monitoring and mitigating voltage rise conditions at the POC by regulating

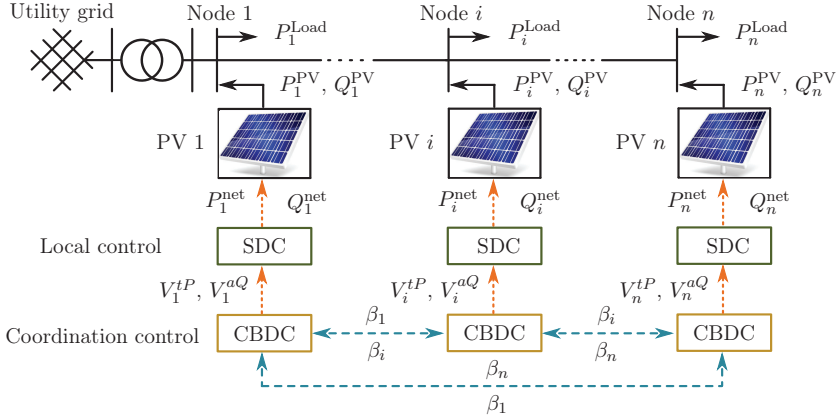


Figure 6.1: Block diagram of a LV distribution network with the proposed control strategy, composed of two control levels: a local control, implemented using SDC; and a coordination control, implemented using CBDC. The orange dotted and blue dashed lines represent the control signals and information exchange, respectively.

active and reactive power of PV units. The coordination control layer, which operates with a lower response speed than the local control layer, is responsible for adequately coordinating PV systems for the voltage level violations by periodically adapting the local control layer. As can be seen in Fig. 6.1, the output power set points of the PV inverters (P^{net} , Q^{net}) are determined by the local control layer, which regulates the APC and RPA scheme of PV units in response to the voltage rise at the POC. Furthermore, the $P-V$ and $Q-V$ droop control parameters, i.e., the threshold levels (V^{tP} and V^{aQ}), are periodically set by the coordination control layer. The operation of this coordination control layer, therefore, can be regarded as a correction process to the local control layer in order to obtain the fair generation curtailment. To complete this process, the coordination control layer first exchanges the PV active power injection ratios (β) between neighboring PV inverters, then reaches the common agreement of β in an iterative manner. The proposed control strategy is discussed next in more detail.

6.3.1 ε -Decomposition technique

In order to determine various control areas for the proposed control strategy, the decomposition of the network is done such that, the decomposed network consists of a series of sub-networks. Consider the fact that the voltage rise is a local problem, grouping these buses into sub-networks, monitoring and solving the sub-networks independently appear promising [173]. Each sub-network bounds the coverage range of the communication network in this area. Given this boundary, the coordination mechanism can be executed among PV

systems located in the same control area.

The ε -decomposition technique is identified by the graph theory. In this technique, a value of ε is pre-defined with $0 < \varepsilon < 1$, which is regarded as a threshold of the interconnection strength among sub-areas. Let us assume a graph $\mathcal{G} = (\mathcal{V}, \xi)$ with the set of vertices \mathcal{V} (i.e., PV units) and the set of edges ξ (i.e., communication links between PV units). If there exists an edge between neighboring sub-graphs that is smaller than the threshold value of ε , such edge is specified as a weak connection of the graph [173]. This link, accordingly, will be disconnected from the graph and a series of sub-graphs will be identified. By mapping this decomposed graph to the original network, the decomposition of a network is attained with mutual coupling among sub-network not greater than a given ε value [174]. A different series of decomposed sub-systems can be generated by varying ε value as it decides the sub-system size [173].

More specifically, our study involves using $n \times n$ admittance matrix, \mathbf{Y} for the implementation of the ε -decomposition method. The basic principle is to associate a graph \mathcal{G} with the matrix \mathbf{Y} , identify the edges $(\mathcal{V}_i, \mathcal{V}_j) \subset \xi$ with magnitude smaller than or equal to a prescribed positive value of ε . Decomposed matrix $\bar{\mathbf{Y}}$ of original matrix \mathbf{Y} is achievable if a permutation matrix \mathbf{P} exists such that Eq. (6.2) is satisfied.

$$\bar{\mathbf{Y}} = \mathbf{P}^T \mathbf{Y} \mathbf{P} \quad (6.2)$$

where $\bar{\mathbf{Y}}$ is assumed as an $M \times M$ block matrix with $M_p \times M_q$ blocks $\bar{\mathbf{Y}}_{pq} = (\bar{y}_{ij}^{pq})$ given by Eq. (6.3). \mathbf{P} can be identified equivalently to dividing the graph \mathcal{G} associated with \mathbf{Y} into M sub-graphs in the manner that the coupling magnitude of these sub-graphs in \mathcal{G} less than ε [173].

$$|\bar{y}_{ij}^{pq}| \leq \varepsilon \quad \forall p, q \in N, p \neq q, i \in N_p, j \in N_q \quad (6.3)$$

$\bar{\mathbf{Y}}$ can be conventionally represented as

$$\bar{\mathbf{Y}} = \bar{\mathbf{Y}}_0 + \varepsilon_1 \bar{\mathbf{Y}}_1 + \varepsilon_2 \bar{\mathbf{Y}}_2 + \cdots + \varepsilon_m \bar{\mathbf{Y}}_m \quad (6.4)$$

where $\bar{\mathbf{Y}}_0$ is a block diagonal matrix and $\bar{\mathbf{Y}}_1, \cdots, \bar{\mathbf{Y}}_m$ are decomposed matrices with all elements less than or equal to ε , and m is a series a prescribed positive value, ε satisfying $\varepsilon_1 > \varepsilon_2 > \cdots > \varepsilon_m$. A comprehensive description of the ε -decomposition approach can be founded in [173].

6.3.2 Local control layer

In the local control layer, the SDC mechanism, as discussed in Chapter 4 (Sec. 4.3.3), is implemented integrating $Q - V$ and $P - V$ droop control. It is worth mentioning that solar irradiance and PV module temperature are constantly changing in time, then the maximum power is also varying. Thus, to function $P - V$ droop control in PV inverter i , the inverter needs to be capable of effectively estimating P_i^{MPP} while operating at a curtailed active power output. Several maximum power point estimation (MPPE) methods for PV active power control have been proposed in [155, 175–177]. In fact, in [155], the PV inverter periodically switches to the MPPT mode performed by the inside MPPT algorithm for a certain time window, then recapturing the actual maximum power. However, the droop control function remains regularly deactivated and activated, making the power outputs largely fluctuated and then voltage rise problems not fully solved. An interesting alternative introduced in [175] utilizes irradiance and temperature measurements to extrapolate the datasheet information to actual PV module parameters, then fits a linear regression model to determine the polynomial function coefficients for MPPE. In [176, 177], a least-squares curve fitting model is built based on a dataset of voltage and current measured at the dc side to realize MPPE. These two latter MPPE methods allow the PV inverters to continuously estimate the maximum power and simultaneously function the active power curtailment. Since the sequential droop control parameters will be periodically modified in a real-time manner by the consensus-based distributed control as described in the next section, the MPPE approaches in [175–177] appear to be promising ones. Nevertheless, none of these approaches is incorporated in this chapter as it is assumed that the maximum power set-points are already provided by a MPPE method.

However, as discussed in Chapter 5, the main drawback of the sequential droop control is the improper use of reactive power capability as well as the unequal generation curtailment of PV systems during voltage rise conditions. In the radial LV feeders, PV units connected to the end of the feeder absorb significantly more reactive power and curtail more active power compared to other PV units. Hence, a coordinated mechanism for enhancing the contribution of PV systems to support voltage rise alleviation needs to be developed.

6.3.3 Coordination control layer

The improper utilization of PV inverter capability for voltage rise alleviation can be solved by the coordination control level, which is based on a CBDC mechanism. Consensus algorithms have been widely used as a basis for distributed control. Following this, each PV inverter communicates and shares its local information as the variable of interest with neighbours following a distributed procedure [74]. The goal of the consensus algorithm is to converge all PV inverters to a common agreement following an iterative manner. The variable of interest can be regarded as a quantity that is agreed by all PV inverters. The consensus

algorithm considers a graph $\mathcal{G} = (\mathcal{V}, \xi)$ which represents the communication topology of the PV units. The set of buses $\mathcal{V} = \{1, \dots, n\}$ describes the set of PV inverters, whereas the set of edges $\xi \subset \mathcal{V} \times \mathcal{V}$ describes the set of communication links between PV inverters. Define for the PV inverter i a variable of interest x_i and define $\mathcal{N}_i = \{j \in \mathcal{V} : (i, j) \in \xi\}$ as the set of adjacent PV inverters that communicate with it. Considering the discrete nature of information exchange, the first-order consensus algorithm can be adopted. The discovery law of a variable of interest x_i is then expressed as [74]

$$x_i[k+1] = x_i[k] + \sum_{j \in \mathcal{N}_i} d_{ij}(x_j[k] - x_i[k]) \quad \forall i \in \mathcal{V} \quad (6.5)$$

where k is the iteration counter and d_{ij} is the information weight factor between the unit i and the neighbor unit j .

From a system point of view, the discovery law in Eq. (6.5) can be expressed in a matrix-vector form as

$$\mathbf{X}[k+1] = \mathbf{D}\mathbf{X}[k] \quad (6.6)$$

where $\mathbf{X}[k] = [x_1[k], \dots, x_i[k], \dots, x_n[k]]^T$ and $\mathbf{X}[k+1]$ are the vectors of the discovered variables of interest at k and $k+1$ iterations, respectively, and \mathbf{D} is an information weighted matrix. As discussed in [91], if the values of \mathbf{D} 's elements are non-negative and the sums of \mathbf{D} 's rows and columns are all ones, the convergence of all PV inverters to a consensus will be reached at the average value of the variables of interest which can be expressed as

$$\lim_{k \rightarrow \infty} \mathbf{X}[k] = \lim_{k \rightarrow \infty} \mathbf{D}^k \mathbf{X}[0] = \frac{\mathbf{I} \cdot \mathbf{I}^T}{n} \mathbf{X}[0] \quad (6.7)$$

where $\mathbf{X}[0]$ is the initial value of \mathbf{X} and $\mathbf{I} = [1, 1, \dots, 1]^T$. Notice from Eq. (6.7) that the convergence speed of the variable discovery procedure is a function of \mathbf{D} [74]. Among various methods to define d_{ij} , the Metropolis method introduced in [178] is adopted in this work, given by

$$d_{ij} = \begin{cases} 1/[\max(n_i, n_j)], & \text{if } i \neq j \quad \forall j \in \mathcal{N}_i \\ 1 - \sum_{j \in \mathcal{N}_i} (1/[\max(n_i, n_j)]), & \text{if } i = j \\ 0. & \text{Otherwise} \end{cases} \quad (6.8)$$

where n_i and n_j represent the number of PV inverters that communicate with the PV inverter i and j , respectively. To enable the consensus algorithm to properly operate, a sparse communication network is then established. In this communication network, each PV unit exchanges its local measured data only to adjacent buses. Hence, neither a central controller

nor the extensive high-bandwidth communication network is required.

In the proposed CBDC mechanism, the PV active power injection ratio (β) is defined as the variable of interest, i.e., x in Eq. (6.5). Following this, β of each PV system is shared with the adjacent ones, given by

$$\beta_i[k] = P_i^{\text{net}}[k]/P_i^{\text{MPP}}[k] \quad \forall i \in \mathcal{V} \quad (6.9)$$

where P_i^{MPP} depicts the maximum power of the PV inverter determined by the local control as explained in Sec. 6.3.2.

Replacing x_i in Eq. (6.5) by β_i , all PV units will converge to the same power injection ratio illustrated by

$$\beta_1 = \beta_2 = \dots = \beta_n \quad (6.10)$$

As the consensus can only be reached when $k \rightarrow \infty$, this calls for an introduction of a stopping criterion by comparing the error at $k + 1$ iteration with the consensus convergence tolerance (τ) as [74]

$$\sum_{i \in \mathcal{V}} |\beta_i[k + 1] - \beta_i[k]| < \tau \quad \forall i \in \mathcal{V} \quad (6.11)$$

Having the updated value of β_i at $k + 1$ iteration, the coordination control level calculates the droop control parameter, i.e., $V_i^{tP}[k + 1]$, and then updates the sequential droop control at the local control level with such new value. To complete this modification, the following rule is proposed.

$$V_i^{tP}[k + 1] = \frac{V_i[k + 1] - (1 - \beta_i[k + 1])\bar{V}}{\beta_i[k + 1]} \quad (6.12)$$

That adaptation of the droop control parameters, subsequently, enables the local control to command the PV inverters to fully employ the reactive power absorbing capability and properly share the curtailed active power if needed with other PV inverters. It is important to highlight that the coordinated mechanism is performed by PV inverters bounded on the coverage range of the corresponding communication topology. If the communication topology is built for a specific group of PV inverters, only the PV inverters within this group will follow the coordination. In this sense, the proposed control strategy can be implemented in various control areas in parallel.

6.4 Modelling and simulation

6.4.1 LV distribution network

A real European LV distribution network is used as the test network to investigate the effectiveness of the proposed approach. As depicted in Fig. 6.2, this network is energized from a 125 kVA, 11/0.4 kV distribution transformer and supplies electricity to 39 households, of which 28 are assumed to be equipped with PV units. The network comprises underground power cables with R , X values being listed in Table 6.1. The cable properties are provided in [168].

Table 6.1: R , X values for the power cables of the test network

Cable types	R (Ω/km)	X (Ω/km)	R/X
240 mm ² Al	0.14	0.0818	1.71
150 mm ² Al	0.228	0.0844	2.70
95 mm ² Al	0.353	0.0868	4.07
50 mm ² Al	0.706	0.0924	7.64
35 mm ² Al	0.956	0.0982	9.74

6.4.2 Load profiles and PV system data

4 load profiles of residential households and 4 types of PV capacity are utilized. Table 6.2 exhibits the main properties of load profiles and PV systems. The household loads in the test network are all uncontrollable and derived from 15-minute measurements of real smart meters, as discussed in Chapter 5. The household load demands are in the ranges of 0.54 - 3.67 kW with a PF of 0.98. The installed PV capacities are of residential-scale, ranging between 5.25 and 6.65 kWp. The total installed PV capacity is 168.3 kWp, depicting a penetration level of about 150%, calculated as a ratio of total installed PV capacity to the maximum network load [179]. The input data for the PV systems, comprising the solar irradiation data and the ambient temperature data, are derived from real measurements. Due to the small geographical area of the test network, identical input data is used for all PV systems. For the compliance with the Standard EN 50438 [160], all PV inverters are assumed to operate within a PF of ± 0.9 .

6.4.3 Simulation platform

The simulation is performed in Matlab/Simulink with a time steps of 1 second and executed over two consecutive summer days. Since the proposed approach uses only changes in voltage

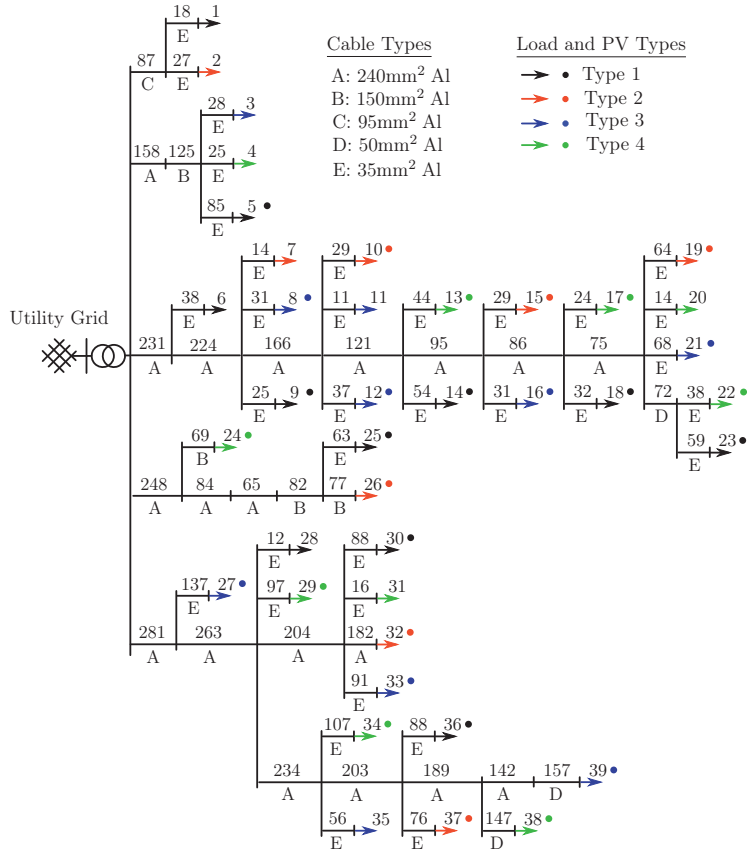


Figure 6.2: The test network based on a real European LV distribution network. The arrows and solid circles represent loads and PV units, respectively, along with their index. The numerical values along the power cable sections denote the cable length in meters, while the uppercase letters denote the cable types.

Table 6.2: Properties of load profiles and PV systems

Properties	Type 1	Type 2	Type 3	Type 4
Load demand range (kW)	0.54-2.37	0.94-3.67	0.64-2.7	0.68-2.53
PF of load demand (-)	0.98	0.98	0.98	0.98
Installed PV capacity (kWp)	5.25	5.95	6.3	6.65
Allowable PF of PV systems (-)	± 0.9	± 0.9	± 0.9	± 0.9

magnitude as the trigger, the simulations were executed in the phasor mode. The proposed control strategy is tested and compared with two other control methods as follows,

- **Method 1:** PV inverters are only embedded with the static SDC scheme (introduced in Sec. 6.3.2) with all the threshold values being constant over simulation time and uniform among PV inverters. Neither the coordination control nor the network decomposition is applied.
- **Method 2:** PV inverters employ the static $Q - V$ droop control and adaptive $P - V$ droop control. The threshold value for $Q - V$ droop control scheme remains constant over simulation time, while the threshold value for $P - V$ droop control scheme is updated by the coordination control layer (mentioned in Sec. 6.3.3). This method is adopted from our previous work presented in [169], where the network decomposition is not applied. This means that the coordination control is implemented for all PV inverters located in the same feeder, e.g., PV units from no. 8 to 23 will converge to a consensus of the power utilization ratio, while PV units from no. 27 to 39 will converge to the other consensus.
- **Method 3:** PV inverters are embedded with the proposed control strategy by which the threshold values for both $Q - V$ and $P - V$ droop control scheme are periodically modified. Reconsidering the aims of lowering the curtailed PV power generation during voltage rise conditions, this method is carried out along with the network decomposition.

In all 3 methods, the local control of PV inverters employs the SDC scheme to tackle voltage rise issues. For the coordination control layer, a convergence tolerance $\tau = 10^{-3}$ is applied as a stopping criterion for the consensus algorithm. Constant time duration of 15 seconds is used as the time interval at which the coordination mechanism updates the $P - V$ droop control parameter.

6.5 Numerical results

6.5.1 Control area determination

Following the ε -decomposition technique described in Sec. 6.3.1, Fig. 6.3 depicts the determined 7 control areas for the test network with a chosen ε value of 0.21. With no loss of generality, this value of ε is chosen to exemplify the decomposition procedure. To this end, \mathbf{Y} matrix of the network is first computed and then normalized before partitioned with given ε value into multiple decomposed matrices. The network was decomposed into sub-networks, in which each of them determines one of the control areas presented in Fig. 6.3.

It is needed to be noted that, since the ε -decomposition technique bases on the admittance matrix \mathbf{Y} of the network, recalculating the decomposition of the network is required when there is any change of the network configuration. In this work, it is assumed that the test network configuration remains constant.

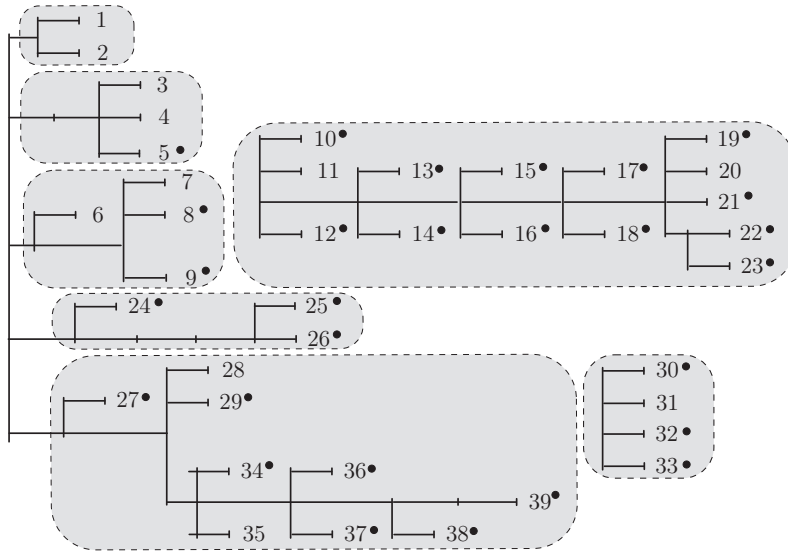


Figure 6.3: Decomposition of the test network for $\varepsilon = 0.21$ and determination of control areas as shaded regions. The solid circles represent PV units along with their index.

Once the network decomposition is completed, the corresponding sparse communication network, which is required for operating the coordination control layer, is established as shown in Fig. 6.4. As can be seen, the coverage range is within each determined control area, meaning that each PV unit only communicates with the other units located in the same area. The information weight factors (d_{ij}) for the established sparse communication network are calculated using Eq. (6.8). Development of the communication infrastructure is considered more in the planning phase for the distribution network by the network operators, which involves long-term planning decisions. In this work, it is assumed that the communication infrastructure is already installed in the test distribution network and the main focus is on evaluating the proposed control strategy more in the operation phase. The planning requirement and cost for the communication infrastructure is, hence, considered beyond of the scope of this study.

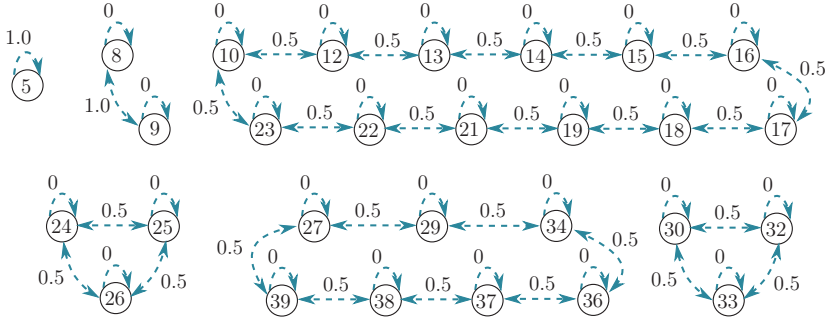


Figure 6.4: A sparse communication network for the decomposed test network with $\varepsilon = 0.21$ presented as a graph. The numerical circles represent PV units. The blue two-end arrow dashed lines represent the bi-directional communication links between PV units, while the numerical values along with the communication links denote the information weight factors (d_{ij}).

6.5.2 Voltage rise mitigation

Fig. 6.5 displays the resulting voltage magnitudes at the POCs of all PV systems in the network without any control mechanism over two consecutive summer days. This figure shows that voltage rise, e.g., above 1.07 p.u. only appears in the feeder no. 3 and 5, where the PV units from no. 8 to 23 and the PV units from no. 27 to 33 are located, respectively. For the sake of comparison, the threshold value $V_i^{tP} = 1.07$ p.u. is used uniformly for the static $P - V$ droop control in Method 1, and applied as a default setting for the adaptive $P - V$ droop control in Method 2 and 3. Meanwhile, the threshold value $V_i^{aQ} = 1.06$ p.u. is applied uniformly for the static $Q - V$ droop control in both Method 1 and 2, and utilized as a default setting for the adaptive $Q - V$ droop control in Method 3. If no voltage rise is detected or if the PV units are not in operation (e.g., at night), Method 2 will automatically reset V_i^{tP} to the default value, while Method 3 resets both V_i^{aQ} and V_i^{tP} .

The decomposed test network along with the sparse communication network resulting from Sec. 6.5.1 are utilized to execute the simulation with Method 3. Recall that the simulation with Method 1 and 2 is performed without the network decomposition procedure. To evaluate the performance of the proposed control strategy, this study adopted an ECDF to visualize the maximum voltage levels occurring in the test network, as illustrated in Fig. 6.6. Without control, the voltage magnitude significantly rises (i.e., above 1.09 p.u.). Visibly, the curves of all 3 methods move far to the left, indicating that the network voltage represents considerably lower magnitudes as compared to the case with no control. Additionally, it is observed that there is a slight difference in the ECDF curves between each of 3 control methods, meaning that the voltage profile of PV systems in 3 methods are comparable; therefore, all 3 methods effectively mitigate the voltage rise issues. This effective support is

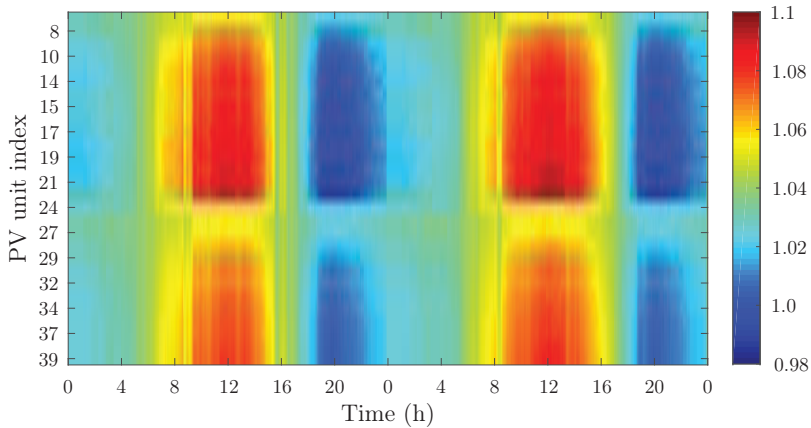


Figure 6.5: Voltage magnitude at the POCs of PV systems in the network without any control mechanism.

derived from employing the SDC scheme in the local controllers of the PV inverters, where both reactive and active power control are sequentially utilized.

Table 6.3 summarizes several performance metrics for 3 control methods. It is evident that Method 3 outperforms Method 1 and 2 in terms of the total curtailed PV energy. More specifically, Method 3 leads to a relatively similar value of the maximum voltage magnitude with the diminished percentage of curtailed energy (i.e., 0.234%) compared to Method 1 and 2 (i.e., 0.363% and 0.982% respectively), corresponding with the reduction of 35.6% and 76.2% compared to Method 1 and 2, respectively. This superiority of Method 3 is derived from the increased reactive power absorption by PV systems compared with Method 1 and 2, which is demonstrated in the next section. This growth in PV reactive power absorption along with a higher PV active power production (i.e., because of lower PV active power curtailment) causes Method 3 to have the slight rises of 1.63% and 3.88% in the network energy losses compared to Method 1 and 2, respectively. In 3 methods, Method 2 has the smallest value of energy losses, resulted from the lowest energy flow in the network. This is due to the smallest quantity of the energy supplied (kWh) of PV inverters in Method 2, meanwhile, its load energy consumption is in the same volume as Method 1 and 3. It can be noted that the performance metrics analyzed in this section correspond with the predefined threshold values V_i^{aQ} and V_i^{tP} . The sensitivity analysis of different threshold values is discussed in Sec. 6.5.4.

Another advanced feature of Method 3 is to significantly reduce the amount of curtailed active power of the PV units located at the end of the feeders (e.g., PV unit no. 23). To

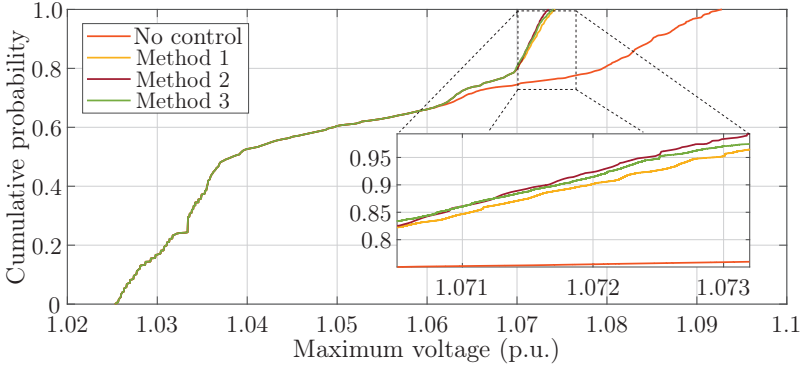


Figure 6.6: Maximum voltage level measured in the network for different control methods using Empirical Cumulative Distribution Function (ECDF).

Table 6.3: Summarized results for 3 control methods

Properties	Method 1	Method 2	Method 3
Maximum network voltage level (p.u.)	1.0743	1.0735	1.0740
Total energy supplied from PV systems (kWh)	2850.8	2833.1	2854.5
Total curtailed energy of PV systems (%)	0.363	0.982	0.234
Total energy losses in the network (kWh)	68.02	66.55	69.13

demonstrate this, Fig. 6.7 plots the calculated active power curtailment and reactive power absorption along with the measured voltage profiles of PV unit no. 23. At the POC of that PV system, the voltage rise above $V_i^{tP} = 1.07$ p.u. predominantly occur (as displayed in Fig. 6.5). In cases of voltage rise, Method 1 results in the highest amount of curtailed active power compared to Method 2 and 3 (with a maximum value of approximately 0.53 kW and 0.71 kW in the first and second day, respectively). Owing to the static $Q - V$ droop control scheme and the consensus-based coordination control mechanism, Method 2 helps to prevent voltage rise situations with a smaller volume of active power reduction (with the maximum value being around 38.5% and 38.7% lower than Method 1). The total amount of curtailed energy of the PV system in Method 2 is 1.7343 kWh (around 40.7% lower than that in Method 1). Finally, the proposed control strategy in Method 3 provides the comparable outcomes of voltage magnitude with the lowest amount of curtailed active power. In this method, the total curtailed PV energy is just nearly 0.69 kWh (approximately 76.5% and 60.3% smaller than that in Method 1 and 2, respectively). Note from Fig. 6.7 that, the absorbed reactive power by the PV unit in Method 3 is higher than that in Method 2. This is because the curtailed active power in Method 3 is less than that in Method 2, leading to P_i^{net} of PV inverters in Method 3 to become greater than Method 3. Accordingly, a greater Q_i is available for $Q - V$ droop control, as defined in Eq. (4.8). Hence, these findings

show the effectiveness of the proposed control strategy to alleviate voltage rise problems as well as significantly decrease the volume of active power curtailment of the PV inverters.

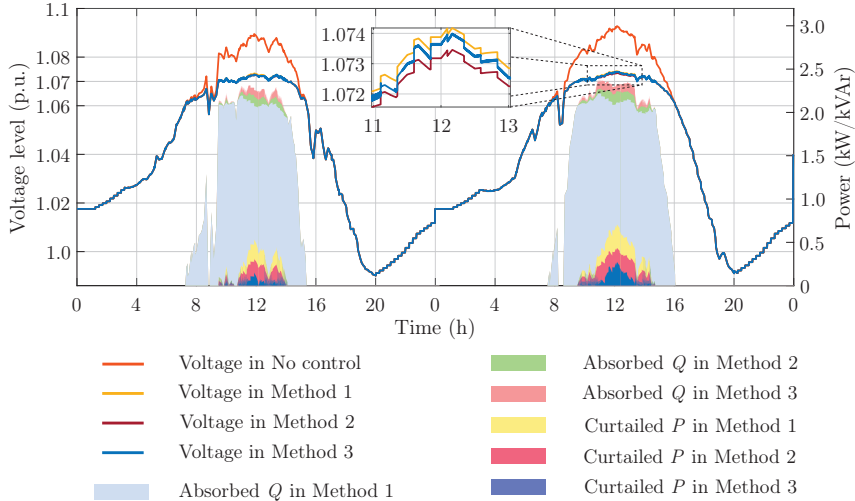


Figure 6.7: Curtailed active power (P), absorbed reactive power (Q) and voltage profiles for different control methods over two consecutive days of PV index no. 23.

6.5.3 PV system contribution to voltage rise mitigation

To verify the contribution of the power control of various PV systems towards alleviating voltage rise issues, the amount of curtailed energy per PV inverters in the feeder no. 3 and 5 for different control methods as a percentage of the energy (kWh) in the case with no control are calculated, as presented in Fig. 6.8. Recall that voltage rise above the threshold setting, i.e., 1.07 p.u., only appears in the feeder no. 3 and 5, as discussed in Sec. 6.5.2. The reduction of active power required for voltage rise alleviation, as a result, is purely done on such feeders.

As can be seen, Fig. 6.8 illustrates that the effective contribution of PV generation curtailment to prevent voltage rise is obtained in Method 3 and also Method 2, in which the coordination control layer was applied. In Method 2, all PV inverters in the same feeder reduce their generation with a relatively equal percentage at the expense of a high volume of the total curtailed energy. In Method 3, although the share of energy reduction is not equal among PV inverters in the same decomposed control areas (i.e., decomposition of the network with $\varepsilon = 0.21$ as demonstrated in Fig. 6.3), the total curtail energy is remarkably

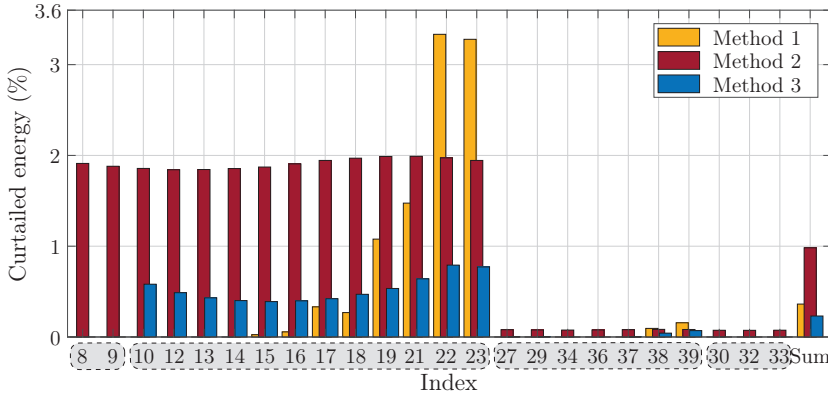


Figure 6.8: Curtailed energy of the PV inverters for different control methods during voltage rise conditions as a percentage of individual PV energy (kWh) in the case with no control. Each index from 8 to 39 represents the corresponding individual PV unit, while the last index, i.e., Sum, represents the total amount. The shaded, rounded rectangles covering the PV index represent the groups of PV inverters within the corresponding control areas in Method 3 with $\varepsilon = 0.21$.

reduced. The reason for the unequal reduction of curtailed energy in Method 3 is that the number of PV systems in several decomposed control areas is still large, e.g., 12 PV systems in the control area for PV inverters from no. 10 to 23. Then all PV inverters could not fully converge to a consensus of the power utilization ratio (β). However, a smaller number of PV units enables the convergence to the consensus as shown in the following section. In contrast, being embedded only with the static SDC scheme, Method 1 caused large deviations of the curtailment among PV units. Noticeably, Method 3 has outstanding performance as compared to Method 1 and 2 because the percentages of total curtailed energy in Method 3 are substantially lower.

As depicted by the absorbed reactive power profile of PV unit no. 10 in Fig. 6.9, the efficient use of reactive power absorption is obtained in Method 3. Although PV unit no. 10 is located closer to the transformer, where voltage rise conditions occur with lower levels (as can be observed in Fig. 6.5), reactive power absorption through the droop control is largely obtained. This is due to the use of the adaptive $Q - V$ droop control scheme, which is regulated by the coordination control mechanism for the control area of PV unit no. 10 as illustrated in Fig. 6.3. On the other hand, in Method 1 and 2, the location of PV unit no. 10 causes the static $Q - V$ droop control scheme to regulate reactive power absorption with considerably lower quantities compared to Method 3. Accordingly, the proposed coordination strategy proved to command PV inverters to not only more effectively contribute to

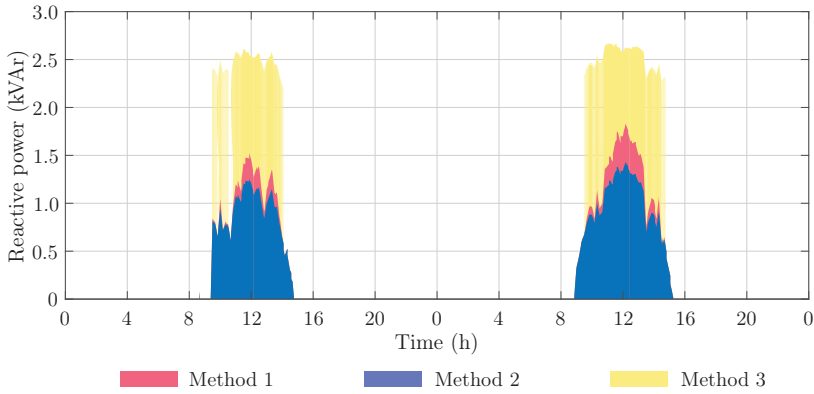


Figure 6.9: Absorbed reactive power (Q) profiles for different control methods over two consecutive days of PV index no. 10.

voltage rise mitigation, but also lower their generation reduction.

Since voltage rise mitigation involves activating the local droop control schemes of multiple PV systems at the same time, fluctuation of PV power output can arise due to interaction between the local controllers. This power fluctuation can result in voltage oscillation in the network [165]. To damp the voltage oscillation, there are several techniques available in the literature, such as applying a low-pass filter represented by a continuous-time transfer function with a time constant for PV power output [165] and limiting the rate of changes of PV power outputs [180]. For this study, the investigation of the voltage oscillation due to the interaction between PV droop controls is left for future researches.

6.5.4 Sensitivity analysis of different threshold values

As mentioned in Sec. 6.5.2, the threshold value settings for the local control play an important role in the performance of the control models. For further comparison of 3 control methods, the impact on the methods' performance metrics for different threshold values is analyzed in this section. The simulations are conducted using the configuration explained in Sec. 6.4 and Sec. 6.5.1 for two pairs of different threshold values for the droop control schemes. Key simulation results for 3 control methods are summarized in Table 6.4. It is observed in the first pair of threshold values $V_i^{aQ} = 1.07$ p.u. and $V_i^{tP} = 1.08$ p.u. that, Method 3 (i.e., the proposed control strategy) effectively solve voltage rise issues and results in the decrease in the curtailed PV energy rate compared to Method 1 and 2, respectively. Regarding system energy losses, 3 control methods are insignificantly different. With the

second pair of threshold values $V_i^{aQ} = 1.08$ p.u. and $V_i^{tP} = 1.09$ p.u., the performance of 3 methods are equivalent. Since the voltage levels (i.e., 1.0873 p.u.) are all lower than V_i^{tP} setting (i.e., 1.09 p.u.), PV active power curtailment mechanism in 3 methods remain inactivated.

Table 6.4: Comparison of different control methods with different threshold values

Properties	$V_i^{aQ} = 1.07$ p.u., $V_i^{tP} = 1.08$ p.u.			$V_i^{aQ} = 1.08$ p.u., $V_i^{tP} = 1.09$ p.u.		
	Method 1	Method 2	Method 3	Method 1	Method 2	Method 3
Maximum network voltage level (p.u.)	1.0809	1.0807	1.08	1.0873	1.0873	1.0873
Total energy supplied from PV systems (kWh)	2860.8	2860	2861	2861.2	2861.2	2861.2
Total curtailed energy of PV systems (%)	0.014	0.042	0.007	0	0	0
Total energy losses in the network (kWh)	63.39	63.33	63.46	61.12	61.12	61.12

As can be seen from Table 6.3 and Table 6.4, when voltage rise conditions activate the $P - V$ droop control scheme, Method 3, i.e., the proposed control strategy, induces the smallest quantity of PV active power reduction compared to Method 1 and 2, as well as adequately limits the voltage rise at the connection points. It is also important to highlight that, increasing threshold values for the droop control schemes allow the decrease in the active power curtailment, and power losses in the network as the differences between the network voltage levels and threshold values become smaller.

6.5.5 Performance evaluation in different control areas

The performance of Method 3 is further evaluated using the network decomposition for various ε values. The values of ε were chosen to decompose the network into a different number of control areas. The percentages of curtailed energy of the PV inverters during voltage rise conditions in Method 3 with various ε values are displayed in Fig. 6.10. The notable changes in the curtailed energy of individual PV units and also the total amount occur when different values of ε are used. Nevertheless, the adequate contribution of PV power control towards voltage rise prevention is achieved as the percentages of curtailed energy are relatively comparable in each case of decomposition.

Notice also from Fig. 6.10 that, with ε from 0.37 to 0.84, the same curtailed energy rate is achieved for PV inverters within the same control areas. In case of $\varepsilon = 0.44$, for instance, the control area for PV no. 19 and 21 has the curtailed energy percentage of 1.4%, while in the control area for PV no. 22 and 23 the percentage is 3.3%. This also illustrates that the introduction of the equal PV energy curtailment rate in each control area provokes the unequal PV energy curtailment rates between different control areas. The reason behind the

fair reduction rates achieved with ε from 0.37 to 0.84 is that the number of PV systems in the control areas is decreased, e.g., a maximum total of 4 PV inverters within a control area for the case of $\varepsilon = 0.37$ as compared to a maximum total of 12 PV inverters for the case of $\varepsilon = 0.21$. This smaller number of PV inverters allows the consensus of the power utilization ratio (β) among them to be properly converged. To illustrate this, Fig. 6.11 shows the iteration number of the consensus of β for a group of PV no. 22 and 23 in case of $\varepsilon = 0.37$. The number of iteration is executed by the consensus algorithm to converge β_{22} and β_{23} of PV no. 22 and 23, respectively, to a common agreement, as considered by Eq. (6.11). For some duration, the iteration numbers reach high values due to the rapid changes in PV power generation as well as load consumption, which in turn induce the rapid changes in the voltage levels and then the power utilization ratio (β) of PV systems. By contrast, the iteration number values are small when the voltage levels vary with low rate.

Furthermore, another number of performance metrics for Method 3 implemented with various ε values are summarized in Table 6.5. This table points out that a larger ε value leads to a growing number of control areas and a declining number of the bi-directional communication links between PV units as more weakly coupling terms between the network buses are identified. With increasing values of ε from 0.21 to 0.37, the percentage of total curtailed energy of PV systems increases. A reason for this is that the partitioned sub-networks, which each of them forms the control areas for PV systems, become gradually decreased in size. The coverage range of the proposed control strategy within individual control areas, subsequently, is for a small group of PV units. The decreasing number of PV units in the control area enables the iteration number for the consensus procedure to decrease, meaning that the consensus procedure converges with shorter time. The control areas, where voltage rise issues appear, receive less contribution from PV reactive power absorption to prevent

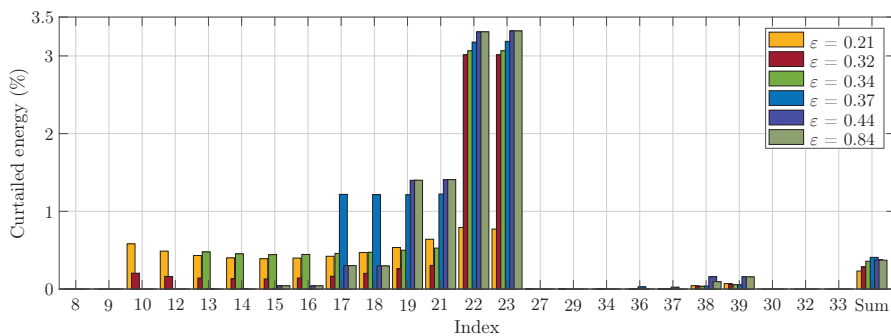


Figure 6.10: Curtailed energy percentages of the PV inverters during voltage rise conditions in Method 3 with various ε values. Each index from 8 to 39 represents the corresponding individual PV unit, while the last index, i.e., Sum, represents the total amount.

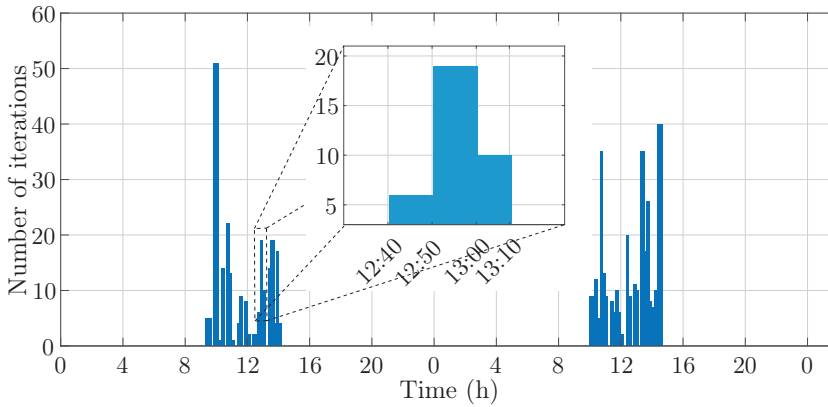


Figure 6.11: Iteration number of the consensus algorithm applied in PV index no. 23 over two consecutive days. The zoomed-in figure in the middle shows the iteration number, i.e., the height of the bar represented in y-axis, for a time duration (hh:mm), i.e., the width of the bar represented in x-axis.

voltage rise problems. Meanwhile, in the neighbouring control areas without voltage rise issues, the available PV reactive power absorption remains unused. Such decrease in the PV systems' active power generation and reactive power absorption provokes the decline of the energy losses in the network.

Table 6.5: Summarized results of applying Method 3 with various ϵ values

Properties	$\epsilon = 0.21$	$\epsilon = 0.32$	$\epsilon = 0.34$	$\epsilon = 0.37$	$\epsilon = 0.44$	$\epsilon = 0.84$
Number of control areas	7	9	10	12	16	22
Number of bi-directional communication links	26	24	23	22	14	12
Total number of consensus iterations	2253	1653	1243	798	469	468
Maximum network voltage level (p.u.)	1.0740	1.0739	1.0741	1.0741	1.0743	1.0743
Total energy supplied from PV systems (kWh)	2854.50	2853.00	2850.90	2849.50	2850.46	2850.54
Total curtailed energy of PV systems (%)	0.234	0.287	0.360	0.409	0.375	0.373
Total energy losses in the network (kWh)	69.13	68.60	68.26	67.95	67.99	68.00

As also indicated from Table 6.5 that when ϵ starts increasing from 0.44 to 0.84, the resulting curtailed energy rates of PV inverters decline. Nevertheless, the variation of PV systems' curtailed energy is insignificant, causing the network energy losses to be remarkably similar.

The rationale behind is that the size of the established control areas becomes small with a few PV units, e.g., a maximum total of 3 PV inverters for the case of $\varepsilon = 0.44$. The available PV reactive power absorption to support voltage rise mitigation, accordingly, is decreasingly exploited. Thus, the outcomes of adapting the SDC schemes of such PV inverters using the proposed control strategy (i.e., Method 3) are roughly similar to that of using the static SDC schemes, (i.e., Method 1), as shown in Table 6.3.

Recognizing that, when considering the number of bi-directional communication links (BCL) and total consensus iteration (CI), identifying ε value can be based on the maximum percentage decrease in two successive values. Based on this criterion, $\varepsilon = 0.44$ is the fitting value for the proposed control strategy applied in the given test network, as can be seen from Fig. 6.12. This value of $\varepsilon = 0.44$ also corresponds to a small amount of the total energy losses in the network, as illustrated in Table 6.5. However, when considering the total curtailed energy of PV systems (%), the fitting value for ε is the value corresponding to the lowest rate, that is $\varepsilon = 0.21$. Hence, the long-term techno-economic analysis is required to select the optimal value for the epsilon decomposition. As the epsilon decomposition will define the size of the communication infrastructure and the curtailed PV energy rate, the long-term techno-economic involves balancing the investment in the communication infrastructure with the decrease in the losses of PV owners' revenue by reducing their curtailed power.

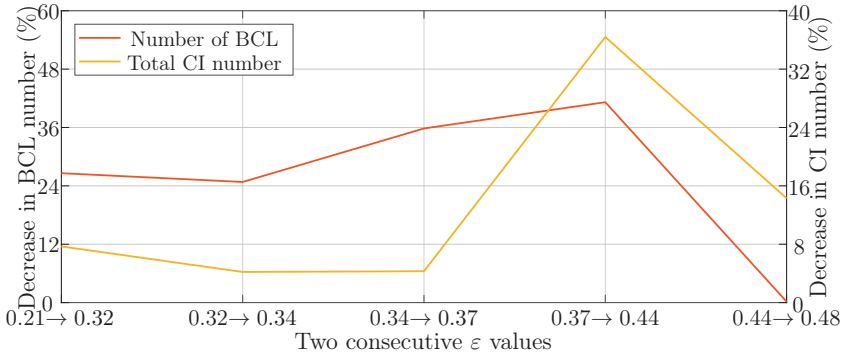


Figure 6.12: Identifying ε value. The x-axis depicts two consecutive ε values. The left y-axis represents the percentage decrease in the number of bi-directional communication links (BCL) associated with two successive ε values, while the right y-axis represents the percentage decrease in the consensus iteration (CI) numbers.

6.6 Summary

The distributed control scheme has been investigated in a number of studies to coordinate PV inverters for the LV network operation support. This chapter has introduced a completely distributed coordination control strategy for PV inverters combined with the ε -decomposition technique to alleviate voltage rise problems in PV-rich LV distribution networks. The ε -decomposition technique is employed to decouple the network into multiple control areas, where the proposed control strategy can be effectively implemented. The proposed control strategy utilises a hierarchical control architecture, which includes the sequential $Q - V$ and $P - V$ droop control scheme discussed in Chapter 4 as the local control of PV inverters. A consensus-based distributed control mechanism is used to implement the coordination control among PV inverters, in charge of periodically tuning and adapting the parameters of both $Q - V$ and $P - V$ droop control scheme within each control area.

The efficacy of the proposed control strategy is evaluated through simulations on a real European LV distribution network, considering a high PV penetration level of about 150%. The proposed control strategy is tested and compared with two other control methods. The obtained results prove that the proposed control strategy adequately prevents voltage rise problems while significantly reducing the total PV generation curtailment by approximately 35.6% and 76.2% when compared with the static sequential droop control and the static $Q - V$ droop control and adaptive $P - V$ droop control, respectively. Simultaneously, the effective contribution of all PV systems towards voltage rise mitigation, i.e., by the efficient use of reactive power absorption, is guaranteed. However, the proposed control strategy does not provide the fair curtailment of PV generations in some cases of small ε values. Thus, further evaluation of the proposed control strategy has been performed with multiple ε values. Larger ε values result in the fairness of PV generation curtailment, a decline in system energy losses, and faster convergence for the consensus-based distributed control in the control areas, but in some cases increased volume of total curtailed energy of the PV systems. Selecting the optimal ε value should be based on the long-term techno-economic analysis, which thoroughly assesses the investment in the communication infrastructure and the impact of reduced PV power curtailment on PV owners' revenue.

The proposed control strategy can provide DSOs with better control in voltage rise mitigation with more effective contribution and fair treatment of PV systems. The proposed control strategy can also assist the PV owners in decreasing their revenue losses by reducing their curtailed power.

In this research, the consensus procedure among PV inverters is simulated using fast communications without delays and no interaction between PV droop controllers. Future research can be conducted to investigate the potential impact of communication delays and failure on the consensus-based coordination control and the voltage oscillation due to the interaction of multiple local droop controllers.

7

Conclusions

This final chapter presents the conclusions from the research conducted in this thesis. First, the key findings and insights from the studies in relation to the research questions are summarised. Next, the scientific contributions of the thesis are discussed. Finally, several recommendations for future research are provided.

7.1 Research summary

In recent years, distribution networks have been undergoing a transition to active systems. This transition has been derived from the expanding integration of RES and the rapid digital transformation at the grid edges, i.e., interface points between the LV networks and the end-user installations. The transition to the active systems with the RES integration poses challenges for the network operation and the power quality. These challenges can involve, for instance, managing the transformer congestion or thermal overloading and voltage rise problems. However, a conventional method to tackle these challenges by performing network reinforcement typically involves high investment costs, consequently having low economic viability. Therefore, an alternative solution is expected to effectively use the network assets, such as by controlling the RES inverters in LV distribution networks (so-called grid-edge control). Besides, the proper monitoring of the network operation is critical for the DSOs

to ensure stable and reliable operation and manage new connections, especially with the increasing share of RES with its intermittent and unpredictable nature.

The main objective of the research described in this thesis has been to develop a suitable grid-edge monitoring and control strategy that will help in stimulating the integration of RES in LV distribution networks and support the network operation. The developed grid-edge monitoring and control strategy focuses on solving the congestion and voltage rise problems by exploiting the RES controllability and digital transformation in the LV distribution networks. Several research questions were formulated and addressed in the previous chapters to achieve the above objective. Brief summaries of the key findings and insights from the studies with the research questions are given in the following sections.

7.1.1 Grid-edge monitoring and control

Chapter 2 provides a comprehensive overview of grid-edge monitoring and control for LV distribution networks. The increasing proliferation of RES creates challenges for the network operation and planning. These challenges have arisen from the nature of RES associated with the uncertainty, variability, and no inertia and the regulation related to the system operation. Main challenges can include but not limited to system-demand balancing, power quality, network congestion, stability issues and changes in the regulatory framework. Conventional approaches, e.g., network reinforcement, are normally not financially viable. Thus, the RES control strategy at the grid edges, i.e., the secondary side of LV distribution transformers (so-called grid-edge control), can be a promising alternative to support LV distribution network operation. This new paradigm calls for data-driven methods to capture the uncertainty and complexity natures of RES. Meanwhile, the coexistence between the grid and RES control strategy must be adopted.

On the other hand, the rapid digital transformation at the grid edges provides opportunities to improve network performance. This digital transformation, which arises from the uses of smart meters (SM), the Internet-of-Things and ICT, can increase the network monitoring for the operation support. Furthermore, an appropriate combination of the digital transformation with the RES control can effectively use the inherent controllability of RES and the availability of the digital transformation at the grid edges. This new paradigm, subsequently, can facilitate the efficient coordination of RES at the grid edges. Therefore, the increasing integration of RES into LV distribution networks becomes feasible while the system stability and reliability can be maintained appropriately.

The first research question (Q1) is addressed in this chapter. First, the challenges from the energy transition in LV distribution networks are presented. Thereafter, the context of grid-edge monitoring and control is elaborated, including the role of these approaches in supporting the distribution network operation. Finally, technological aspects of grid-edge monitoring and control, including modellings, architectures, and strategies, are also discussed.

7.1.2 Transformer loading monitoring

Chapter 3 responds to the second research question (Q2) by investigating the relationships between the data from residential SM in terms of voltage magnitudes and the LV distribution transformer loading. A data-driven approach is developed to estimate the transformer loading by adopting the machine learning-based regression models and leveraging the residential SM readings. As the SM readings are vital for this data-driven approach, it is proposed that this approach will be implemented by the LECs as they can access the end-user's SMs. To facilitate the implementation of the data-driven approach, a comprehensive framework with all the essential stages is provided, consisting of training data generation, exploratory data analysis, feature selection, model selection and algorithm selection. Following this comprehensive framework, different machine learning algorithms will be implemented, validated and compared.

Simulations were performed in the unbalanced IEEE European LV network with 55 houses to test the proposed approach. A thoroughly conducted analysis of the relationships between the transformer loading and the nodal voltage magnitude data from residential SMs reveals clear V-shaped patterns between these two variables. Subsequently, with the voltage magnitude data from only a reduced set of residential SMs within a particular LEC being utilised, the machine learning-based regression model effectively estimates the transformer loading, i.e., with the Pearson correlation coefficient R and RMSE calculated for the real values and the estimated values of around 0.98 and 0.87, respectively. This data-driven approach, simultaneously, can preserve customers' privacy rights as only the voltage readings (not power consumption) are used. Hence, the proposed approach can provide an alternative to implementing transformer congestion monitoring in LV distribution networks. Moreover, the self-management capability of the LECs in the regional network can be enhanced.

7.1.3 Local control for voltage regulation

Chapter 4 answers the third and fourth research questions (Q3, Q4). It presents a procedure for comprehensively assessing the technical and economical impact of the residential-scale PV systems operating with local voltage control on the LV distribution networks and the PV system owners. The local voltage control, which is installed in the PV inverters, utilises locally available information to regulate the PV power outputs when the voltage at the POC violates the threshold values of the local voltage level. To realise this control function, the SDC mechanism is presented, which consists of RPA and APC scheme. For the impact assessments, a Monte Carlo-based stochastic approach is adopted along with the conditional Copula method to generate a large set of time series input data. Several impact metrics are used to assess the network and the PV owners, both technically and economically.

A simulation case study on the IEEE European LV test network is carried out with various

permutations of the threshold settings for the SDC-based local voltage control, PV penetration levels, and one-year time-series data scenarios. The simulation results indicate that the SDC-based local voltage control effectively solves the voltage rise problems by regulating the power outputs of PV systems in a sequence with the RPA scheme before the APC scheme. The technical and economical impact of the PV inverter control on the network and the PV owners relies on how fast the SDC mechanism responds to voltage rise conditions in different PV penetration levels. Overall, the faster the RPA scheme reacts (by setting a lower threshold level), the network can be more adversely affected while less adversely affected by the PV owners.

7.1.4 Centralised control for voltage regulation

Chapter 5 responds to the fifth research question (Q5) by discussing a coordination control of reactive power outputs from residential-scale PV systems in real-time operation for voltage rise mitigation in LV distribution networks. A centralised control strategy is developed by employing the hierarchical control architecture to integrate local and centralised control algorithms. The local control algorithm, i.e., embedded in each PV inverter, continuously monitors and tackles voltage rise issues by adopting the SDC mechanism discussed in Chapter 4. The centralised control algorithm, i.e., executed in a central controller, aims to optimally steer the performance of the local control algorithm in PV inverters. The performance steering is performed in discrete time steps by solving the optimisation problem of PV power outputs and calculating new threshold settings for the SDC mechanism-based local control. The threshold settings are regularly transmitted to each PV unit to support the voltage violation regulation. Solving the optimisation problem of PV power outputs involves applying the linear programming technique while calculating the new local control parameters utilising the concept of the Jacobian matrix.

Simulations were performed on a typical Dutch LV distribution network with a real data set for household consumption and PV generation from the Netherlands. The proposed control strategy is shown to be adequate to alleviate the voltage rise issues while significantly reducing the curtailed amount of PV energy. The centralised control algorithm correctly solves the optimisation problems of PV power outputs, and then efficiently coordinates the local control algorithms in all relevant PV units by periodically providing the threshold settings for the SDC mechanisms. This centralised control strategy, however, causes unfair power curtailment among the PV systems since the voltage problems appear mainly towards the end of the LV feeders. An alternative approach should be considered to achieve a fair curtailment of PV power.

7.1.5 Distributed control for voltage regulation

Chapter 6 addresses the final research question (Q6). The variation in the impact of PV power generation on voltage regulation in LV distribution networks is analysed. A distributed coordination control strategy for residential-scale PV systems is proposed, in combination with the ε -decomposition technique to support the voltage rise mitigation. The objective is to mitigate voltage rise conditions in LV distribution networks with a more effective contribution and fair power curtailment of PV units. To achieve this objective, a coordination control among PV units is implemented in a hierarchical control architecture comprising a continuous local voltage control and a distributed control applied in discrete time steps. The ε -decomposition technique decouples the network into multiple control areas with the strong coupling nature of PV systems, aiming to facilitate coordination control among PV inverters. The local voltage control is based on the SDC mechanism discussed in Chapter 4. The distributed control is developed without a centralised controller that adopts the consensus algorithm to coordinate PV systems. The distributed control periodically tunes and adapts the local control parameters (i.e., threshold levels of the SDC mechanism) for every PV inverter within each control area.

A simulation case study on a real European LV distribution network with high PV penetration demonstrates that the proposed control strategy adequately prevents voltage rise problems while substantially decreasing the total PV generation curtailment by up to 76.2% compared with non-coordination control approaches. Simultaneously, the effective contribution of all PV systems towards voltage rise mitigation, i.e., by an efficient use of reactive power absorption, is achieved. Furthermore, applying the ε -decomposition technique with large ε values results in the fairness of PV generation curtailment, a decline in system energy losses, and faster convergence for the consensus-based distributed control in the control areas.

7.2 Contributions

The main contributions of this thesis are summarised in the following sections.

- **A thorough analysis of voltage rise mitigation support by residential PV systems**
An essential contribution of this thesis is to obtain a thorough analysis of voltage rise mitigation support by residential-scale PV systems. Due to the widespread and increasing integration of residential-scale PV units, leveraging the controllability of the existing PV inverters for RPA and APC is emerging as a promising one to support voltage rise mitigation. In this regard, an analysis of the short-term (i.e., real-time) operation and long-term operation of PV units equipped with these control functions,

if thoroughly implemented, can be the foundation for a wide range of applications in future distribution networks.

- **A data-driven method for congestion monitoring of distribution transformers**

A regression-based method is introduced in combination with a limited series of residential SM data for transformer loading estimation. In this regard, a thorough analysis based on summary statistics and graphical visualisation are implemented to discover the relationships between the transformer loading and voltage magnitudes measured at the POC of the houses. Furthermore, a comprehensive comparison with various ML algorithms is also conducted to select the best-performing regression model.

- **A comprehensive procedure for transformer congestion monitoring**

A comprehensive procedure is proposed to implement, validate and compare different machine learning algorithms for the transformer loading estimation from the LECs' perspective. This procedure covers all the essential stages in deploying a data-driven technique, consisting of training data generation, exploratory data analysis, feature selection, model selection and algorithm selection. With this respect, some state-of-the-art advances in machine learning research have been integrated, such as XGBR algorithm and Nested CV technique. This procedure can enable self-management capability of the LECs via transformer congestion monitoring in LV distribution networks.

- **Long-term technical and economic impact assessment of local voltage control**

A comprehensive procedure is proposed to implement, validate and compare different machine learning algorithms for the transformer loading estimation from the LECs' perspective. This procedure covers all the essential stages in deploying a data-driven technique, consisting of training data generation, exploratory data analysis, feature selection, model selection and algorithm selection. With this respect, some state-of-the-art advances in machine learning research have been integrated, such as the eXtreme Gradient Boosting Regression algorithm and Nested CV technique. Furthermore, this procedure can enable the self-management capability of the LECs via transformer congestion monitoring in LV distribution networks.

- **Centralised coordination control for voltage rise mitigation**

Aiming to gain a more efficient contribution of PV reactive power capability for voltage rise mitigation, the centralised coordination control is built to coordinate PV units in real-time operation. The deficient employment of PV reactive power capability occurs when only local voltage control is used by PV inverters that purely take the locally available information for the control decision. Therefore, the centralised coordination control is formulated to maximise reactive power absorption by PV inverters to maintain the voltage levels at all the POCs within the allowable range while reducing the curtailment of active power injection from PV units. As a result, coordinating local

voltage control by a centralised controller in discrete time steps is successfully executed in real-time operation.

- **Distributed coordination control for voltage rise mitigation**

A distributed coordination control scheme is proposed that adapts the SDC parameters of the PV inverters to reduce the amount of curtailed generation and guarantee the effective contribution of all PV systems while alleviating voltage rise problems. In addition, an ε -decomposition technique is used to decompose the network into multiple control areas, where the proposed control is implemented for PV units located in the same control area. The distributed control uses a sparse communication network with a significantly low bandwidth requirement, enabling this control architecture to be less costly and less complex. Furthermore, considering the widespread integration of residential-scale PV units, the distributed control is highly suitable for the LV distribution network. Hence, this proposed control strategy can provide DSOs with better control in voltage rise problems with more effective contribution and fair treatment of PV systems. Besides, it can assist the PV owners in reducing their revenue losses by decreasing their PV curtailed power.

7.3 Recommendations

Conducting the work presented in this thesis poses some interesting open questions that can be considered to extend the research. Therefore, several recommendations for future research directions are described below in this section.

7.3.1 Grid-edge monitoring in LV distribution networks

- **Regulatory framework modifications**

The data-driven approach to estimating the distribution transformer loading heavily hinges on the existence of the LECs and their ability to access the residential SMs. The LECs will use the SM readings as historical and real-time operational data for the regression model preparation and deployment. In this respect, modifications of the existing regulatory framework regarding the LECs' business model and the accessibility to the residential SMs will be required.

- **Intelligent adaptability with network topology and PV penetration level**

The transformer loading estimating approach is currently developed for the LV distribution network with a fixed topology and a specific PV penetration level. Accordingly, this existing approach is not adaptive to grid topology changes or increasing PV installation, inherent in the grid operation and evolution. These changes will induce

variations in the correlation between the transformer power and nodal voltage levels, which needs to be re-captured by the regression model. Therefore, periodically assessing the regression model performance and afterwards re-training the model is essential. A more intelligent data-driven approach that can automatically adapt to variations in the network topology and PV penetration levels could be considered.

- **Transformer loading estimation in distribution networks with mesh topology**

A typical LV distribution network with a radial configuration is considered for the transformer loading estimating approach. However, for LV distribution networks with mesh topology, the application of the proposed approach can face challenges. For example, the relationship between the transformer power and the nodal voltage magnitude can deviate from the V-shaped pattern. Thus, this relationship can be more complicated for regression models, and the accuracy of estimated transformer loading can be degraded. Thus, further research is required to consider the mesh networks more efficiently.

7.3.2 Grid-edge control in LV distribution networks

- **More comparative analysis for local voltage control**

Using the SDC-based local voltage control method, the advantages of using more reactive power absorption for the PV owners are made at the expense of a higher transformer loading and the system power losses, which are significant concerns of DSOs. Therefore, a more comparative analysis of the technical and economic impact is expected to identify the parameters for local voltage control that harmonise the impact on the PV owners and DSOs. On the other hand, the impact on each PV owner is unobserved, yet because the obtained assessment is performed for the network as a whole. Further research for the impact assessment on the individual PV units, thus, can be conducted.

- **Interaction of PV inverters operating with local droop control**

The SDC schemes of multiple residential-scale PV systems located closely in the same LV feeder can activate simultaneously when the voltage at the POC violates the threshold values of the local voltage level. Fluctuation of PV power outputs, subsequently, can occur due to the interaction between those local droop controllers. This power fluctuation can result in voltage oscillation in the network. The investigation of such voltage oscillation can be a topic for future research. Several techniques available in the literature, such as applying a low-pass filter and limiting the rate of changes in PV power outputs, can be considered.

- **Effect of communication delay on real-time coordination control**

The centralised and distributed control approach presented in this thesis assumes fast

communications between the network components. However, communication delays are inevitable and can considerably affect real-time coordination control. Future research can investigate the potential effect of communication delays on both centralised and distributed-based coordination control. The research can be carried out in the laboratory environment and in field experiments.

A

Load characteristics and PV capacity data

As discussed in Chapter 3, the test network based on the IEEE European LV distribution network is unbalanced grid consisting of a 250 kVA, 11/0.4 kV distribution transformer and 55 houses with single-phase connections: 21 houses on phase A, 19 houses phase B, and 15 houses on phase C [127]. The household load characteristics and installed PV capacities for phase A is given in Chapter 3. In this appendix, the properties of load and PV systems for phase B and C are listed in Table A.1, and Table A.2, respectively.

Table A.1: *Summary of household load characteristics and PV installations in phase B*

House No.	Node No.	Peak load (kW)	Installed PV capacity (kWp)	House No.	Node No.	Peak load (kW)	Installed PV capacity (kWp)
H2	47	3.6	5.8	H36	676	3.1	5.6
H6	83	3.3	4.7	H37	682	3.2	5.2
H7	178	2.9	6.0	H38	688	3.4	4.4
H10	248	3.0	4.5	H40	702	3.6	5.9
H11	249	2.8	4.2	H41	755	3.8	5.7
H13	276	3.5	4.3	H44	785	3.5	5.9
H15	314	3.3	4.3	H45	813	2.8	4.5
H23	406	3.3	6.2	H50	886	3.2	5.6
H26	522	3.8	4.4	H53	899	2.9	4.8
H35	639	4.2	5.8				

Table A.2: *Summary of household load characteristics and PV installations in phase C*

House No.	Node No.	Peak load (kW)	Installed PV capacity (kWp)	House No.	Node No.	Peak load (kW)	Installed PV capacity (kWp)
H8	208	4.6	4.7	H28	556	2.8	5.7
H12	264	3.6	5.1	H32	614	3.5	6.2
H16	320	3.5	5.7	H33	619	4.4	6.1
H17	327	3.9	5.6	H39	701	2.8	5.3
H18	337	3.2	4.4	H42	778	4.1	4.1
H19	342	2.5	5.6	H43	780	3.6	4.1
H24	458	3.9	4.1	H47	835	3.9	6.0
H27	539	3.1	4.7				

Every household is assumed to own a PV system. The rated capacities of PV systems in the test network are randomly chosen between 4.06 and 6.27 kWp [126], which is derived from the information on the real residential PV installations in the Netherlands.

B

Results of exploratory data analysis

Exploratory Data Analysis (EDA) implementation is crucial for the deployment of any data-driven technique. EDA is used to examine the data from various angles to discover interesting features, such as patterns, relationships among input variables, relationships between input and output variables, and anomalies [131, 132].

In Chapter 3, EDA is implemented for the transformer phase A loading (S_{trans}^A), voltage magnitudes (V) at the POC, net active power (P^{net}) and net reactive power (Q^{net}) of houses connecting to the same phase, using two methods: summary statistic and graphical visualisation. Parts of the EDA results are included in Chapter 3 and the remaining EDA results are shown in this appendix.

Fig. B.1, and Fig. B.2 show pair plots computed for S_{trans}^A and V at the POC of the houses on the same phase. It is noted that the explanation of the pair plots is given the Chapter 3. These two figures show a strong correlation between S_{trans}^A and V with clear V-shaped patterns. Thus, applying regression models is possible to compute power flow through the transformer from the nodal voltage magnitudes.

Fig. B.3, and Fig. B.4 show pair plots for S_{trans}^A and P^{net} of the houses on the same phase, while Fig. B.5, and Fig. B.6 show pair plots for S_{trans}^A and Q^{net} . The first two figures illustrate high correlation coefficients between S_{trans}^A and P^{net} . The next two figures indicate very low correlation coefficients between S_{trans}^A and Q^{net} . In all four figures, the scatter

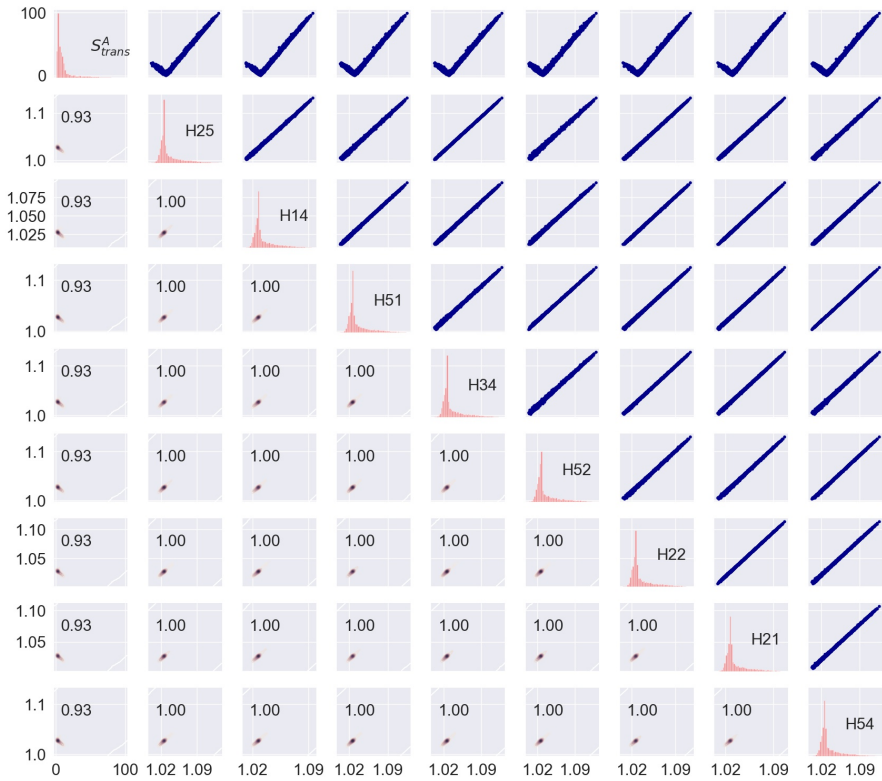


Figure B.1: A pair plot for the transformer phase A loading (S_{trans}^A) and voltage magnitudes (V) at the POC of the houses H25, H14, H51, H34, H52, H22, H21, and H54 connecting to the same phase. This pair plot consists of histogram plots along the diagonal, Pearson correlation coefficients below the diagonal, and scatter plots above it.

plots show the relationship between S_{trans}^A and P^{net} , and S_{trans}^A and Q^{net} with less clear patterns than the relationship between S_{trans}^A and V (Fig. B.1, and Fig. B.2). Hence, active and reactive power data from SMs are considered as unsuitable input candidates for the data-driven monitoring of transformer loading.



Figure B.2: A pair plot for the transformer phase A loading (S_{trans}^A) and voltage magnitudes (V) at the POC of the houses H5, H30, H4, H9, H49, H20, H55, and H46 connecting to the same phase. This pair plot consists of histogram plots along the diagonal, Pearson correlation coefficients below the diagonal, and scatter plots above it.

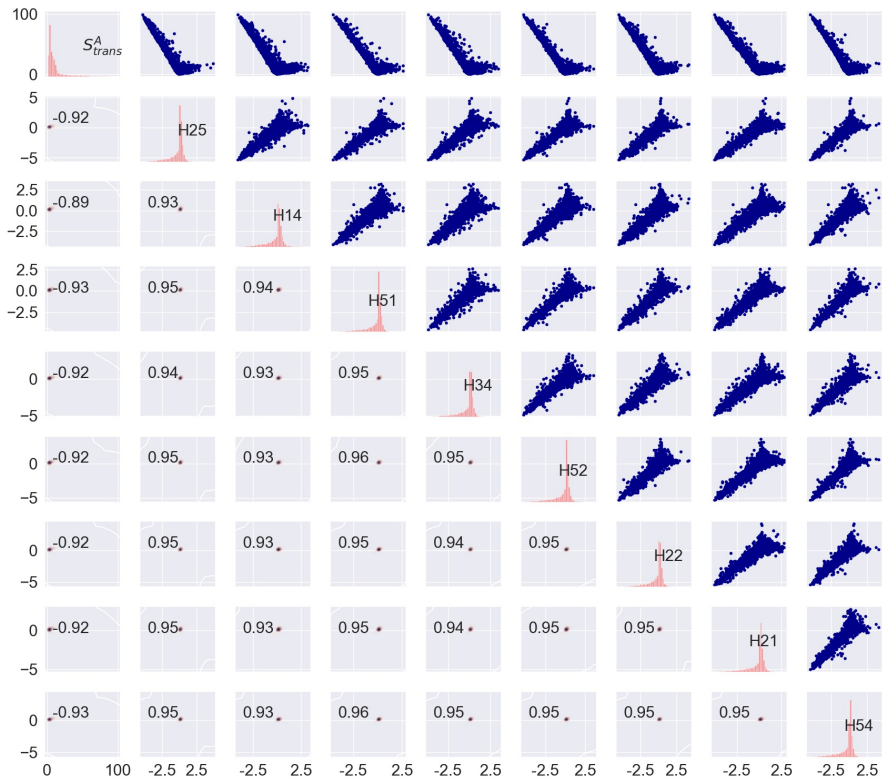


Figure B.3: A pair plot for the transformer phase A loading (S_{trans}^A) and net active power (P^{net}) of houses H25, H14, H51, H34, H52, H22, H21, and H54 connecting to the same phase. This pair plot consists of histogram plots along the diagonal, Pearson correlation coefficients below the diagonal, and scatter plots above it.

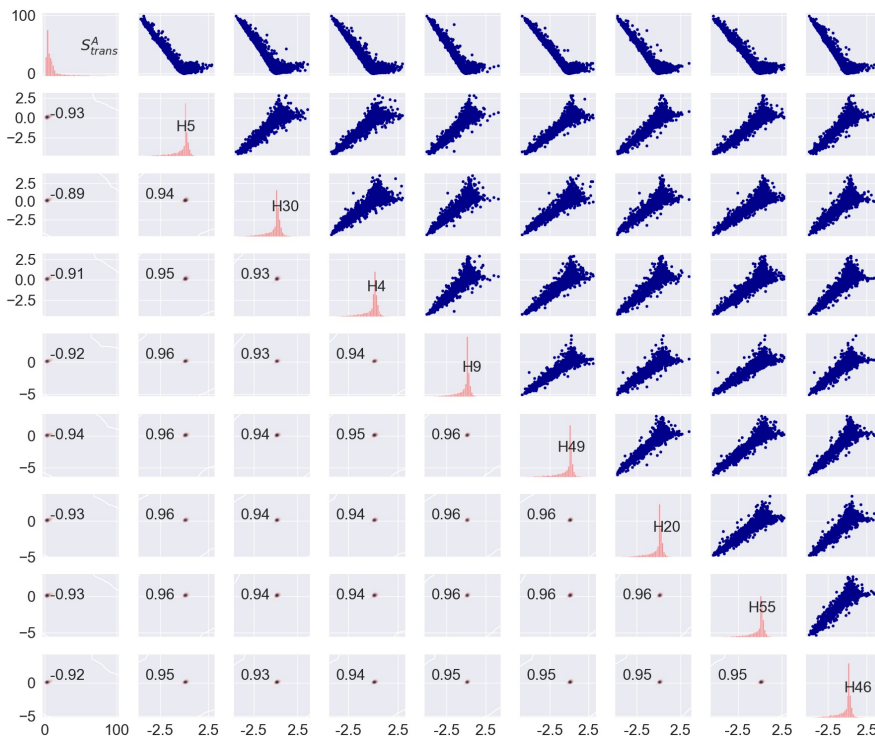


Figure B.4: A pair plot for the transformer phase A loading (S_{trans}^A) and net active power (P^{net}) of houses H5, H30, H4, H9, H49, H20, H55, and H46 connecting to the same phase. This pair plot consists of histogram plots along the diagonal, Pearson correlation coefficients below the diagonal, and scatter plots above it.

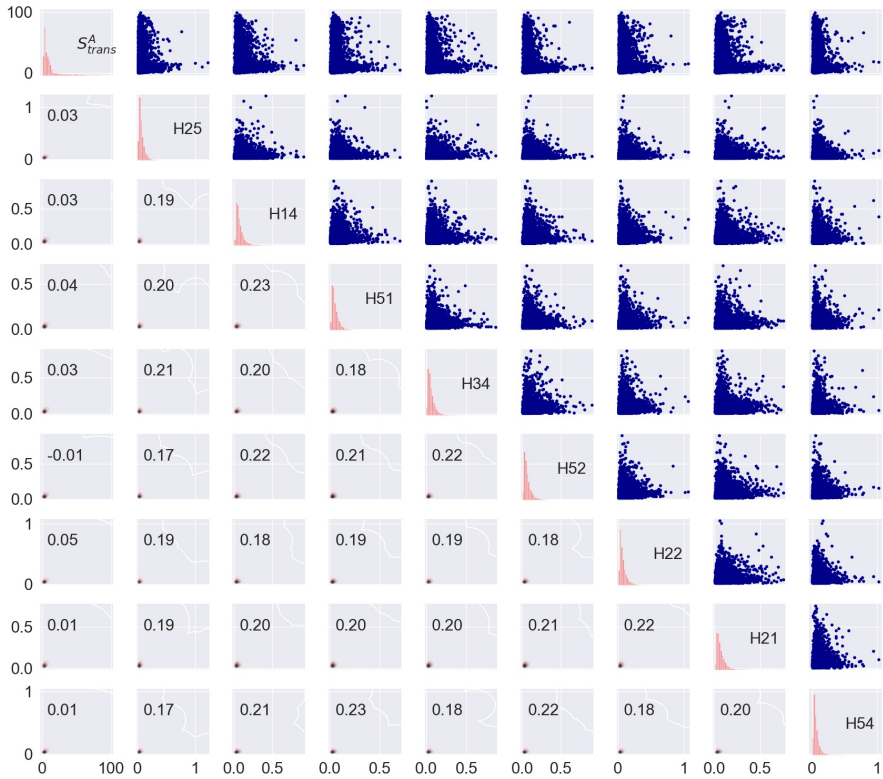


Figure B.5: A pair plot for the transformer phase A loading (S_{trans}^A) and net reactive power (Q_{net}) of houses H25, H14, H51, H34, H52, H22, H21, and H54 connecting to the same phase. This pair plot consists of histogram plots along the diagonal, Pearson correlation coefficients below the diagonal, and scatter plots above it.

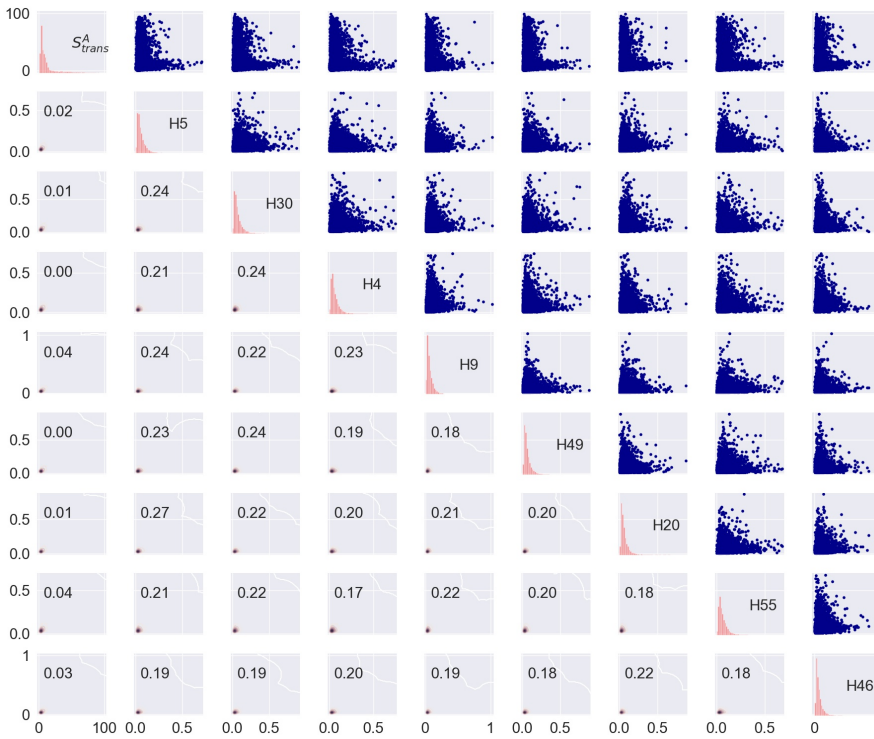


Figure B.6: A pair plot for the transformer phase A loading (S_{trans}^A) and net reactive power (Q^{net}) of houses H5, H30, H4, H9, H49, H20, H55, and H46 connecting to the same phase. This pair plot consists of histogram plots along the diagonal, Pearson correlation coefficients below the diagonal, and scatter plots above it.

C

Additional results of the assessment of PV local voltage control

As discussed in Chapter 4, a Monte Carlo-based stochastic approach is used to assess the impact of PV systems operating with the sequential droop control (SDC) mechanism on both LV distribution networks and PV owners. The threshold levels (V_i^{tP} and V_i^{aQ}) of the SDC mechanism play an important role in the performance of this mechanism. In total 9 simulation cases categorised into 3 groups with different threshold levels (see Table 4.1) have been performed. The simulation results for the cases in Group A are discussed in Chapter 4. The simulation results for the cases in Group B and Group C are given in this appendix.

Table C.1: *Group B and Group C simulation cases for the impact assessment*

Group	Cases	Threshold levels of SDC mechanism	
		V_i^{aQ} (p.u.)	V_i^{tP} (p.u.)
Group B	Case 4	1.04	1.07
	Case 5	1.05	1.07
	Case 6	1.06	1.07
Group C	Case 7	1.05	1.08
	Case 8	1.06	1.08
	Case 9	1.07	1.08

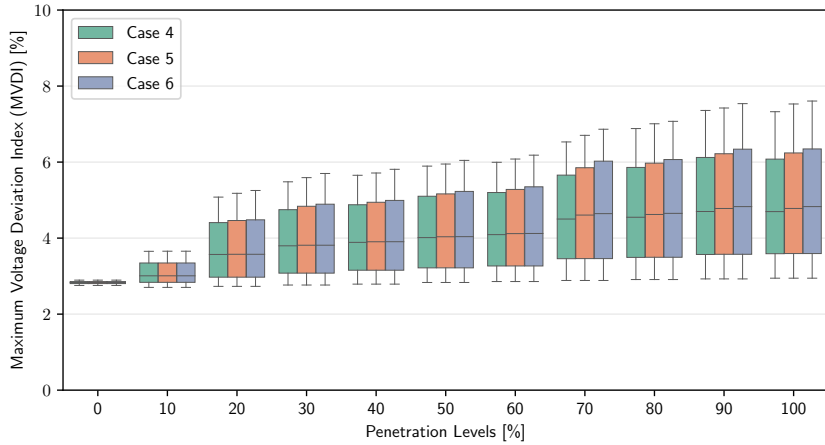


Figure C.1: Maximum voltage deviation index at the POCs of the PV units with Group B cases.

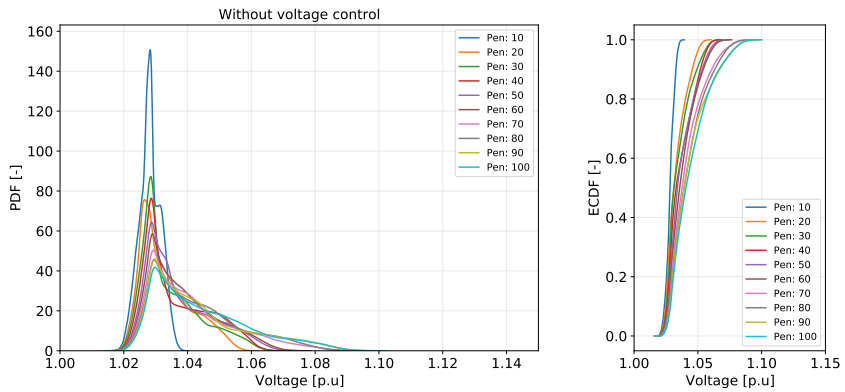


Figure C.2: PDF and ECDF of the voltage levels in the network with Group B cases.

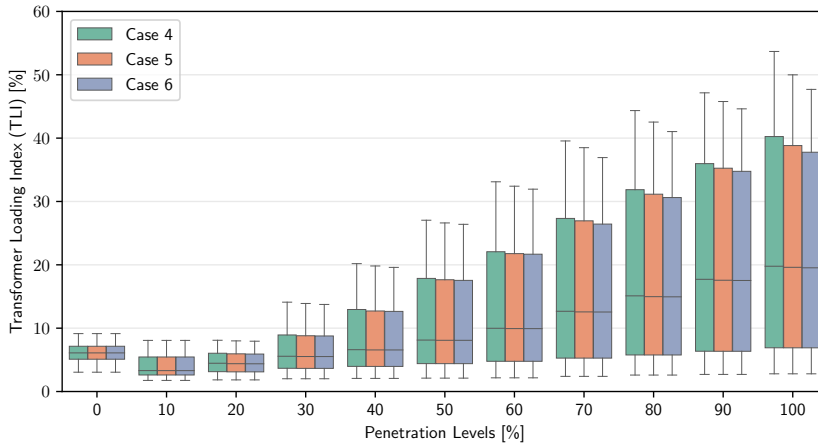


Figure C.3: Transformer loading index with Group B cases.

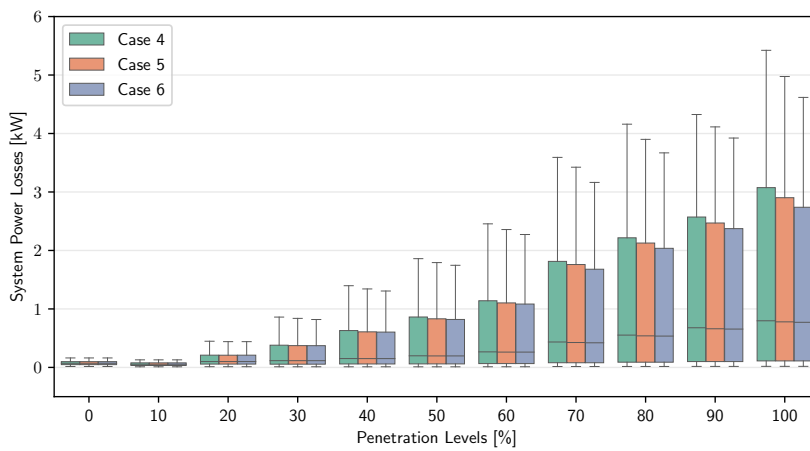


Figure C.4: System power losses with Group B cases.

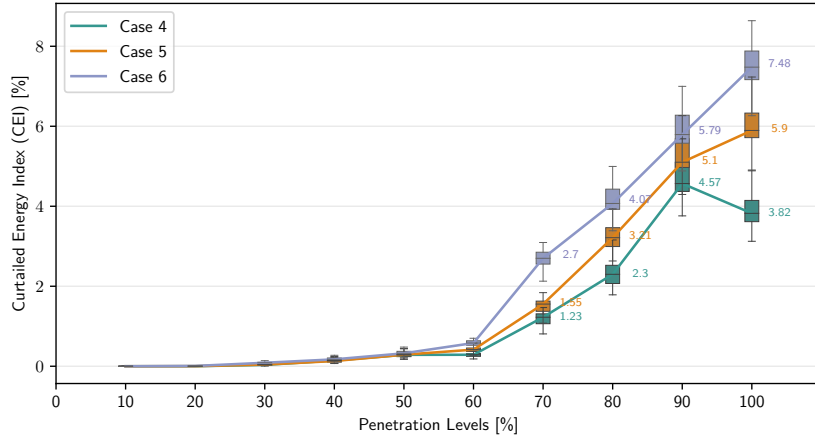


Figure C.5: Curtailed energy index with Group B cases.

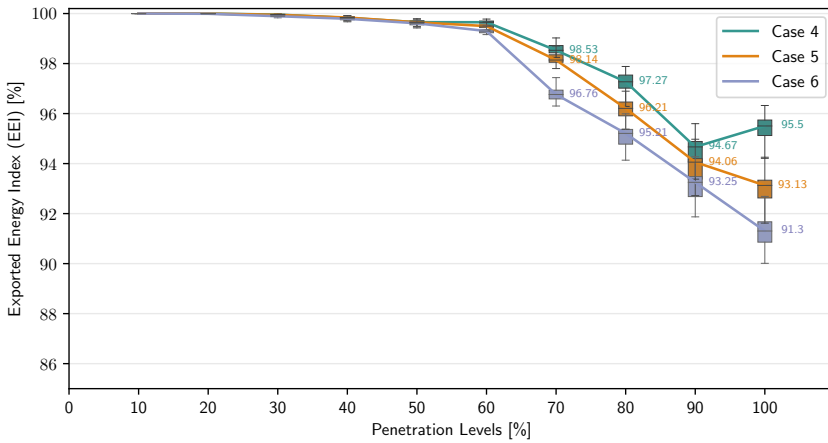


Figure C.6: Exported energy index with Group B cases.

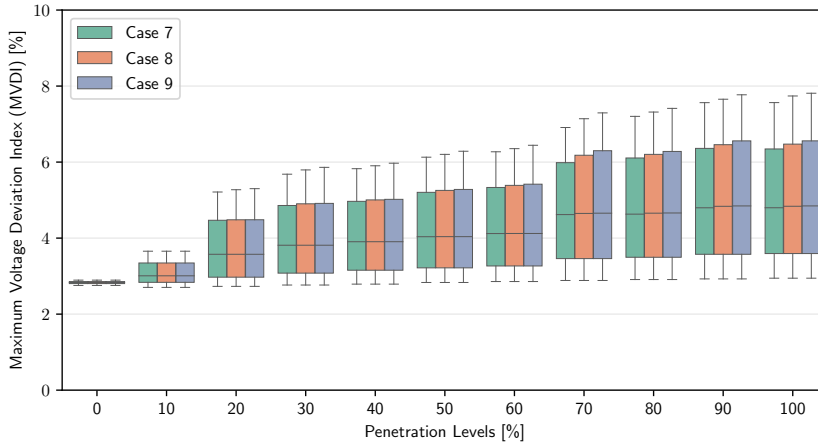


Figure C.7: Maximum voltage deviation index at the POCs of the PV units with Group C cases.

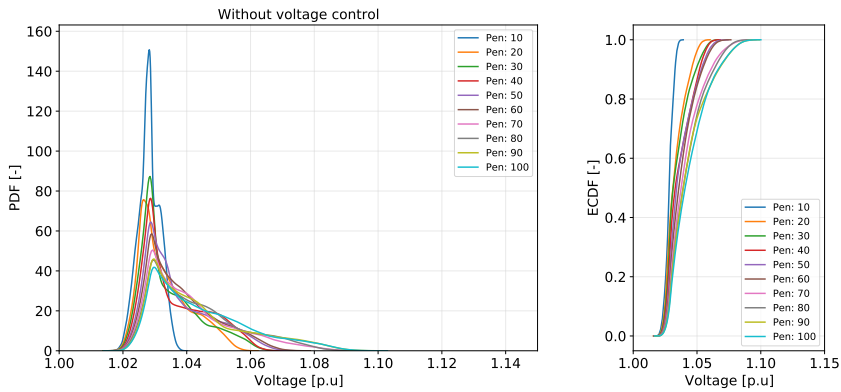


Figure C.8: PDF and ECDF of the voltage levels in the network with Group C cases.

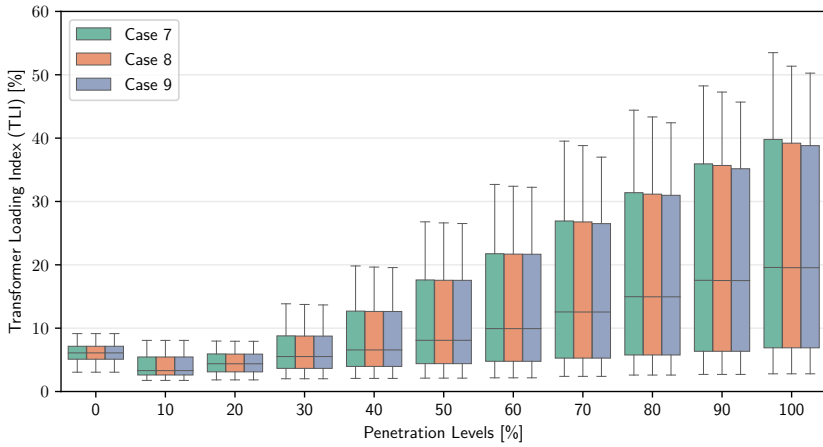


Figure C.9: Transformer loading index with Group C cases.

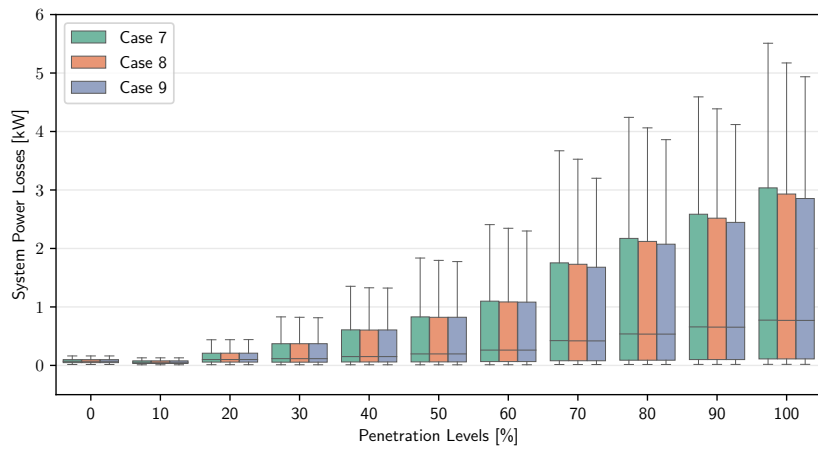


Figure C.10: System power losses with Group C cases.

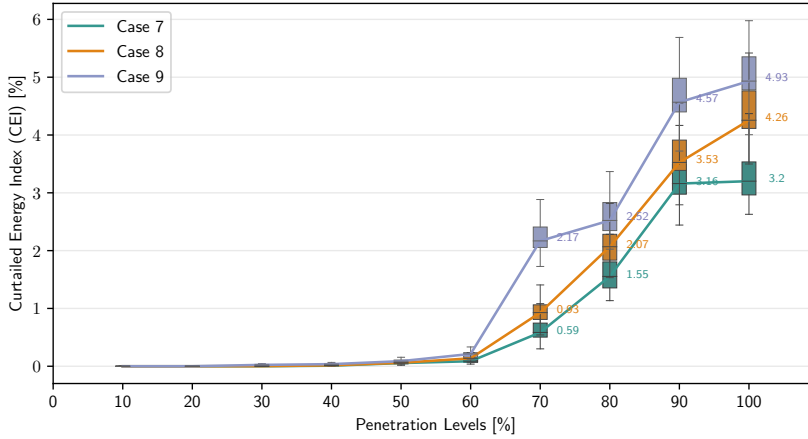


Figure C.11: Curtailed energy index with Group C cases.

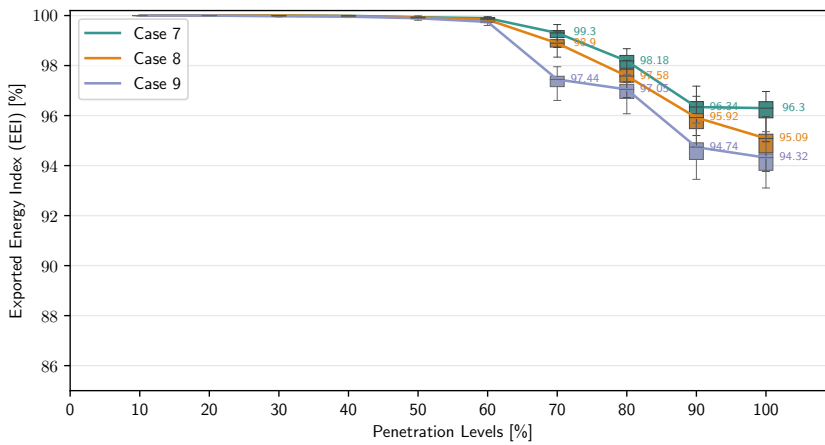


Figure C.12: Exported energy index with Group C cases.

References

- [1] United Nation Climate Change Conference UK2021, “COP26 goals,” 2021. [Online]. Available: <http://https://ukcop26.org/cop26-goals/>
- [2] European Parliament, Fact Sheets on the European Union, “Renewable energy,” 2021. [Online]. Available: <https://www.europarl.europa.eu/factsheets/en/sheet/70/renewable-energy>
- [3] Government of the Netherlands, “Dutch goals within EU,” 2021. [Online]. Available: <https://www.government.nl/topics/climate-change/eu-policy>
- [4] S. Minniti, N. Haque, P. Nguyen, and G. Pemen, “Local Markets for Flexibility Trading : Key Stages,” *Energies*, vol. 11, no. 11, pp. 1–21, 2018.
- [5] International Energy Agency (IEA), “Renewables 2021 - Analysis and forecast to 2026,” Tech. Rep., 2021.
- [6] I. Colak, S. Sagiroglu, G. Fulli, M. Yesilbudak, and C. F. Covrig, “A survey on the critical issues in smart grid technologies,” *Renewable and Sustainable Energy Reviews*, vol. 54, pp. 396–405, 2016. [Online]. Available: <http://dx.doi.org/10.1016/j.rser.2015.10.036>
- [7] T. Mai, A. Haque, T. Vo, P. Nguyen, and M. Pham, “Development of ICT Infrastructure for Physical LV Microgrids,” in *IEEE International Conference on Environment and Electrical Engineering and IEEE Industrial and Commercial Power Systems Europe, EEEIC/I and CPS Europe*, 2018.
- [8] T. T. Mai, P. H. Nguyen, Q. Tuan, T. Alessia, C. Giovanni, and D. C. Yassine, “An overview of grid edge control with the digital transformation,” *Electrical Engineering*, 2021. [Online]. Available: <https://doi.org/10.1007/s00202-020-01209-x>
- [9] M. Alberto, G. M. Soares, L. R. Silva, C. A. Duque, I. C. Decker, P. F. Ribeiro, E. L. Junio, A. D. Fvaro, and L. F. Passos, “Newly Implemented Real-Time PQ Monitoring for Transmission 4.0 Substations,” *Electric Power Systems Research*, vol. 204, no. May 2021, p. 107709, 2022. [Online]. Available: <https://doi.org/10.1016/j.epsr.2021.107709>

- [10] T. Morstyn, B. Hredzak, and V. G. Agelidis, "Control Strategies for Microgrids with Distributed Energy Storage Systems: An Overview," *IEEE Transactions on Smart Grid*, vol. 9, no. 4, pp. 3652–3666, 2018.
- [11] J. Liu, Y. Xiao, S. Li, W. Liang, and C. L. P. Chen, "Cyber Security and Privacy Issues in Smart Grids," *IEEE Communications Surveys Tutorials*, vol. 14, no. 4, pp. 981–997, 2012.
- [12] M. H. Andishgar, E. Gholipour, and R. Allah Hooshmand, "An overview of control approaches of inverter-based microgrids in islanding mode of operation," *Renewable and Sustainable Energy Reviews*, vol. 80, no. August, pp. 1043–1060, 2017.
- [13] Z.-j. Wang and Z.-z. Guo, "Uncertain models of renewable energy sources," *The Journal of Engineering*, vol. 2017, no. 13, pp. 849–853, 2017.
- [14] F. Martin-Martínez, A. Sánchez-Miralles, and M. Rivier, "A literature review of Microgrids: A functional layer based classification," *Renewable and Sustainable Energy Reviews*, vol. 62, pp. 1133–1153, 2016.
- [15] M. M. Haque and P. Wolfs, "A review of high PV penetrations in LV distribution networks: Present status, impacts and mitigation measures," *Renewable and Sustainable Energy Reviews*, vol. 62, pp. 1195–1208, 2016. [Online]. Available: <http://dx.doi.org/10.1016/j.rser.2016.04.025>
- [16] K. E. Antoniadou-ptytaria, I. N. Kouveliotis-lysikatos, S. Member, P. S. Georgilakis, S. Member, and N. D. Hatziargyriou, "Distributed and Decentralized Voltage Control of Smart Distribution Networks : Models , Methods , and Future Research," *IEEE Transactions on Smart Grid*, vol. 8, no. 6, pp. 2999–3008, 2017.
- [17] The Union of the Electricity Industry (Eurelectric), "Active Distribution System Management A key tool for the smooth integration," *Euroelectric paper*, no. February, 2013.
- [18] R. Bayindir, E. Hossain, E. Kabalci, and R. Perez, "A Comprehensive Study on Microgrid Technology," *International Journal of Renewable Energy Research*, vol. 4, no. 4, pp. 1094–1107, 2014.
- [19] M. Karimi, H. Mokhlis, K. Naidu, S. Uddin, and A. H. Bakar, "Photovoltaic penetration issues and impacts in distribution network - A review," *Renewable and Sustainable Energy Reviews*, vol. 53, pp. 594–605, 2016. [Online]. Available: <http://dx.doi.org/10.1016/j.rser.2015.08.042>
- [20] B. M. Chen and H. V. Poor, "High-Frequency Power Electronics at the Grid Edge: A Bottom-Up Approach Toward the Smart Grid," *IEEE Electrification Magazine*, no. 3, pp. 6–17, 2020.

- [21] R. Fonteijn, M. Amstel, P. Nguyen, J. Morren, G. Maarten Bonnema, and H. Slootweg, "Evaluating flexibility values for congestion management in distribution networks within Dutch pilots," *The Journal of Engineering*, vol. 2019, no. 18, pp. 5158–5162, 2019.
- [22] A. Haque, P. Nguyen, T. Vo, and F. Blik, "Agent-based unified approach for thermal and voltage constraint management in LV distribution network," *Electric Power Systems Research*, vol. 143, pp. 462–473, 2017.
- [23] E. Veldman, "Power Play Impacts of flexibility in future residential electricity demand on distribution network utilisation," Ph.D. dissertation, Technische Universiteit Eindhoven, 2013.
- [24] A. G. Anastasiadis, G. P. Kondylis, A. Polyzakis, and G. Vokas, "Effects of increased electric vehicles into a distribution network," *Energy Procedia*, vol. 157, pp. 586–593, 2019. [Online]. Available: <https://doi.org/10.1016/j.egypro.2018.11.223>
- [25] H. Han, X. Hou, J. Yang, J. Wu, M. Su, and J. M. Guerrero, "Review of power sharing control strategies for islanding operation of AC microgrids," *IEEE Transactions on Smart Grid*, vol. 7, no. 1, pp. 200–215, 2016.
- [26] L. Shang, J. Hu, X. Yuan, and Y. Chi, "Understanding inertial response of variable-speed wind turbines by defined internal potential vector," *Energies*, vol. 10, no. 1, pp. 1–17, 2017.
- [27] U. Tamrakar, D. Shrestha, M. Maharjan, B. Bhattarai, T. Hansen, and R. Tonkoski, "Virtual Inertia: Current Trends and Future Directions," *Applied Sciences*, vol. 7, no. 7, p. 654, 2017. [Online]. Available: <http://www.mdpi.com/2076-3417/7/7/654>
- [28] M. Ferdowsi, A. Benigni, A. Lowen, B. Zargar, A. Monti, and F. Ponci, "A scalable data-driven monitoring approach for distribution systems," *IEEE Transactions on Instrumentation and Measurement*, vol. 64, no. 5, pp. 1292–1305, 2015.
- [29] European Commission, "Directive (EU) 2018/2001 of the European Parliament and of the Council on the promotion of the use of energy from renewable sources," *Official Journal of the European Union*, vol. 2018, no. 328, pp. 82–209, 2018.
- [30] B. P. Koirala, E. Koliou, J. Friege, R. A. Hakvoort, and P. M. Herder, "Energetic communities for community energy: A review of key issues and trends shaping integrated community energy systems," *Renewable and Sustainable Energy Reviews*, vol. 56, pp. 722–744, 2016.
- [31] S. Energy2I, "WhitePaper Layered Energy System," Tech. Rep. November, 2018.

- [32] A. Barbato, A. Dedè, D. Della, G. Massa, A. Angioni, G. Lipari, F. Ponci, and S. Repo, "Lessons learnt from real-time monitoring of the low voltage distribution network," *Sustainable Energy, Grids and Networks*, vol. 15, pp. 76–85, 2018.
- [33] M. A. Khan and B. Hayes, "PTP-based time synchronisation of smart meter data for state estimation in power distribution networks," *IET Smart Grid*, vol. 3, no. 5, pp. 705–712, 2020.
- [34] Y. L. Lo, S. C. Huang, and C. N. Lu, "Transformational benefits of AMI data in transformer load modeling and management," *IEEE Transactions on Power Delivery*, vol. 29, no. 2, pp. 742–750, 2014.
- [35] M. Pau, E. Patti, L. Barbierato, A. Estebasari, E. Pons, F. Ponci, and A. Monti, "Low voltage system state estimation based on smart metering infrastructure," *IEEE International Workshop on Applied Measurements for Power Systems (AMPS 2016)*, 2016.
- [36] C. S. Kumar, K. Rajawat, S. Chakrabarti, and B. C. Pal, "Robust distribution system state estimation with hybrid measurements," *IET Generation, Transmission and Distribution*, vol. 14, no. 16, pp. 3250–3259, 2020.
- [37] F. Ni, P. Nguyen, J. Cobben, H. V. den Brom, and D. Zhao, "Three-phase state estimation in the medium-voltage network with aggregated smart meter data," *Electrical Power and Energy Systems*, vol. 98, pp. 463–473, 2018.
- [38] Y. Kinoshita, K. Iwabuchi, and Y. Miyazaki, "Distribution voltage monitoring and control utilising smart meters," in *International Conference and Exhibition on Electricity Distribution (CIRED)*, vol. 2017, Glasgow, 2017, pp. 1043–1047.
- [39] K. Nainar, "Smart Meter Measurement-Based State Estimation for Monitoring of Low-Voltage Distribution Grids," *Energies*, vol. 13, 2020.
- [40] S. Lu, S. Repo, D. D. Giustina, F. A. C. Figuerola, A. Lof, and M. Pikkarainen, "Real-Time Low Voltage Network Monitoring - ICT Architecture and Field Test Experience," *IEEE Transactions on Smart Grid*, vol. 6, no. 4, pp. 2002–2012, 2015.
- [41] B. Yildiz, J. I. Bilbao, J. Dore, and A. B. Sproul, "Recent advances in the analysis of residential electricity consumption and applications of smart meter data," *Applied Energy*, vol. 208, pp. 402–427, 2017.
- [42] L. M. Candanedo, V. Feldheim, and D. Deramaix, "Data driven prediction models of energy use of appliances in a low-energy house," *Energy and Buildings*, vol. 140, pp. 81–97, 2017.

- [43] R. K. Jain, K. M. Smith, P. J. Culligan, and J. E. Taylor, "Forecasting energy consumption of multi-family residential buildings using support vector regression: Investigating the impact of temporal and spatial monitoring granularity on performance accuracy," *Applied Energy*, vol. 123, pp. 168–178, 2014.
- [44] N. Yampikulsakul, E. Byon, S. Huang, S. Sheng, and M. You, "Condition monitoring of wind power system with nonparametric regression analysis," *IEEE Transactions on Energy Conversion*, vol. 29, no. 2, pp. 288–299, 2014.
- [45] D. Zafirakis, G. Tzanesa, and J. K. Kaldellisa, "Forecasting of wind power generation with the use of Artificial Neural Networks and Support Vector Regression Models," *Energy Procedia*, vol. 159, pp. 509–514, 2019. [Online]. Available: <https://doi.org/10.1016/j.egypro.2018.12.007>
- [46] M. Hassanzadeh and C. Y. Evrenosoğlu, "A regression analysis based state transition model for power system dynamic state estimation," *NAPS 2011 - 43rd North American Power Symposium*, 2011.
- [47] M.-Q. Tran, A. S. Zamzam, P. H. Nguyen, and G. Pemen, "Multi-Area Distribution System State Estimation Using Decentralized Physics-Aware Neural Networks," *Energies*, vol. 14, no. 3025, pp. 1–13, 2021.
- [48] S. Wang, P. Dong, and Y. Tian, "A novel method of statistical line loss estimation for distribution feeders based on feeder cluster and modified XGBoost," *Energies*, vol. 10, no. 2067, pp. 1–17, 2017.
- [49] M. V. Suganyadevi, C. K. Babulal, and S. Kalyani, "Assessment of voltage stability margin by comparing various support vector regression models," *Soft Computing*, vol. 20, pp. 807–818, 2016. [Online]. Available: <http://dx.doi.org/10.1007/s00500-014-1544-x>
- [50] H. D. Abbood and A. Benigni, "Data-Driven Modeling of a Commercial Photovoltaic Microinverter," *Modelling and Simulation in Engineering*, vol. 2018, pp. 1–11, 2018.
- [51] O. Abdel-Rahim, H. Funato, and J. Haruna, "Grid-connected boost inverter for low-power PV applications with model predictive control," *The Journal of Engineering*, vol. 2017, no. 7, pp. 318–326, 2017.
- [52] N. C. Sintamarean, F. Blaabjerg, H. Wang, and Y. Yang, "Real field mission profile oriented design of a SiC-Based PV-inverter application," *IEEE Transactions on Industry Applications*, vol. 50, no. 6, pp. 4082–4089, 2014.
- [53] A. Halu, A. Scala, A. Khiyami, and M. C. González, "Data-driven modeling of solar-powered urban microgrids," *Science Advances*, vol. 2, no. 1, 2016.

- [54] R. Relan, Y. Firouz, J. M. Timmermans, and J. Schoukens, "Data-Driven Nonlinear Identification of Li-Ion Battery Based on a Frequency Domain Nonparametric Analysis," *IEEE Transactions on Control Systems Technology*, vol. 25, no. 5, pp. 1825–1832, 2017.
- [55] J. Windahl, H. Runvik, and S. Velut, "Platform for Microgrid Design and Operation," in *13th International Modelica Conference, Regensburg, Germany*, vol. 157, 2019, pp. 405–412.
- [56] O. Abrishambaf, P. Faria, L. Gomes, Z. Vale, and J. M. Corchado, "Implementation of a Real-Time Microgrid Simulation Platform Based on Centralized and Distributed Management," *Energies*, vol. 10, no. 6, 2017.
- [57] R. AhmadiAhangar, A. Rosin, A. N. Niaki, I. Palu, and T. Korótko, "A review on real-time simulation and analysis methods of microgrids," *International Transactions on Electrical Energy Systems*, vol. 29, no. 11, pp. 1–16, 2019.
- [58] A. Cagnano, E. De Tuglie, and P. Mancarella, "Microgrids: Overview and guidelines for practical implementations and operation," *Applied Energy*, vol. 258, no. November 2019, p. 114039, 2020. [Online]. Available: <https://doi.org/10.1016/j.apenergy.2019.114039>
- [59] A. Rojas and T. Rousan, "Microgrid Control Strategy: Derived from Stakeholder Requirements Analysis," *IEEE Power and Energy Magazine*, vol. 15, no. 4, pp. 72–79, jul 2017. [Online]. Available: <http://ieeexplore.ieee.org/document/7947249/>
- [60] D. K. Molzahn, F. Dörfler, H. Sandberg, S. H. Low, S. Chakrabarti, R. Baldick, and J. Lavaei, "A Survey of Distributed Optimization and Control Algorithms for Electric Power Systems," *IEEE Transactions on Smart Grid*, vol. 8, no. 6, pp. 2941–2962, 2017.
- [61] A. Dimeas, A. Tsikalakis, G. Kariniotakis, and G. Korres, "Microgrid Control Issues," in *Microgrids Architectres and Control*, 2014, p. 315.
- [62] D. E. Olivares, A. Mehrizi-Sani, A. H. Etemadi, C. A. Cañizares, R. Iravani, M. Kazerani, A. H. Hajimiragha, O. Gomis-Bellmunt, M. Saadifard, R. Palma-Behnke, G. A. Jiménez-Estévez, and N. D. Hatziaargyriou, "Trends in microgrid control," *IEEE Transactions on Smart Grid*, vol. 5, no. 4, pp. 1905–1919, 2014.
- [63] M. Yazdani and A. Mehrizi-Sani, "Distributed control techniques in microgrids," *IEEE Transactions on Smart Grid*, vol. 5, no. 6, pp. 2901–2909, 2014.
- [64] S. Karagiannopoulos, P. Aristidou, and G. Hug, "Data-Driven Local Control Design for Active Distribution Grids Using Off-Line Optimal Power Flow and Machine Learning Techniques," *IEEE Transactions on Smart Grid*, vol. 10, no. 6, pp. 6461–6471, 2019.

- [65] J. Rocabert, A. Luna, F. Blaabjerg, and I. Paper, "Control of Power Converters in AC Microgrids," *IEEE Transactions on Power Electronics*, vol. 27, no. 11, pp. 4734–4749, 2012.
- [66] J. M. Guerrero, M. Chandorkar, T. Lee, and P. C. Loh, "Advanced Control Architectures for Intelligent Microgrids; Part I: Decentralized and Hierarchical Control," *Industrial Electronics, IEEE Transactions on*, vol. 60, no. 4, pp. 1254–1262, 2013.
- [67] O. Palizban, K. Kauhaniemi, and J. M. Guerrero, "Microgrids in active network management - Part I: Hierarchical control, energy storage, virtual power plants, and market participation," *Renewable and Sustainable Energy Reviews*, vol. 36, pp. 428–439, 2014. [Online]. Available: <http://dx.doi.org/10.1016/j.rser.2014.01.016>
- [68] L. Meng, E. R. Sanseverino, A. Luna, T. Dragicevic, J. C. Vasquez, and J. M. Guerrero, "Microgrid supervisory controllers and energy management systems: A literature review," *Renewable and Sustainable Energy Reviews*, vol. 60, pp. 1263–1273, 2016. [Online]. Available: <http://dx.doi.org/10.1016/j.rser.2016.03.003>
- [69] S. Anand, B. G. Fernandes, and J. M. Guerrero, "Distributed control to ensure proportional load sharing and improve voltage regulation in low-voltage DC microgrids," *IEEE Transactions on Power Electronics*, vol. 28, no. 4, pp. 1900–1913, 2013.
- [70] M. Shahidehpour, Z. Li, S. Bahramirad, Z. Li, and W. Tian, "Networked Microgrids: Exploring the Possibilities of the IIT-Bronzeville Grid," *IEEE Power and Energy Magazine*, vol. 15, no. 4, pp. 63–71, jul 2017. [Online]. Available: <http://ieeexplore.ieee.org/document/7947305/>
- [71] J. M. Guerrero, J. C. Vasquez, J. Matas, L. G. De Vicuña, and M. Castilla, "Hierarchical control of droop-controlled AC and DC microgrids - A general approach toward standardization," *IEEE Transactions on Industrial Electronics*, vol. 58, no. 1, pp. 158–172, 2011.
- [72] L. Ortiz, J. W. Gonz, L. B. Gutierrez, and O. Llanes-santiago, "A review on control and fault-tolerant control systems of AC/DC microgrids," *Heliyon*, vol. 6, no. 8, 2020.
- [73] F. Olivier, P. Aristidou, D. Ernst, and T. V. Cutsem, "Active Management of Low-Voltage Networks for Mitigating Overvoltages Due to Photovoltaic Units," *IEEE Transactions on Smart Grid*, vol. 7, no. 2, pp. 926–936, 2016.
- [74] M. Zeraati, M. E. H. Golshan, and J. M. Guerrero, "A Consensus-Based Cooperative Control of PEV Battery and PV Active Power Curtailment for Voltage Regulation in Distribution Networks," *IEEE Transactions on Smart Grid*, vol. 3053, no. 1, pp. 1–11, 2017.

- [75] M. J. Morshed and A. Fekih, "A Fault-Tolerant Control Paradigm for Microgrid-Connected Wind Energy Systems," *IEEE Systems Journal*, pp. 1–13, 2016.
- [76] S. Minniti, A. N. Haque, N. G. Paterakis, and P. H. Nguyen, "A hybrid robust-stochastic approach for the day-ahead scheduling of an EV aggregator," in *IEEE PES Powertech 2019 Milano*. IEEE, 2019, pp. 1–6.
- [77] X. Chen, Y. Du, and H. Wen, "Forecasting Based Power Ramp-Rate Control For PV Systems Without Energy Storage," in *2017 IEEE 3rd International Future Energy Electronics Conference and ECCE Asia (IFEEC 2017 - ECCE Asia)*. IEEE, 2017, pp. 733–738.
- [78] M. Lei, Z. Yang, Y. Wang, H. Xu, L. Meng, J. C. Vasquez, and J. M. Guerrero, "An MPC-Based ESS Control Method for PV Power Smoothing Applications," *IEEE Transactions on Power Electronics*, vol. 33, no. 3, pp. 2136–2144, 2018.
- [79] T. Degner, N. Soultanis, A. Engler, and A. G. de Muro, "Intelligent local controllers," in *Microgrids: Architectures and Control*, 2013, pp. 81–116.
- [80] J. Kim, J. M. Guerrero, P. Rodriguez, R. Teodorescu, and K. Nam, "Mode adaptive droop control with virtual output impedances for an inverter-based flexible AC microgrid," *IEEE Transactions on Power Electronics*, vol. 26, no. 3, pp. 689–701, 2011.
- [81] Y. Yang, K. A. Kim, F. Blaabjerg, and A. Sangwongwanich, "Flexible active power control of PV systems," in *Advances in Grid-Connected Photovoltaic Power Conversion Systems*, 2019, pp. 153–185.
- [82] X. Liu, A. Aichhorn, and L. Liu, "Coordinated Control of Distributed Energy Storage System With Tap Changer Transformers for Voltage Rise Mitigation Under High Photovoltaic Penetration," vol. 3, no. 2, pp. 897–906, 2012.
- [83] M. J. E. Alam, K. M. Muttaqi, and D. Sutanto, "Mitigation of Rooftop Solar PV Impacts and Evening Peak Support by Managing Available Capacity of Distributed Energy Storage Systems," vol. 28, no. 4, pp. 3874–3884, 2013.
- [84] —, "Distributed Energy Storage for Mitigation of Voltage-rise Impact caused by Rooftop Solar PV," in *IEEE PES General Meeting*. IEEE, 2012, pp. 1–8.
- [85] Y. Wang, K. T. Tan, X. Y. Peng, and P. L. So, "Coordinated Control of Distributed Energy-Storage Systems for Voltage Regulation in Distribution Networks," *IEEE Transactions on Power Delivery*, vol. 31, no. 3, pp. 1132–1141, 2016.
- [86] F. Marra, G. Yang, C. Træholt, J. Østergaard, S. Member, and E. Larsen, "A Decentralized Storage Strategy for Residential Feeders With Photovoltaics," vol. 5, no. 2, pp. 974–981, 2014.

- [87] M. N. Kabir, Y. Mishra, G. Ledwich, Z. Y. Dong, and K. P. Wong, "Coordinated control of grid-connected photovoltaic reactive power and battery energy storage systems to improve the voltage profile of a residential distribution feeder," *IEEE Transactions on Industrial Informatics*, vol. 10, no. 2, pp. 967–977, 2014.
- [88] M. Chamana, B. H. Chowdhury, and F. Jahanbakhsh, "Distributed control of voltage regulating devices in the presence of high PV penetration to mitigate ramp-rate issues," *IEEE Transactions on Smart Grid*, vol. 9, no. 2, pp. 1086–1095, 2018.
- [89] R. K. Lam and H.-g. Yeh, "PV Ramp Limiting Controls with Adaptive Smoothing Filter through a Battery Energy Storage System," in *2014 IEEE Green Energy and Systems Conference (IGESC)*. IEEE, 2014, pp. 55–60.
- [90] A. Samadi, E. Shayesteh, R. Eriksson, B. Rawn, and L. Söder, "Multi-objective coordinated droop-based voltage regulation in distribution grids with PV systems," *Renewable Energy*, vol. 71, no. 3, pp. 315–323, 2014.
- [91] J. Li, K. Cheng, S. Wang, F. Morstatter, R. P. Trevino, J. Tang, and H. Liu, "Feature selection: a data perspective," *ACM Computing Survey*, vol. 50, no. 6, pp. 163–193, 2017.
- [92] V. M. Mansoor, P. H. Nguyen, and W. L. Kling, "An integrated control for over-voltage mitigation in the distribution network," in *IEEE PES Innovative Smart Grid Technologies Conference Europe*, 2015, pp. 1–6.
- [93] Q. C. Zhong, "Robust droop controller for accurate proportional load sharing among inverters operated in parallel," *IEEE Transactions on Industrial Electronics*, vol. 60, no. 4, pp. 1281–1290, 2013.
- [94] S. Ghosh, S. Rahman, and M. Pipattanasomporn, "Distribution Voltage Regulation Through Active Power Curtailment With PV Inverters and Solar Generation Forecasts," *IEEE Transactions on Sustainable Energy*, vol. 8, no. 1, pp. 13–22, 2017.
- [95] E. Dall'Anese, S. V. Dhople, B. B. Johnson, and G. B. Giannakis, "Optimal dispatch of photovoltaic inverters in residential distribution systems," *IEEE Transactions on Sustainable Energy*, vol. 5, no. 2, pp. 487–497, 2014.
- [96] T. Stetz, F. Marten, and M. Braun, "Improved low voltage grid-integration of photovoltaic systems in Germany," *IEEE Transactions on Sustainable Energy*, vol. 4, no. 2, pp. 534–542, 2013.
- [97] M. J. Alam, K. M. Muttaqi, and D. Sutanto, "A multi-mode control strategy for VAR support by solar PV inverters in distribution networks," *IEEE Transactions on Power Systems*, vol. 30, no. 3, pp. 1316–1326, 2015.

- [98] F. Marra, Y. T. Fawzy, T. Bülo, and B. Blažič, “Energy Storage Options for Voltage Support in Low-Voltage Grids with High Penetration of Photovoltaic,” pp. 1–7, 2012.
- [99] P. Chaudhary and M. Rizwan, “Voltage regulation mitigation techniques in distribution system with high PV penetration: A review,” *Renewable and Sustainable Energy Reviews*, vol. 82, pp. 3279–3287, 2018. [Online]. Available: <https://doi.org/10.1016/j.rser.2017.10.017>
- [100] J. Von Appen, T. Stetz, M. Braun, and A. Schmiegel, “Local voltage control strategies for PV storage systems in distribution grids,” *IEEE Transactions on Smart Grid*, vol. 5, no. 2, pp. 1002–1009, 2014.
- [101] G. De Carne, G. Buticchi, and M. Liserre, “Current-type Power Hardware in the Loop (PHIL) evaluation for smart transformer application,” in *Proceedings - 2018 IEEE International Conference on Industrial Electronics for Sustainable Energy Systems, IESES 2018*, vol. 2018-Janua. IEEE, 2018, pp. 529–533.
- [102] K. Turitsyn, P. Šulc, S. Backhaus, and M. Chertkov, “Options for control of reactive power by distributed photovoltaic generators,” *Proceedings of the IEEE*, vol. 99, no. 6, pp. 1063–1073, 2011.
- [103] H. Shareef, M. Islam, and A. Mohamed, “A review of the stage-of-the-art charging technologies , placement methodologies , and impacts of electric vehicles,” *Renewable and Sustainable Energy Reviews*, vol. 64, no. December 2017, pp. 403–420, 2016. [Online]. Available: <http://dx.doi.org/10.1016/j.rser.2016.06.033>
- [104] S. Weckx, C. Gonzalez, and J. Driesen, “Combined central and local active and reactive power control of PV inverters,” *IEEE Transactions on Sustainable Energy*, vol. 5, no. 3, pp. 776–784, 2014.
- [105] S. Ghosh, S. Rahman, and M. Pipattanasomporn, “Local distribution voltage control by reactive power injection from PV inverters enhanced with active power curtailment,” *IEEE Power and Energy Society General Meeting*, vol. 2014-October, no. October, 2014.
- [106] A. Garg, M. Jalali, V. Kekatos, V. Tech, S. Antonio, and S. Antonio, “Kernel-based learning for smart inverter control,” in *2018 IEEE Global Conference on Signal and Information Processing*. IEEE, 2018, pp. 875–879.
- [107] R. Dobbe, O. Sondermeijer, D. Fridovich-keil, D. Arnold, D. Callaway, and C. Tomlin, “Toward Distributed Energy Services : Decentralizing Optimal Power Flow With Machine Learning,” *IEEE Transactions on Smart Grid*, vol. 11, no. 2, pp. 1296–1306, 2020.

- [108] O. Sondermeijer, R. Dobbe, D. Arnold, and C. Tomlin, "Regression-based Inverter Control for Decentralized Optimal Power Flow and Voltage Regulation," in *2016 IEEE Power Energy Society General Meeting*, 2016, pp. 1–5.
- [109] S. Li, Y. Sun, and M. Ramezani, "Artificial Neural Networks for Volt / VAR Control of DER Inverters at the Grid Edge," *IEEE Transactions on Smart Grid*, vol. 10, no. 5, pp. 5564–5573, 2019.
- [110] J. Salpakari and P. Lund, "Optimal and rule-based control strategies for energy flexibility in buildings with PV," *Applied Energy*, vol. 161, pp. 425–436, 2016. [Online]. Available: <http://dx.doi.org/10.1016/j.apenergy.2015.10.036>
- [111] B. Zhang, A. Y. S. Lam, and A. D. Domínguez-garcía, "An Optimal and Distributed Method for Voltage Regulation in Power Distribution Systems," *IEEE Transactions on Power Systems*, vol. 30, no. 4, pp. 1714–1726, 2015.
- [112] S. Alyami, Y. Wang, C. Wang, J. Zhao, and B. Zhao, "Adaptive real power capping method for fair overvoltage regulation of distribution networks with high penetration of PV systems," *IEEE Transactions on Smart Grid*, vol. 5, no. 6, pp. 2729–2738, 2014.
- [113] V. Loia, S. Member, A. Vaccaro, S. Member, and K. Vaisakh, "A Self-Organizing Architecture Based on Cooperative Fuzzy Agents for Smart Grid Voltage Control," *IEEE Transactions on Industrial Informatics*, vol. 9, no. 3, pp. 1415–1422, 2013.
- [114] T. L. Nguyen, Y. Wang, Q. T. Tran, R. Caire, Y. Xu, and Y. Besanger, "Agent-based Distributed Event-Triggered Secondary Control for Energy Storage System in Islanded Microgrids - Cyber-Physical Validation," *Proceedings - 2019 IEEE International Conference on Environment and Electrical Engineering and 2019 IEEE Industrial and Commercial Power Systems Europe, IEEEICIE and CPS Europe 2019*, pp. 0–5, 2019.
- [115] Y. Wang, T.-L. Nguyen, Y. Xu, Q.-T. Tran, and R. Caire, "Peer-to-Peer Control for Networked Microgrids: Multi-Layer and Multi-Agent Architecture Design," *IEEE Transactions on Smart Grid*, vol. 3053, no. c, pp. 1–11, 2020.
- [116] S. Weckx, R. D'Hulst, B. Claessens, and J. Driesensam, "Multi-agent charging of electric vehicles respecting distribution transformer loading and voltage limits," *IEEE Transactions on Smart Grid*, vol. 5, no. 6, pp. 2857–2867, 2014.
- [117] G. Valverde and T. Van Cutsem, "Model predictive control of voltages in active distribution networks," *IEEE Transactions on Smart Grid*, vol. 4, no. 4, pp. 2152–2161, 2013.
- [118] G. Reynders, T. Nuytten, and D. Saelens, "Potential of structural thermal mass for demand-side management in dwellings," *Building and Environment*, vol. 64, no. April, pp. 187–199, 2013.

- [119] Y. Yang, K. A. Kim, F. Blaabjerg, and A. Sangwongwanich, "Power electronic technologies for PV systems," *Advances in Grid-Connected Photovoltaic Power Conversion Systems*, pp. 15–43, 2019.
- [120] T. Mai, M. Salazar, A. Haque, and P. Nguyen, "Stochastic modelling of the correlation between transformer loading and distributed energy resources in LV distribution networks," in *International Conference and Exhibition on Electricity Distribution (CIRED)*, Berlin, Germany, 2020, pp. 1–5.
- [121] T. T. Mai, P. H. Nguyen, N. A. Haque, and G. A. Pemen, "Exploring regression models to enable monitoring capability of local energy communities for self-management in low-voltage distribution networks," *IET Smart Grid*, vol. 5, no. 1, pp. 25–41, 2022.
- [122] P. P. Vergara, T. T. Mai, A. Burstein, and P. H. Nguyen, "Feasibility and Performance Assessment of Commercial PV Inverters Operating with Droop Control for Providing Voltage Support Services," *IEEE PES Innovative Smart Grid Technologies Europe (ISGT-Europe)*, pp. 2–6, 2019.
- [123] A. N. Haque, P. H. Nguyen, F. W. Bliet, and J. G. Slootweg, "Demand response for real-time congestion management incorporating dynamic thermal overloading cost," *Sustainable Energy, Grids and Networks*, vol. 10, pp. 65–74, 2017.
- [124] D. Alahakoon and X. Yu, "Smart Electricity Meter Data Intelligence for Future Energy Systems : A Survey," *IEEE Transactions on Industrial Informatics*, vol. 12, no. 1, pp. 425–436, 2016.
- [125] Y. Wang, S. Member, Q. Chen, and S. Member, "Review of Smart Meter Data Analytics : Applications , Methodologies , and Challenges," *IEEE Transactions on Smart Grid*, vol. 10, no. 3, pp. 3125–3148, 2019.
- [126] P. P. Vergara, M. Salazar, T. T. Mai, P. H. Nguyen, and H. Slootweg, "A comprehensive assessment of PV inverters operating with droop control for overvoltage mitigation in LV distribution networks," *Renewable Energy*, vol. 159, pp. 172–183, 2020.
- [127] F. Ni, P. H. Nguyen, and J. F. Cobben, "Basis-Adaptive Sparse Polynomial Chaos Expansion for Probabilistic Power Flow," *IEEE Transactions on Power Systems*, vol. 32, no. 1, pp. 694–704, 2017.
- [128] A. Dobos, "PVWatts Version 5 Manual - Technical Report NREL/TP-6A20-62641," Tech. Rep., 2014.
- [129] "Royal Netherlands Meteorological Institute (KNMI) - Hourly weather data in the Netherlands," 2020. [Online]. Available: <http://projects.knmi.nl/klimatologie/uurgegevens/selectie.cgi>

- [130] M. Ferdowsi, A. Benigni, A. Monti, and F. Ponci, "Measurement Selection for Data-Driven Monitoring of Distribution Systems," *IEEE Systems Journal*, vol. 13, no. 4, pp. 4260–4268, 2019.
- [131] S. Morgenthaler, "Exploratory data analysis," *WIREs Computational Statistics*, vol. 1, no. 1, pp. 33–44, 2009.
- [132] H. J. Seltman, "Chapter 4 Exploratory Data Analysis," in *Experimental Design and Analysis*. Carnegie Mellon University, 2018, pp. 61–100.
- [133] J. Miao and L. Niu, "A Survey on Feature Selection," *Procedia Computer Science*, vol. 91, pp. 919–926, 2016.
- [134] B. Xue, M. Zhang, W. N. Browne, and X. Yao, "A Survey on Evolutionary Computation Approaches to Feature Selection," *IEEE Transactions on Evolutionary Computation*, vol. 20, no. 4, pp. 606–626, 2016.
- [135] G. Chandrashekar and F. Sahin, "A survey on feature selection methods," *Computers and Electrical Engineering*, vol. 40, no. 1, pp. 16–28, 2014.
- [136] S. Raschka, "Model Evaluation , Model Selection, and Algorithm Selection in Machine Learning," 2018.
- [137] G. C. McDonald, "Ridge regression," *WIREs Computational Statistics*, vol. 1, no. 1, pp. 93–100, 2009.
- [138] J. Hawkins, "Support Vector Regression," in *Efficient Learning Machines*. Apress, Berkeley, CA, 2015, pp. 67–80.
- [139] E. Scornet, "Random forests and kernel methods," *IEEE Transactions on Information Theory*, vol. 62, no. 3, pp. 1485–1500, 2016.
- [140] M. W. Ahmad, J. Reynolds, and Y. Rezgui, "Predictive modelling for solar thermal energy systems: A comparison of support vector regression, random forest, extra trees and regression trees," *Journal of Cleaner Production*, vol. 203, pp. 810–821, 2018. [Online]. Available: <https://doi.org/10.1016/j.jclepro.2018.08.207>
- [141] T. Chen and C. Guestrin, "XGBoost : A Scalable Tree Boosting System," in *Proceedings of the 22nd ACM SIGKDD International Conference on Knowledge Discovery and Data*, 2016, pp. 785–794.
- [142] H. Lu, F. Cheng, X. Ma, and G. Hu, "Short-term prediction of building energy consumption employing an improved extreme gradient boosting model: A case study of an intake tower," *Energy*, vol. 203, p. 117756, 2020. [Online]. Available: <https://doi.org/10.1016/j.energy.2020.117756>

- [143] G. James, D. Witten, T. Hastie, and R. Tibshirani, *An introduction to statistical learning with applications in R*. Springer, 2013.
- [144] G. Li and P. Niu, “An enhanced extreme learning machine based on ridge regression for regression,” *Neural Computing and Applications*, vol. 22, pp. 803–810, 2013.
- [145] O. Kramer, *Machine learning for evolution strategies*, 2016.
- [146] T. Hastie, R. Tibshirani, and J. Friedman, *The elements of statistical learning*. Springer, 2008.
- [147] A. Vehtari, A. Gelman, and J. Gabry, “Practical Bayesian model evaluation using leave-one-out cross-validation and WAIC,” *Statistics and Computing*, vol. 27, pp. 1413–1432, 2017.
- [148] E. Mocanu, P. H. Nguyen, M. Gibescu, and W. L. Kling, “Deep learning for estimating building energy consumption,” *Sustainable Energy, Grids and Networks*, vol. 6, pp. 91–99, 2016.
- [149] O. Maimon, L. Rokach, and S. Edition, *Data mining and knowledge discovery*, second ed. Springer, Boston, MA, 2010.
- [150] V. N. Vapnik, “Kernel Ridge Regression,” in *Empirical Inference*. Springer, Berlin, Heidelberg, 2013, pp. 105–116.
- [151] E. Mocanu, P. H. Nguyen, W. L. Kling, and M. Gibescu, “Unsupervised energy prediction in a Smart Grid context using reinforcement cross-building transfer learning,” *Energy and Buildings*, vol. 116, pp. 646–655, 2016. [Online]. Available: <http://dx.doi.org/10.1016/j.enbuild.2016.01.030>
- [152] V. Klonari, J. F. Toubeau, T. L. Vandoorn, B. Meersman, Z. De Grève, J. Lobry, and F. Vallée, “Probabilistic framework for evaluating droop control of photovoltaic inverters,” *Electric Power Systems Research*, vol. 129, pp. 1–9, 2015.
- [153] D. V. Bozalakov, J. Laveyne, J. Desmet, and L. Vandeveld, “Overvoltage and voltage unbalance mitigation in areas with high penetration of renewable energy resources by using the modified three-phase damping control strategy,” *Electric Power Systems Research*, vol. 168, no. April 2018, pp. 283–294, 2019. [Online]. Available: <https://doi.org/10.1016/j.epsr.2018.12.001>
- [154] E. M. S. Duque, P. P. Vergara, P. H. Nguyen, A. Van Der Molen, and J. G. Slootweg, “Conditional Multivariate Elliptical Copulas to Model Residential Load Profiles from Smart Meter Data,” *IEEE Transactions on Smart Grid*, vol. 12, no. 5, pp. 4280–4294, 2021.

- [155] M. M. Viyathukattuva Mohamed Ali, M. Babar, P. H. Nguyen, and J. F. Cobben, "Overlaying control mechanism for solar PV inverters in the LV distribution network," *Electric Power Systems Research*, vol. 145, pp. 264–274, 2017.
- [156] G. Mokhtari, G. Nourbakhsh, F. Zare, and A. Ghosh, "Overvoltage prevention in LV smart grid using customer resources coordination," *Energy and Buildings*, vol. 61, pp. 387–395, 2013. [Online]. Available: <http://dx.doi.org/10.1016/j.enbuild.2013.02.015>
- [157] R. Tonkoski, L. A. Lopes, and T. H. El-Fouly, "Coordinated active power curtailment of grid connected PV inverters for overvoltage prevention," *IEEE Transactions on Sustainable Energy*, vol. 2, no. 2, pp. 139–147, 2011.
- [158] L. Collins and J. K. Ward, "Real and reactive power control of distributed PV inverters for overvoltage prevention and increased renewable generation hosting capacity," *Renewable Energy*, vol. 81, pp. 464–471, 2015.
- [159] S. Y. Mousazade Mousavi, A. Jalilian, M. Savaghebi, and J. M. Guerrero, "Coordinated control of multifunctional inverters for voltage support and harmonic compensation in a grid-connected microgrid," *Electric Power Systems Research*, vol. 155, pp. 254–264, 2018. [Online]. Available: <http://dx.doi.org/10.1016/j.epsr.2017.10.016>
- [160] European Committee for Standards - Electrical, "EN 50438:2013 - Requirements for micro-generating plants to be connected in parallel with public low-voltage distribution networks," 2013.
- [161] T. R. Ricciardi, K. Petrou, J. F. Franco, and L. F. Ochoa, "Defining Customer Export Limits in PV-Rich Low Voltage Networks," *IEEE Transactions on Power Systems*, vol. 34, no. 1, pp. 87–97, 2019.
- [162] IEEE PES AMPS DSAS Test Feeder Working Group, "2015 Test Feeder Cases - European Low Voltage Test Feeder." [Online]. Available: <https://site.ieee.org/pes-testfeeders/resources/>
- [163] T. T. Mai, N. A. N. M. M. Haque, H. T. Vo, and P. H. Nguyen, "Coordinated active and reactive power control for overvoltage mitigation in physical LV microgrids," *The Journal of Engineering*, vol. 2019, no. 18, pp. 5007–5011, 2019.
- [164] C. Long and L. F. Ochoa, "Voltage control of PV-rich LV networks: OLTC-fitted transformer and capacitor banks," *IEEE Transactions on Power Systems*, vol. 31, no. 5, pp. 4016–4025, 2016.
- [165] P. Jahangiri and D. C. Aliprantis, "Distributed Volt/VAr control by PV inverters," *IEEE Transactions on Power Systems*, vol. 28, no. 3, pp. 3429–3439, 2013.

- [166] J. J. Grainger and W. D. Stevenson, *Power System Analysis*. New York: McGraw-Hill Education, 1994.
- [167] A. N. M. Haque, "Smart Congestion Management in Active Distribution Networks," Ph.D. dissertation, 2017.
- [168] Nexans, "Nexans Olex New Zealand Power Cable Catalogue," 2012. [Online]. Available: <https://www.nexans.co.nz/NewZealand/2013/PowerCableCatalogueFullversion2012.pdf>
- [169] T. T. Mai, A. N. M. M. Haque, and P. H. Nguyen, "Consensus-Based Distributed Control for Overvoltage Mitigation in LV Microgrids," in *IEEE PES Powertech*, Milan, 2019.
- [170] T. T. Mai, A. N. M. Haque, P. P. Vergara, P. H. Nguyen, and G. Pemen, "Adaptive coordination of sequential droop control for PV inverters to mitigate voltage rise in PV-Rich LV distribution networks," *Electric Power Systems Research*, vol. 192, pp. 1–13, 2021. [Online]. Available: <https://doi.org/10.1016/j.epsr.2020.106931>
- [171] D. Shi, X. Chen, Z. Wang, X. Zhang, Z. Yu, X. Wang, and D. Bian, "A Distributed Cooperative Control Framework for Synchronized Reconnection of a Multi-Bus Microgrid," *IEEE Transactions on Smart Grid*, vol. 9, no. 6, pp. 6646–6655, 2018.
- [172] E. Demirok, P. C. González, K. H. Frederiksen, D. Sera, P. Rodriguez, and R. Teodorescu, "Local reactive power control methods for overvoltage prevention of distributed solar inverters in low-voltage grids," *IEEE Journal of Photovoltaics*, vol. 1, no. 2, pp. 174–182, 2011.
- [173] D. D. Šiljak, "Chapter 7 Nested Epsilon Decompositions," in *Decentralized Control of Complex Systems*, 1991, vol. 184, pp. 374–413.
- [174] M. M. M. Ali, N. G. Paterakis, P. H. Nguyen, and J. F. Cobben, "A LV network overvoltage mitigation strategy based on epsilon-decomposition," in *IEEE Manchester PowerTech*. Manchester: IEEE, 2017.
- [175] A. F. Hoke, M. Shirazi, S. Chakraborty, E. Muljadi, and D. Maksimovic, "Rapid Active Power Control of Photovoltaic Systems for Grid Frequency Support," *IEEE Journal of Emerging and Selected Topics in Power Electronics*, vol. 5, no. 3, pp. 1154–1163, 2017.
- [176] E. I. Batzelis, G. E. Kampitsis, and S. A. Papathanassiou, "Power Reserves Control for PV Systems With Real-Time MPP Estimation via Curve Fitting," *IEEE Transactions on Sustainable Energy*, vol. 8, no. 3, pp. 1269–1280, 2017.

-
- [177] E. I. Batzelis, S. A. Papathanassiou, and B. C. Pal, "PV System Control to Provide Active Power Reserves under Partial Shading Conditions," *IEEE Transactions on Power Electronics*, vol. 33, no. 11, pp. 9163–9175, 2018.
- [178] A. Olshevsky, "Linear Time Average Consensus on Fixed Graphs and Implications for Decentralized Optimization and Multi-Agent Control," in *IFAC Workshop on Distributed Estimation and Control in Networked Systems*, no. 22, 2015, pp. 94–99.
- [179] T. Aziz and N. Ketjoy, "PV Penetration Limits in Low Voltage Networks and Voltage Variations," *IEEE Access*, vol. 5, pp. 16 784–16 792, 2017.
- [180] P. Lusi, L. L. Andrew, A. Liebman, and G. Tack, "Interaction between Coordinated and Droop Control PV Inverters," in *e-Energy 2020 - Proceedings of the 11th ACM International Conference on Future Energy Systems*, 2020, pp. 314–324.

List of Figures

1.1	Percentage of wind and solar PV in total electricity generation [5].	2
1.2	Percentage of wind and solar PV generation curtailment [5].	3
1.3	Visualisation of the thesis outline and the correlation between the chapters and the research questions (Q1 - Q6).	6
2.1	The concept of the grid-edge monitoring and control.	10
2.2	Main challenges for grid operation and planning due to high RES penetration.	11
2.3	Types of modelling and simulations of the grid-edge control.	16
2.4	Classification of grid-edge control strategies based on their communication network: (a) Centralised control, (b) Decentralised control, (c) Distributed control. The green circles represent RES, while the orange circle represent a central controller. The dashed blue lines represent two-way communication links.	17
2.5	Active power control based on (a) - $P - f$ droop control and (b) - $P - V$ droop control.	23
2.6	(a) - FPF method for reactive power control of a RES system: the orange curve represents the apparent power S , P^{rated} and P denotes the rated and injected active power, respectively, and \bar{Q} denotes maximum reactive power. (b) - VPF(P) method for reactive power control of a RES system: PF^{LIM} Capacitive and Inductive represent PF limit values in capacitive and inductive operation, P_{th}^{min} and P_{th}^{max} denote threshold active power for PF^{LIM} Capacitive and Inductive, respectively. P_{db}^{lower} and P_{db}^{upper} denote lower and upper values of the dead-band interval.	24
2.7	Operation regions of RES power outputs demonstrated by the dash-line regions for two control strategies: (a) - without minimum allowed PF requirement and (b) - with the minimum allowed PF requirement.	26
3.1	Methodological framework.	33
3.2	Single-line diagram of the IEEE European LV test network. The numerical value denotes the number of the node where the load is connected [127].	36

3.3	A pair plot for the transformer phase A loading (S_{trans}^A) and voltage magnitudes (V) at the POC of the houses H3, H1, H31, H29, and H48 connecting to the same phase. This pair plot consists of histogram plots along the diagonal, Pearson correlation coefficients below the diagonal, and scatter plots above it.	38
3.4	A pair plot for the transformer phase A loading (S_{trans}^A) and net active power (P^{net}) of houses H3, H1, H31, H29, and H48 connecting to the same phase. This pair plot consists of histogram plots along the diagonal, Pearson correlation coefficients below the diagonal, and scatter plots above it.	39
3.5	A pair plot for the transformer phase A loading (S_{trans}^A) and net reactive power (Q^{net}) of houses H3, H1, H31, H29, and H48 connecting to the same phase. This pair plot consists of histogram plots along the diagonal, Pearson correlation coefficients below the diagonal, and scatter plots above it.	40
3.6	Feature importance and selection with the LASSO approach. H_i with $\forall i \in \mathcal{N}^A$ denotes the house number as listed in Table 3.1. The vertical red dashed line represents the importance threshold with $\omega = 2.5$	42
3.7	Methodology of model evaluation and selection for a ML algorithm based on the k -fold CV inner loop of Nested CV.	48
3.8	Spread of RMSE results across each fold of the CV outer loop for ML algorithms.	50
3.9	PDF of the absolute values of transformer loading.	53
3.10	PDF of the errors between the measurements and the estimations by the models.	53
4.1	Droop characteristics for local voltage control of PV systems. (a) $P - V$ droop control, (b) $Q - V$ droop control.	60
4.2	(a) The SDC mechanism applied for PV unit i consisting of $Q - V$ droop control (dark blue curve) and $P - V$ droop control (red curve). (b) The operation region (shaded triangle) of the PV inverter i determined by the apparent power S_i (orange curve), rated active power P_i^{rated} , maximum reactive power \bar{Q}_i , and PF requirement ($\cos \varphi = \text{PF}$).	62
4.3	PDF and ECDF of the voltage levels in the network without any control mechanism.	67
4.4	Maximum voltage deviation index at the POCs of the PV units with Group A cases.	68
4.5	PDF and ECDF of the voltage levels in the network with Group A cases.	69
4.6	Transformer loading index with Group A cases.	70
4.7	System power losses with Group A cases.	70
4.8	Curtailed energy index with Group A cases.	71
4.9	Exported energy index with Group A cases.	72

5.1	Schematic representation of a LV distribution network with the proposed control strategy, consisting of local control (LC) and centralised control (CC). The orange dotted lines represent the control signals, while the blue dashed lines represent the information exchange.	77
5.2	SDC mechanism applied for two PV inverters in different locations of a radial LV feeder.	78
5.3	Integration of local control (LC) and centralised control (CC) (adjusted from [167]).	81
5.4	Methodology for integrating local control and centralised control. APC depicts active power curtailment of PV inverters. N-R denotes Newton-Raphson algorithm. LP represents Linear Programming technique.	82
5.5	The test network based on a Dutch LV distribution network. The arrows and solid circles represent loads and PV units, respectively, along with their index. The numerical values along the power cable sections denote the cable length in meters, while the uppercase letters denote the cable types.	84
5.6	Solar irradiation and ambient temperature profiles used in the simulation.	85
5.7	Measured voltage levels at the POCs of all the houses during the simulated two days without any control algorithms. Each index represents the corresponding individual house.	87
5.8	PDF and ECDF of the voltage levels for different control methods.	88
5.9	Percentage of curtailed energy of PV systems.	89
5.10	(a) Full view and (b) Zoomed-in view for the profiles of the measured voltage (V_i) and the adaptation of the droop control parameters (V_i^{tP}) of PV unit no. 1 and 6 when operating with Method 3. The dashed-line rectangular in Fig. (a) indicates the region of the zoomed-in view shown in Fig. (b).	90
6.1	Block diagram of a LV distribution network with the proposed control strategy, composed of two control levels: a local control, implemented using SDC; and a coordination control, implemented using CBDC. The orange dotted and blue dashed lines represent the control signals and information exchange, respectively.	96
6.2	The test network based on a real European LV distribution network. The arrows and solid circles represent loads and PV units, respectively, along with their index. The numerical values along the power cable sections denote the cable length in meters, while the uppercase letters denote the cable types.	102
6.3	Decomposition of the test network for $\varepsilon = 0.21$ and determination of control areas as shaded regions. The solid circles represent PV units along with their index.	104

6.4	A sparse communication network for the decomposed test network with $\varepsilon = 0.21$ presented as a graph. The numerical circles represent PV units. The blue two-end arrow dashed lines represent the bi-directional communication links between PV units, while the numerical values along with the communication links denote the information weight factors (d_{ij}).	105
6.5	Voltage magnitude at the POCs of PV systems in the network without any control mechanism.	106
6.6	Maximum voltage level measured in the network for different control methods using Empirical Cumulative Distribution Function (ECDF).	107
6.7	Curtailed active power (P), absorbed reactive power (Q) and voltage profiles for different control methods over two consecutive days of PV index no. 23.	108
6.8	Curtailed energy of the PV inverters for different control methods during voltage rise conditions as a percentage of individual PV energy (kWh) in the case with no control. Each index from 8 to 39 represents the corresponding individual PV unit, while the last index, i.e., Sum, represents the total amount. The shaded, rounded rectangles covering the PV index represent the groups of PV inverters within the corresponding control areas in Method 3 with $\varepsilon = 0.21$	109
6.9	Absorbed reactive power (Q) profiles for different control methods over two consecutive days of PV index no. 10.	110
6.10	Curtailed energy percentages of the PV inverters during voltage rise conditions in Method 3 with various ε values. Each index from 8 to 39 represents the corresponding individual PV unit, while the last index, i.e., Sum, represents the total amount.	112
6.11	Iteration number of the consensus algorithm applied in PV index no. 23 over two consecutive days. The zoomed-in figure in the middle shows the iteration number, i.e., the height of the bar represented in y-axis, for a time duration (hh:mm), i.e., the width of the bar represented in x-axis.	113
6.12	Identifying ε value. The x-axis depicts two consecutive ε values. The left y-axis represents the percentage decrease in the number of bi-directional communication links (BCL) associated with two successive ε values, while the right y-axis represents the percentage decrease in the consensus iteration (CI) numbers.	114
B.1	A pair plot for the transformer phase A loading (S_{trans}^A) and voltage magnitudes (V) at the POC of the houses H25, H14, H51, H34, H52, H22, H21, and H54 connecting to the same phase. This pair plot consists of histogram plots along the diagonal, Pearson correlation coefficients below the diagonal, and scatter plots above it.	130

B.2	A pair plot for the transformer phase A loading (S_{trans}^A) and voltage magnitudes (V) at the POC of the houses H5, H30, H4, H9, H49, H20, H55, and H46 connecting to the same phase. This pair plot consists of histogram plots along the diagonal, Pearson correlation coefficients below the diagonal, and scatter plots above it.	131
B.3	A pair plot for the transformer phase A loading (S_{trans}^A) and net active power (P^{net}) of houses H25, H14, H51, H34, H52, H22, H21, and H54 connecting to the same phase. This pair plot consists of histogram plots along the diagonal, Pearson correlation coefficients below the diagonal, and scatter plots above it.	132
B.4	A pair plot for the transformer phase A loading (S_{trans}^A) and net active power (P^{net}) of houses H5, H30, H4, H9, H49, H20, H55, and H46 connecting to the same phase. This pair plot consists of histogram plots along the diagonal, Pearson correlation coefficients below the diagonal, and scatter plots above it.	133
B.5	A pair plot for the transformer phase A loading (S_{trans}^A) and net reactive power (Q^{net}) of houses H25, H14, H51, H34, H52, H22, H21, and H54 connecting to the same phase. This pair plot consists of histogram plots along the diagonal, Pearson correlation coefficients below the diagonal, and scatter plots above it.	134
B.6	A pair plot for the transformer phase A loading (S_{trans}^A) and net reactive power (Q^{net}) of houses H5, H30, H4, H9, H49, H20, H55, and H46 connecting to the same phase. This pair plot consists of histogram plots along the diagonal, Pearson correlation coefficients below the diagonal, and scatter plots above it.	135
C.1	Maximum voltage deviation index at the POCs of the PV units with Group B cases.	138
C.2	PDF and ECDF of the voltage levels in the network with Group B cases.	138
C.3	Transformer loading index with Group B cases.	139
C.4	System power losses with Group B cases.	139
C.5	Curtailed energy index with Group B cases.	140
C.6	Exported energy index with Group B cases.	140
C.7	Maximum voltage deviation index at the POCs of the PV units with Group C cases.	141
C.8	PDF and ECDF of the voltage levels in the network with Group C cases.	141
C.9	Transformer loading index with Group C cases.	142
C.10	System power losses with Group C cases.	142
C.11	Curtailed energy index with Group C cases.	143
C.12	Exported energy index with Group C cases.	143

List of Tables

3.1	Summary of household load characteristics and PV installations in phase A	35
3.2	Pre-defined hyperparameters of the compared ML algorithms	46
3.3	Summarised results for model evaluation and selection of SVR	48
3.4	Summary of RMSE results and computational time for individual ML algorithm	50
3.5	Summarised results for model set-up of RFR and XGBR	51
3.6	Summary of model performance	52
3.7	Measurements of simulation time (mm:ss)	54
4.1	Simulation cases for the impact assessment	67
4.2	Q2 results of the system annual billing with Group A cases	73
5.1	Properties of the MV/LV transformer used in the test network	84
5.2	R, X characteristics of the power cables of the test network	84
5.3	Properties of household loads and PV systems	85
5.4	Results summary for all control methods	89
6.1	R, X values for the power cables of the test network	101
6.2	Properties of load profiles and PV systems	102
6.3	Summarized results for 3 control methods	107
6.4	Comparison of different control methods with different threshold values .	111
6.5	Summarized results of applying Method 3 with various ε values	113
A.1	Summary of household load characteristics and PV installations in phase B	127
A.2	Summary of household load characteristics and PV installations in phase C	128
C.1	Group B and Group C simulation cases for the impact assessment	137

List of Abbreviations

APC	Active Power Curtailment
BCL	Bidirectional Communication Links
CBDC	Consensus-Based Distributed Control
CC	Centralised Control
CEI	Curtailed Energy Index
CI	Consensus Iteration
CV	Cross-Validation
DG	Distributed Generation
DSO	Distribution System Operator
ECDF	Empirical Cumulative Distribution Function
EDA	Exploratory Data Analysis
EEL	Export Energy Index
EMS	Energy Management System
ESS	Energy Storage Systems
EU	European Union
EV	Electric Vehicle
FPF	Fixed Power Factor
HP	Heat Pump
HV	High Voltage
ICT	Information and Communication Technology
IoT	Internet of Things
KNMI	Koninklijk Nederlands Meteorologisch Instituut (Royal Dutch Meteorological Institute)
LASSO	Least Absolute Shrinkage and Selection Operator
LC	Local Control
LEC	Local Energy Community
LR	Linear Regression
LV	Low Voltage
MAS	Multi-Agent Systems
ML	Machine Learning
MPC	Model Predictive Control

MPPE	Maximum Power Point Estimation
MPPT	Maximum Power Point Tracking
MV	Medium Voltage
MVDI	Maximum Voltage Deviation Index
OLTC	On-Load Tap Changers
PDF	Probability Density Function
PF	Power Factor
POC	Point of Connection
PV	Photovoltaic
PRC	Power Reduction Control
PRRC	Power Ramp-Rate Control
Q	Question
RES	Renewable Energy Source
RFR	Random Forest Regression
RMSE	Root Mean Square Error
RPA	Reactive Power Absorption
RT	Real Time
RR	Ridge Regression
SAB	System Annual Billing
SDC	Sequential Droop Control
SM	Smart Meter
SVR	Support Vector Regression
TLI	Transformer Loading Index
THD	Total Harmonic Distortion
VPF	Varying Power Factor
VUF	Voltage Unbalance Factor
XGBR	eXtreme Gradient Boosting Regression

List of Publications

Journal papers

- T.T. Mai, P.H. Nguyen, A.N.M.M. Haque, A.J.M. Pemen (2022). Exploring regression models to enable monitoring capability of local energy communities for self-management in low-voltage distribution networks. *IET Smart Grid*, vol. 5, no. 1, pp. 25–41
- T.T. Mai, P.H. Nguyen, T.Q. Tran, A. Cagnano, G. De Carne, Y. Amirat, T.A. Le, E. De Tuglie (2021). An overview of grid-edge control with the digital transformation. *Electrical Engineering*, vol. 103, pp. 1989 – 2007
- T.T. Mai, A.N.M.M. Haque, P.P. Vergara, P.H. Nguyen, A.J.M. Pemen (2020). Adaptive coordination of sequential droop control for PV inverters to mitigate voltage rise in PV-Rich LV distribution networks. *Electric Power Systems Research*, vol. 192, pp. 1 - 13
- P.P. Vergara, M. Salazar, T.T. Mai, P.H. Nguyen, J.G. Slootweg (2020). A comprehensive assessment of PV inverters operating with droop control for overvoltage mitigation in LV distribution networks. *Renewable Energy*, vol. 159, pp. 172 – 183
- T.T. Mai, A.N.M.M. Haque, T. Vo, P.H. Nguyen (2019). Coordinated active and reactive power control for overvoltage mitigation in physical LV Microgrids. *The Journal of Engineering*, vol. 2019, pp. 5007 - 5011

Conference papers

- M.Q. Tran, T.T. Mai, T.T. Tran, P.H. Nguyen (2022). Self-adaptive Controllers for Renewable Energy Communities based on Transformer Loading Estimation. *Accepted at IEEE International Conference on Environment and Electrical Engineering and IEEE Industrial and Commercial Power Systems Europe, 2022, Prague, Czech Republic*

- R. Revaliente-Revuelta, T.T. Mai, H. Khalilnezhad, P.H. Nguyen, A.V.D Molen (2021). Techno-Economic Assessment of Local Control Strategies for PV Inverters in the Dutch LV Distribution Networks. *IEEE International Universities Power Engineering Conference (UPEC), 2021, Middlesbrough, UK*
- T.T. Mai, P.H. Nguyen (2020). Distributed Control of PV for Voltage Rise Mitigation in LV Distribution Networks with Heat Pumps. *International Symposium on Power, Energy, and Cybernetics (ISPEC), 2020, Hanoi, Vietnam*
- T.T. Mai, M. Salazar, A.N.M.M. Haque, P.H. Nguyen (2020). Stochastic Modelling of the Correlation between Transformer Loading and Distributed Energy Resources in LV Distribution Networks. *International Conference and Exhibition on Electricity Distribution (CIRED), 2020, Berlin, Germany, pp. 1 – 5*
- T.T. Mai, A.N.M.M. Haque, P.H. Nguyen (2019). Consensus-Based Distributed Control for Overvoltage Mitigation in LV Microgrids. *IEEE PES PowerTech, 2019, Milan, Italy, pp. 1 – 6*
- P.P. Vergara, T.T. Mai, A. Burstein, P.H. Nguyen (2019). Feasibility and Performance Assessment of Commercial PV Inverters Operating with Droop Control for Providing Voltage Support Services. *IEEE PES Innovative Smart Grid Technologies Europe (ISGT-Europe), 2019, Bucharest, Romania, pp. 1 – 5*
- F.K. Adiguno, T.T. Mai, P.H. Nguyen (2019). Mitigating Impact of Large-Scale PV Integration on MV Distribution Network with Sequential Control Functions: A Case Study in Noordwolde Grid, The Netherland. *International Conference and Exhibition on Electricity Distribution (CIRED), 2019, Madrid, Spain, pp. 1 – 5*
- T.T. Mai, A.N.M.M. Haque, T.H. Vo, P.H. Nguyen, M.C. Pham (2018). Development of ICT Infrastructure for Physical LV Microgrids. *IEEE International Conference on Environment and Electrical Engineering and IEEE Industrial and Commercial Power Systems Europe, 2018, Palermo, Italy, pp. 1 – 6*

Peer reviewed EU project deliverable

- K.E. Antoniadou-Plytaria, I. Bouloumpasis, T.T. Mai (2019). Report on physical micro-grid interface with real test-site validation. *m2M-GRID project deliverable, D4.3, 2019*
- T.Q. Tran, G. Mouloud, T.T. Mai, M.C. Pham (2019). Control algorithms for micro-grid local controllers. *m2M-GRID project deliverable, D4.1, 2019*
- K.E. Antoniadou-Plytaria, T.T. Mai, G. Mouloud (2019). Preparation for demonstration sites. *m2M-GRID project deliverable, D2.3, 2019*

Peer reviewed Dutch project deliverable

- P.P. Vergara, T.T. Mai, P.H. Nguyen (2019). Theoretical background of PQ in Control. *TKI Project Power Quality (PQ) in Control project deliverable, D3.2, 2019*

Acknowledgments

I thought that it would be very far and challenging to reach the stage of writing the thesis. I still remember the stressful days when I struggled to develop the research ideas for the first scientific article and then the other ones. Also, many sleepless nights I devoted myself to debugging the simulation models. Besides, the PhD completion was the most critical deadline and always hung above my head in the last four years. It is still hard to believe that I overcame these challenges and managed to write this final chapter. It would never have been completed without the valuable support of many people. I gratefully acknowledge all their support and would like to thank some people in particular.

I would like to sincerely thank my first promotor and supervisor, Dr. Phuong Nguyen, as without him it would never have been possible. In the supervisor role, Phuong constantly supported me throughout my PhD in various ways: his earnestness and solemnity for my research; his thoughtfulness and encouragement when I struggled. Additionally, Phuong always gave his guidance flexibly and timely whenever I asked with his in-depth knowledge, constant drive to be “proactive and flexible”, and immense patience with me, for which I am deeply grateful. In the promotor role, Phuong’s guidance made the thesis finalisation so smooth and well-organised, and his detailed feedback has improved the thesis content. His support and guidance have been invaluable for my PhD research and enlightened me during the most difficult years, which shaped a turning point in my life.

My special thank goes to my second promotor, Professor Guus Pemen for his guidance during my PhD years and his valuable feedback of the thesis. Also, Professor Guus Pemen has arranged support from his scientific family, the EES group, for my research. It has truly been an honor working with you.

I am grateful to my co-promotor, Dr. Niyam Haque, for all his kind support I have received during my PhD. Dr. Niyam Haque acted as a daily supervisor of my PhD with his continuously shared scientific experience, thoughtful advice, and the MATLAB simulation models, which significantly helped to focus my research and write the scientific articles. In addition, his critical review had a high contribution to improve this thesis.

My sincere gratitude goes to Professors Paulo Ribeiro, Johan Driesen, Sjeff Cobben and Dr. Anh Tuan Le for their roles as the doctoral committee members in my PhD defence. Their

feedback was invaluable both for the thesis and for future work.

I would like to extend my thanks to a partner of my PhD research project, m2M-GRID, Professor Quoc Tuan Tran, for helping me with a research exchange at the Grenoble Institute of Technology in 2017 and sharing a LV distribution network model.

I am immensely thankful for my PhD colleagues in the EES group. They are Simone, Niels, and Mansoor, who helped me by sharing the simulation models and research topics and being friendly persons to socialise. In addition, they are Babar, Bram, Mana, Lindsey, Ravi, Stanislav, Arpit, Siam, Nijhuis, Irena and Andrew for having cheerful social talks and their feedback. Next, my special thanks go to Pedro for his competent advice on scientific writing, including Latex using guidance and sharing research ideas; to Mauricio for sharing Python programming techniques and machine learning knowledge. I highly appreciated the excellent collaboration with Pedro and Mauricio for our joint papers. Finally, I would like to especially thank Quan and An for the time together with great ‘meaningful’ discussions, memorable typical Dutch lunches, and healthy after-lunch walking on the beautiful routes on the TU/e campus from season to season.

I would like to thank my colleague in DNV PSP NL team, Mr. Jan Frederik Groeman for helping me in Dutch translation of the thesis summary.

I would like to acknowledge the great help from my ‘brother’ also my EES colleague, Dr. Thai Hau Vo. He offered me a place to live free of charge when I had just arrived in Eindhoven, for which I also would like to thank his wife, Thanh Ngoc Ton Nu. Besides, Dr. Thai Hau Vo meticulously guided me in MATLAB modelling, shared his PhD experience with me in the challenging early days, and spent his time debugging my simulation models. His help all meant a lot to me, especially during the difficult early days. Additionally, I would like to thank another ‘brother’, Dr. Dai Nguyen, for inspiring me to apply for a PhD when I was about to finish my Master degree in Australia.

I was lucky to have such wonderful Vietnamese friends in Eindhoven, such as Trang, Hai, Vinh, Mai and many others that are not listed due to an insufficient space here. They assisted my family and me immerse smoothly in life here and having enjoyable moments. With their assistance, my life was balanced out of work, which in turn helped me conduct my PhD.

This thesis is dedicated to my family. To my wife, Hai, and two of my sons, Pisu and Mon, for their unconditional support and companionship with me on this journey. They have always been there to share every bit of the ups and downs I had during my PhD and motivate me to keep moving forward. My heartfelt deep love and gratitude to Hai, Pisu and Mon!. To my parents and my parents-in-law for all their great love and favour on me to pursue this PhD. Especially to my mother: I can make you more proud of me for now obtaining this PhD, and our family and I always love you!.

Curriculum Vitae

Tam Thanh Mai (Vietnamese: Mai Thanh Tâm) was born on 02nd May, 1985 in Nam Dinh, Vietnam. He received the Bachelors degree in Electrical Engineering in Power Systems at Hanoi University of Science and Technology (HUST), Vietnam in June 2008. Upon graduation, he joined as a Power Systems Engineer in the Electricity Authority Regulatory of Vietnam (ERAV), Vietnam. From October 2008 to May 2010, he attended an intensive Transmission System Operation Training program at the National Load Dispatch Center (EVNNLDC), Vietnam. As a result, he gained in-depth knowledge of the high-voltage grid and power generation technologies and operational planning. Also, he developed a deep understanding of the real-time operating procedures for the national high-voltage grid and power generation dispatch. At the end of the training program, he was well qualified for the final training to be a (national) transmission system operator. During the next five years working for ERAV, his main duties were to daily supervise power generation dispatch and power network operation for stable performance of power systems. Besides, he analysed/appraised the annual planning for power generation dispatch and power network expansion, complying with Grid Code and Distribution Code. In 2015 he was awarded the Australia Awards Scholarship (AAS) funded by the Australian Government to pursue the MSc program "Master of Engineering Management (MEM)" at the University of Technology Sydney (UTS), Australia. From May 2017, he joined as a PhD student at the Electrical Energy Systems (EES) group at Eindhoven University of Technology (TU/e) and has been working on monitoring and controlling low-voltage distribution networks with high renewable energy penetration. His research interests include coordination control, data-driven approach, and integration of renewable energy resources.